2010-01-01

Iron And Manganese Based Nanomaterials For The Removal Of Selenite And Selenate From Aqueous Solution

Christina Marie Gonzalez
University of Texas at El Paso, cgonzalez13@miners.utep.edu

IRON AND MANGANESE BASED NANOMATERIALS FOR THE REMOVAL OF SELENITE AND SELENATE FROM AQUEOUS SOLUTION

CHRISTINA MARIE GONZALEZ

Department of Chemistry

APPROVED:

_____
Jorge Gardea-Torresdey, Ph.D. Chair

_____
Jose R. Peralta-Videa, Ph.D.

_____
John McClure, Ph.D.

_____
Patricia D. Witherspoon, Ph.D.
Dean of the Graduate School

Dedication

I dedicate this work to my parents, David and Helen R. Gonzalez.

IRON AND MANGANESE BASED NANOMATERIALS FOR THE REMOVAL OF SELENITE AND SELENATE FROM AQUEOUS SOLUTION

By

CHRISTINA MARIE GONZALEZ, B.S.

THESIS

Presented to the Faculty of the Graduate School of

The University of Texas at El Paso

in Partial Fulfillment

of the Requirements

for the Degree of

MASTER OF SCIENCE

Department of Chemistry

THE UNIVERSITY OF TEXAS AT EL PASO

August 2010

Acknowledgements

I would like to express my sincere gratitude to my parents David and Helen R. Gonzalez for all their support and the many sacrifices they have made for me during my studies. I am also extremely grateful for the rest of my family whom have been there for me throughout this experience.

I would also like to thank Dr. Jorge Gardea-Torresdey for giving me the opportunity to join such a talented research group. I am extremely grateful for the support, knowledge, and advice he has given me throughout my studies. I also acknowledge Dr. Jose Peralta-Videa for his knowledge and his many contributions on my drafts of my manuscripts, as well as my thesis. I am also thankful for having the opportunity to work with Dr. Jason Parsons and Dr. Laura Lopez-Moreno who were able to help me with any problems I encountered with my experiments and especially with the ICP-MS. In addition, I would like to thank Dr. Parsons for his assistance with the XAS studies. I would also like to express my appreciation to my lab group for their support, team work, and friendship they have offered me throughout my research.

I would also like to acknowledge the financial support of the National Science Foundation Graduate Teaching Fellows in K-12 Education (DGE #0538623), the National Science Foundation and the Environmental Protection Agency under Cooperative Agreement Number EF 0830117, USDA grant number 2008-38422-19138**,** the Toxicology Unit of the BBRC (NIH NCRR Grant # 2G12RR008124-16A1) and the NSF Grant # CHE-0840525. Portions of this research were carried out at the Stanford Synchrotron Radiation Laboratory, a national user facility operated by Stanford University on behalf of the U.S. Department of Energy, Office of Basic Energy Sciences. The SSRL Structural Molecular Biology Program is supported by the Department of Energy, Office of Biological and Environmental Research, and

by the National Institutes of Health, National Center for Research Resources, Biomedical Technology Program. I also acknowledge the Department of Chemistry, College of Science, UTEP Graduate School, and National Society for the Advancement of Chicanos and Native Americans in Science for the funding they rewarded me in order to travel to the many conferences I have attended throughout my graduate studies to present my research findings.

Finally, I would like to thank all of my friends who have supported me and believed in me throughout my studies.

Abstract

Selenium, a naturally occurring element in the environment, is an essential nutrient for humans and animals. However, there is a narrow range between selenium deficiency and toxicity. Selenium in natural waters generally has a concentration of < 10 ppb (parts per billion); however, in the San Joaquin Valley of California concentrations of selenium ranging from 140 to 1400 ppb have been observed. Anthropogenic practices such as agricultural irrigation drainage, coal burning power plants, combustion of fossil fuels, and mining operations are increasing selenium concentrations in aqueous environments. Once in aqueous environments, selenium exists primarily as the two inorganic oxoanions selenite (SeO_3^{2-}) and selenate (SeO_4^{2-}). Both of these selenium oxoanions are known to bioaccumulate and can cause embryotoxic and teratogenic effects to waterfowl. There has been a variety of treatment technologies developed for remediation of both selenium oxoanions in water including bacterial reduction, membrane filtration, chemical reduction, reverse osmosis, and solar ponds. However, these treatment technologies are not cost efficient. In this study an alternative treatment technique known as adsorption was used with three synthetic nanomaterials consisting of an iron oxide, manganese oxide, and an iron/manganese oxide. The pH profiles, time dependencies, competitive anion effects, and adsorption isotherms were performed with each of the nanomaterials for both selenite and selenate. In addition, X-ray absorption spectroscopy (XAS) studies were performed to determine both the oxidation state and binding coordination of the selenium oxoanion binding to the nanomaterials.

The investigation revealed the non microwave-assisted and microwave-assisted synthetic Fe_3O_4 and Mn_3O_4 nanomaterials, as well as the non microwave-assisted synthetic $MnFe_2O_4$ nanomaterial had the phases of magnetite, hausmannite, and Jacobsite, while the grain sizes were

27, 25, 25, 34, and 27 nm, respectively. The optimal binding of selenium oxoanions for all nanomaterials examined was reached at pH 4. Both non microwave-assisted and microwave-assisted Fe_3O_4 and non-microwave-assisted $MnFe_2O_4$ had binding times of 5 min while non microwave-assisted and microwave-assisted Mn_3O_4 nanomaterials had a binding time of 10 min. The presence of Cl^- ions only significantly decreased selenate binding to Mn_3O_4 nanomaterials while the NO_3^- ion significantly decreased selenate binding to microwave-assisted Fe_3O_4 and Mn_3O_4 nanomaterials. The inclusion of the SO_4^{2-} ion deceased selenite binding to only Mn_3O_4 nanomaterials and decreased selenate binding to all nanomaterials. Both selenite and selenate binding to all nanomaterials tested was significantly decreased by the addition of the PO_4^{3-} ion. Non microwave-assisted and microwave-assisted Fe_3O_4, non microwave-assisted and microwave-assisted Mn_3O_4, and non microwave-assisted $MnFe_2O_4$ displayed binding capacities of 1893, 2380, 507, 1000, and 6573.76 mg selenite/kg nanomaterial and 1428, 2369, 800, 934.5, and 769.23 mg selenate/kg nanomaterial, respectively. X-ray Absorption Near Edge Structure (XANES) studies revealed all nanomaterials tested do not change the oxidation state of selenite and selenate once binding has occurred. The results of Extended X-ray Absorption Fine Structure (EXAFS) displayed the possible binding modes of selenium oxoanions to all materials tested is, binuclear bidentate.

Table of Contents

List of Tables

Page

List of Figures

Page

1. Introduction

1.1 Selenium

Selenium (Se) is a naturally occurring trace element with semi-metallic characteristics that is introduced into the environment by the dissolution and weathering of selenium bearing minerals and marine sediments such as Cretaceous marine shale rock [1]. Due to its characteristics, Se has been used in a variety of applications such as photocells, rectifiers, xerography equipment, glass pigment, laser technology, infrared photography, drugs, rubber, lubricating oils, manufacture of dandruff shampoo, and for coating of stainless steel and copper [2,3]. Consequently, many of these industrial practices generate effluents that can contain considerable amounts of soluble selenium which could increase environmental Se to dangerous levels [4]. Also, many agricultural activities such as the irrigation of seleniferous soils for crop production are a major source of selenium introduction into the environment [1]. Selenium can exist as elemental selenium (Se^0), selenite (SeO_3^{2-}), selenide (Se^{2-}), and selenate (SeO_4^{2-}) [5]. In aqueous environments, selenium exists predominantly as the oxoanions selenite and selenate [5].

Selenium is an essential element for both human and animal health [6]. Selenocysteine is functionally one of the most used selenium species in biochemical processes because it is a component of glutathione peroxidase, an enzyme that catalyzes the removal of toxic peroxides that are commonly formed during aerobic metabolic processes [1,7]. Interest in the determination of selenium in the environment, especially aqueous selenium, has been growing due to the extremely narrow range between selenium deficiency and toxicity [6]. It has been reported that selenium deficiency in humans occurs when daily consumption of selenium is less than 0.1 mg/kg of body weight while consumption of levels above 1 mg/kg of body weight are considered toxic [1]. According to the Material Safety Data Sheets, the acute oral toxicity

(LD_{50}) for sodium selenite and sodium selenate in rats is 7.0 and 1.6 mg/kg, respectively. The United States Environmental Protection Agency has set the Maximum Contamination Level (MCL) of selenium in drinking water to be 0.05 mg/L due to this narrow range [8]. Typically, natural waters generally have Se concentrations < 10 μg/L [9]. However, there have been elevated levels of selenium reported in the San Joaquin Valley of California which have reported selenium concentrations in the range of 140-1400 μg/L as well as in the Salton Sea region with concentrations of Se in the range of 3-300 μg/L [10]. Adverse effects on humans due to excess selenium have included hair or fingernail loss, numbness in fingers or toes, circulation problems, and liver damage [11,12].

In aquatic systems, selenium has been known to bioaccumulate [9]. Bioaccumulation of selenium occurs when plankton, plants, algae, and benthic invertebrates accumulate selenium, which are than eaten by fish and other wildlife [1]. It has also been stated that the biomagnifications of selenium, which is the accumulation of progressively greater concentrations by successive trophic levels of the food chain, can result in the range of 2-6 times between the primary producer (plants, algae, etc.) and the lower consumer (invertebrates and fish) [1]. As a result, concentrations of selenium in fish that eat the contaminated plankton could contain 500 times the selenium concentration of their surrounding water environment [1]. This bioaccumulation of selenium causes serious hazards to wildlife living in regions with high levels of selenium. It has been reported that high levels of selenium in wildlife can result in reproductive failure, deformities, tissue damages, and the extirpation of fish populations [1,13]. In waterfowl, high concentrations of selenium can be both embryotoxic and teratogenic [14]. Due to the harmful effects of excess selenium concentrations in aqueous environments as described above, a removal technique for both selenite and selenate is needed.

1.2 Previous Selenium Removal Techniques

There have been a variety of treatment technologies that have been developed in the attempts to remove aqueous selenium. These technologies focus primarily on the removal of the two predominant selenium species in aqueous environments, selenite and selenate. These include coagulation, lime precipitation, sand filtration, ion exchange, nanofiltration, reverse osmosis, solar ponds, bioremediation, and phytoremediation [1,15,16,17]. The high cost and complexity of regeneration of ion exchange resins makes ion exchange treatment methods unsuitable for large treatments of water despite its elevated efficiency for removal of selenium oxoanions [18]. The use of a bioremediation system using the bacterial species *Thauera selenatis* was able to reduce selenate and selenite in agricultural drainage water by 98% [19]. However, it has been shown this treatment technique was not cost efficient for full-scale operation [10]. Coagulation and lime softening were reported to be ineffective for the removal of selenium from wastewater [18]. Therefore, an effective and simple technique for selenium oxoanion removal is needed.

1.3 Adsorption

"Sorption" describes the loss of a chemical species from aqueous phase to a contiguous solid phase by three separate mechanisms known as adsorption, precipitation, and absorption [20]. There has been an increase in selenium sorption studies because sorption plays a significant factor in the mobility, transport, transformation, and the ultimate fate of selenium in both soil and aquatic systems [21]. A promising, cost efficient treatment process for the removal of selenium oxoanions is adsorption. An assortment of adsorbents have been investigated for the treatment of aqueous solutions with excess selenium which include sulphuric acid-treated peanut shell, hydrocalumite, ettringite, $AlPO_4$, biopolymeric materials, aluminum-based water treatment

residuals, hardened cement paste, cement minerals, aluminum oxides, iron oxyhydroxides, iron coated sand, zero-valent iron, montnorillonite, and manganese nodule leached residues [4,5,6,10,13,22-27]. However, not all the aforementioned adsorbents investigated the removal of both selenium oxoanions [4,5,10,22,27]. Also, not all previous materials investigated have high capacities for both selenite and selenate or have fast equilibrium times for adsorption. Additionally, naturally occurring anions in the environment such as Cl^-, NO_3^-, SO_4^{2-}, or PO_4^{3-} were not tested which could act as possible competitive anions for the active sites on the adsorbent surface for selenium oxoanion binding.

1.4 Nanomaterials for use as enhanced adsorbents

The use of synthetic nanomaterials could increase the rate of adsorption and capacity of metal oxides for selenium oxoanion removal which may not naturally occur at the nanoscale. For example, a study by Martinez *et al*. [28] has shown the naturally occurring and magnetic metal oxide magnetite (Fe_3O_4) with a particle size <5 μm is capable of binding selenite and selenate at acidic pH. Mayo *et al.* [29] demonstrated an increase of adsorption capacities up to 200 times of both As(III) and As(V) when the particle size of magnetite was decreased from 300 to 12 nm. Decreasing the size of magnetite for selenium oxoanion adsorption could also have a significant increase in adsorption capacities.

Another synthetic nanomateial that has shown to be a good adsorbent is the magnetic, substituted metal oxide Jacobsite ($MnFe_2O_4$). Hu *et al*. [30] reported 10 nm surface-modified Jacobsite removed Cr(VI) at high capacities within only 5 min. Parsons *et al.* [31] synthesized a 12 nm Jacobsite which had binding capacities for As(III) and As(V) of 718 and 2125 μg As/g $MnFe_2O_4$, respectively within 5 min. However, the use of Jacobsite has not been investigated as an adsorbent for selenium oxoanions. Jacobsite's ability to remove other anions with high

capacities could make it a potential adsorbent for selenium with high capacities and equilibrium time.

Synthetic manganese oxides have shown to have the capability of adsorbing selenite in a previous study [32]. The manganese oxide hausmannite (Mn_3O_4) has not been studied for its ability to remove selenite and selenate from aqueous solutions. The synthesis of nanonsize Mn_3O_4 has been gaining attention due to its wide range of applications, one of which is molecular adsorption [33]. The application of a synthetic nanosized hausmannite which would have an increased surface area may display a high performance for selenium oxoanion removal.

1.5 Objectives

The general objective of this research was to study the selenite and selenate binding capability of the nanomaterials Fe_3O_4, Mn_3O_4, and $MnFe_2O_4$. A series of batch experiments were performed to determine the effects of pH, time, and the presence of various anions (Cl^-, NO_3^-, SO_4^{2-}, PO_4^{3-}) on the binding capabilities of the aforementioned nanomaterials. In addition, the adsorption data was fitted using the Langmuir isotherm equation to determine the adsorption capacities of the aforementioned nanomaterials. Finally, the oxidation state and coordination of the selenium oxoanions following binding to the nanomaterials were tested using X-ray Absorption Near Edge Spectroscopy (XANES) and Extended X-ray Absorption Fine Structure (EXAFS).

1.6 Hypotheses

This research was conducted under the hypothesis that at least one of the nanomaterials, Fe_3O_4, Mn_3O_4, or $MnFe_2O_4$, will adsorb both selenium oxoanions in acidic pH ranges, with equilibrium times of less than one hour, and in the presence of various anions. Also, at least one

of the aforementioned nanomaterials will display increased adsorption capacities for both selenite and selenate. Finally, the oxidation state for both selenium oxoanions will remain the same after binding to the nanomaterials has occurred.

2. Removal of selenite and selenate from aqueous solutions using nano-magnetite

Abstract

The sorption of selenite (SeO_3^{2-}) and selenate (SeO_4^{2-}) onto Fe_3O_4 nanomaterials produced by non microwave-assisted or microwave-assisted synthetic techniques was investigated through use of the batch technique. The crystal structures of both synthetic nanomaterials were determined to be magnetite by X-ray Diffraction. The average size of non microwave-assisted and microwave-assisted synthetic Fe_3O_4 were determined to be 27 and 25 nm, respectively through use of the Scherrer's equation. Sorption of selenite was pH independent in the pH range of 2-6, while sorption of selenate decreased at pH 5 and 6. The addition of Cl^- had no significant effect on selenite or selenate binding, while the addition of NO_3^- only affected selenate binding to the microwave assisted Fe_3O_4. A decrease of selenate binding to both synthetic particles was observed after the addition of SO_4^{2-} while selenite binding was not affected. The addition of PO_4^{3-} had the most prominent effect on the binding of both selenite and selenate beginning at concentrations of 0.1 ppm added. The capacities of binding were found to be 1923 and 1428 mg Se /kg of non microwave-assisted Fe_3O_4 and 2380 and 2369 mg Se/ kg of microwave-assisted Fe_3O_4 for selenite and selenate, respectively through use of Langmuir isotherms.

2.1 Introduction

The narrow range between selenium deficiency and toxicity in humans is of concern today. Selenium deficiency in humans occurs when there is less than 0.1 mg Se/kg of body weight while selenium consumption of levels above 1 mg Se/kg of body weight are considered toxic [1]. The United States Environmental Protection Agency has set the maximum

contamination level (MCL) of selenium in drinking water to be 0.05 mg/L, as drinking water is a primary source in which selenium can enter the human body [2-3]. Animals are also at risk when high concentrations of selenium are present in water systems. It has been reported in waterfowl, high levels of selenium are embryotoxic and teratogenic [4]. In water, selenium exists predominately as the inorganic forms: selenite (SeO_3^{2-}, where the Se is present as the Se^{4+} ion) and selenate (SeO_4^{2-}, where the Se is present as the Se^{6+} ion) [5].

There has been a variety of treatment technologies developed for remediation of both selenium oxoanions in water by many researchers including bacterial reduction, membrane filtration, chemical reduction, reverse osmosis, and solar ponds [6-8]. However, these treatment technologies are not cost effective. An alternative treatment technique that has been gaining increasing attention in study over the past decade is adsorption. A variety of adsorbents for the removal of selenium have been tested, which include sulphuric acid-treated peanut shell, hydrocalumite, ettringite, $AlPO_4$, biopolymeric materials, aluminum-based water treatment residuals, hardened cement paste, cement minerals, aluminum oxides, iron oxyhydroxides, iron coated sand, and zero valent iron [8-17]. The use of magnetic materials as adsorbents may emerge as an even more efficient form of treatment technology. Magnetic materials are promising materials for adsorption because they can easily be removed from aqueous effluents by a simple process known as magnetic separation [18]. These materials are also useful because they produce no further contaminants such as flocculants and are capable of treating large amount of wastewater within a short amount of time [19].

The iron oxide magnetite (Fe_3O_4) is an adsorbent with magnetic properties. A study by Martinez *et al.* [20] has shown naturally occurring magnetite with a particle size <5 μm has been capable of binding selenite and selenate at acidic pH. Lopez de Arroyabe Loyo *et al.* [21]

reported rapid selenite binding to ultra small Fe_3O_4 and Fe/Fe_3C particles, but did not test the capacity of the material nor its ability for selenate adsorption. These studies indicate magnetite may be a promising adsorbent for selenium removal. However, many previous studies for selenium oxoanion removal do not investigate the ability of the adsorbent to remove both selenite and selenate. Also, the effects of naturally occurring potential competitive anions Cl^-, NO_3^-, SO_4^{2-}, or PO_4^{3-} on selenium oxoanion removal have not been thoroughly investigated.

In this study, we have synthesized the magnetic iron oxide Fe_3O_4 by both non microwave-assisted and microwave-assisted synthetic techniques. The nanomaterials produced by both of these techniques were determined to have the crystal structure of magnetite. The Fe_3O_4 nanomaterials' adsorption capacities for selenite and selenate were tested in the pH range of 2 through 6 and as a function of time. The effects of the addition of individual competitive anions Cl^-, NO_3^-, SO_4^{2-}, or PO_4^{3-} added to solution in a range of 0.1 to 100 ppm were also investigated. Finally, the capacities of both synthetic nanomaterials for selenite or selenate binding were studied using selenium concentrations of 0.25 through 10 ppm and fitted with Langmuir isotherms.

2.2 Methodology

2.2.1 Solution preparation

Reagent grade Na_2SeO_3 (Aldrich), Na_2SeO_4 (Alfa Aesar), NaCl (Aldrich), $Mg(NO_3)_2 \cdot 6H_2O$ (Mallinckrodt), K_2SO_4 (J.T. Backer), and $Na_3PO_4 \cdot 12H_2O$ (EM Science) chemicals were dissolved in Millipore (18 mΩ) water to obtain stock solutions of selenite, selenate, chloride, nitrate, sulfate and phosphate, respectively. The prepared stock solutions were diluted to proper concentrations for the following research experiments.

2.2.2 Synthesis of the iron oxide nanomaterial

The iron oxide nanomaterials were prepared from two separate 1.0 L solutions of 30 mM Fe(II) (from $FeCl_2$, EM Science). Both solutions were slowly titrated separately for 1 h with 90 mL of 1.0 M NaOH solution (from NaOH, VWR International) to obtain a ratio of 1:3 ratio of $Metal^+$:OH^-. The slow rate of titration was to prevent the precipitation of $Fe(OH)_3$ from occurring. After completion of the titration, one of the titrated solutions was heated to 90° C for 1 h on a heating plate and resulted in the non microwave-assisted nanomaterial. The other solution was transferred into sealed vessels and placed in a Perkin Elmer Mulitwave 2000 system (Shelton CT, USA). The sealed vessels were heated to a temperature of 90° C and held constant for 25 min at a pressure of 75 bars and resulted in the microwave-assisted nanomaterial. The nanomaterials were cooled to room temperature and centrifuged at 3000 rpm (Fisher Scientific 8K, Houston, TX) for 5 min after both techniques were completed. The samples were then washed twice with deionized water (DI) to remove any byproducts that may have been produced during the synthesis. The samples were than dried in a VWR 1305U oven (VWR International, West Chester, PA) at 100° C for 24 h. Lastly, the samples were homogenized into a powder using a mortar and pestle for experimental use.

2.2.3 XRD characterization

Both synthetic nanomaterials were characterized by powder X-ray diffraction (XRD) and fitted using FullProf Suite programs. A Siemens D5000 X-ray diffractometer (Bruker AXS GmbH, Germany) was used to acquire XRD patterns of both synthetic nanomaterials. The samples were placed on a platinum sample holder and diffracted from 25-60° in 2θ using 8 s counting time and a stepping rate of 0.007°/min at room temperature. A Le Bail fitting of both patterns was performed using FullProf Suite programs and crystallographic data from the

literature [22]. A Gaussian fitting to three diffraction peaks on both patterns applied to the Scherer's equation was performed to obtain the average particle size of each nanomaterial.

2.2.4 Binding pH profile

In these studies, the binding of either selenite or selenate to both synthetic nanomaterials were determined over a pH range of 2 to 6. The pH of the 100 ppb selenite or selenate solutions were adjusted to pH 2, 3, 4, 5, or 6 using dilute hydrochloric acid or sodium hydroxide prior to reactions. The reactions were then carried out in 5 mL polyethylene reaction tubes containing 10 mg of either nanomaterial with a 4 mL aliquot of 100 ppb of selenite or selenate. The reaction tubes were than rocked (Specimix, Thermo Scientific) and allowed to equilibrate for 60 min at room temperature. The samples were than centrifuged at 3000 rpm for 7 min and the resulting supernatants were collected for analysis using the inductively-coupled plasma-mass spectrometer (ICP-MS) ELAN DRCII (Perkin Elmer, Shelton, CT) to determine the amount of selenium oxoanion removed. In addition, control samples containing only selenite or selenate oxoanions were treated the same as the samples to determine the effects of the methodology and polyethylene reaction tubes had on the selenium oxoanion binding. All experiments in this study and subsequent experiments were conducted in triplicate for statistical purposes.

2.2.5 Time dependency studies

The time required for either selenite or selenate to equilibrate was determined using 100 ppb of selenite or selenate adjusted to pH 4 reacted with 10 mg of each nanomaterial separately at different time intervals. The pH of 4 was chosen for these experiments because the nanomaterials are both stable at this pH and there was no significant change in binding above this pH level found in the previous study. The pH adjustment was carried out as described in the

pH binding study. A 4 mL aliquot of either 100 ppb selenite or selenate solution was added to 10 mg of either non microwave-assisted nanomaterial or microwave-assisted nanomaterial and was allowed to equilibrate for 5, 10, 15, 20, or 30 min. The samples were centrifuged and the supernatant collected for analysis using DR-ICP-MS.

2.2.6 Competitive anion studies

The possible competition for active adsorption sites on both synthetic nanomaterials between selenite and selenate in the presence of varying concentrations of Cl^-, NO_3^-, SO_4^{2-}, or PO_4^{2-} added to 100 ppb selenium oxoanion solutions were investigated and adjusted to pH 4. A 4 mL aliquot solution containing 100 ppb of selenite or selenate solution and either 0.1, 1, 10, or 100 ppm of the possible interfering ion of Cl^-, NO_3^-, SO_4^2, or PO_4^{3-} was reacted with either synthetic nanomaterial and allowed to equilibrate for 1 h. After reaction time was completed, the samples were centrifuged and the supernatant was collected for ICP-MS analysis.

2.2.7 Adsorption Isotherms

The capacities of both non microwave-assisted and microwave-assisted synthesized nanomaterial for selenium oxoanions was investigated using varying concentrations of either selenite and selenate in the range of 0.25 to 10 ppm. For these reactions a 4 mL aliquot of either selenite or selenate at concentrations of 0.25, 0.5, 1, 5, or 10 ppm adjusted to pH 4 were reacted on a rocker with 10 mg of either synthetic nanomaterial for a period of 15 min. The reaction was performed in triplicate with control samples as mentioned previously. The samples were centrifuged after the reaction time was completed and the supernatant was collected for analysis by ICP-MS. The obtained data was then fitted to the Langmuir isotherm equation shown below,

where C_e is equilibrium concentration of Se(IV/VI), Q_e is the amount of Se(IV/VI) adsorbed to the nanomaterial at equilibrium, and *Qm* and *b* are constants based on ionic strength and pH.

$$\frac{C_e}{Q_e} = \frac{1}{(bQ_m)} + \frac{1}{(Q_m)} C_e$$

2.2.8 DRC-ICP-MS Analysis

A Perkin Elmer Elan DRC II ICP-MS with ELAN software was used for selenium quantification of the supernatants obtained from the experiments described above. The operational parameters of the DRC-ICP-MS for selenium analysis are described in Table 2.1. To reduce interferences on the selenium ions the samples were ran in dynamic reaction cell (DRC) mode using oxygen gas. The Se-O *m/z* 96 was the chosen ion used for analysis as Se-O production is favored under these conditions. All concentrations of selenium were obtained based on calibration curves with a correlation coefficient (r^2) of 0.99 or better.

Table 2.1. ICP-MS settings used for the determination of Se concentration in collected supernatants upon reaction with either non microwave-assisted or microwave-assisted synthesized nanomaterial.

Parameter	Setting
RF Power	1200W
Nebulizer	Meinhard Type A Quartz
Nebulizer flow	0.95 L/min
Spray chamber	Glass cyclonic
Injector	Quartz
Plasma flow (Ar)	15 L/min
CeO/Ce	<5%
Ba^+/Ba^{++}	<5%
O_2	0.85 mL/min

2.2.9 Statistical Analysis

The binding percentages of the selenium oxoanions to both sets of synthetic Fe_3O_4 were analyzed with one-way analysis of variance (ANOVA) using SPSS software, version 12.0 (SPSS, Chicago, IL). The Tukey-HSD (honestly significant difference) test was used to determine significant differences between treatments. References to significant differences between treatment means were based on a probability of $p < 0.05$, unless otherwise stated.

2.3 Results and Discussion

2.3.1 X-ray diffraction characterization of nanomaterial

Characterization of both the non microwave-assisted and microwave-assisted materials by powder X-ray diffraction determined both sets of nanomaterial had the chemical structure of magnetite Fe_3O_4 and diffraction patterns can be seen in Figure 2.1. Both patterns displayed the diffraction peaks of 220, 311, 400, 422, and 511 and correspond to the phase of magnetite (Fe_3O_4) as reported in the literature [22]. The other observed diffraction peaks of 111 and 200 correspond to the platinum sample holder used for pattern collection. The average grain sizes of each of the synthesized nanomaterials was determined from the full width half maximum (FWHM) of the diffraction peaks collected through use of the Scherer's equation. It was determined the non microwave-assisted and microwave-assisted synthetic nanomaterials had the average grain sizes of 27 and 25 nm, respectively. Both of the two synthetic techniques of Fe_3O_4 in this study did not result in oxidation of Fe_3O_4 to γ-Fe_2O_3 though it has been reported this oxidation may possibly occur [23]. The size difference in Fe_3O_4 between the two synthetic techniques could be attributed to the pressure of the microwave. Both synthetic techniques are advantageous due to their simplicity and cost effectiveness compared to other previously

reported preparation techniques of magnetic materials which involve many steps, special chemicals, and procedures [18].

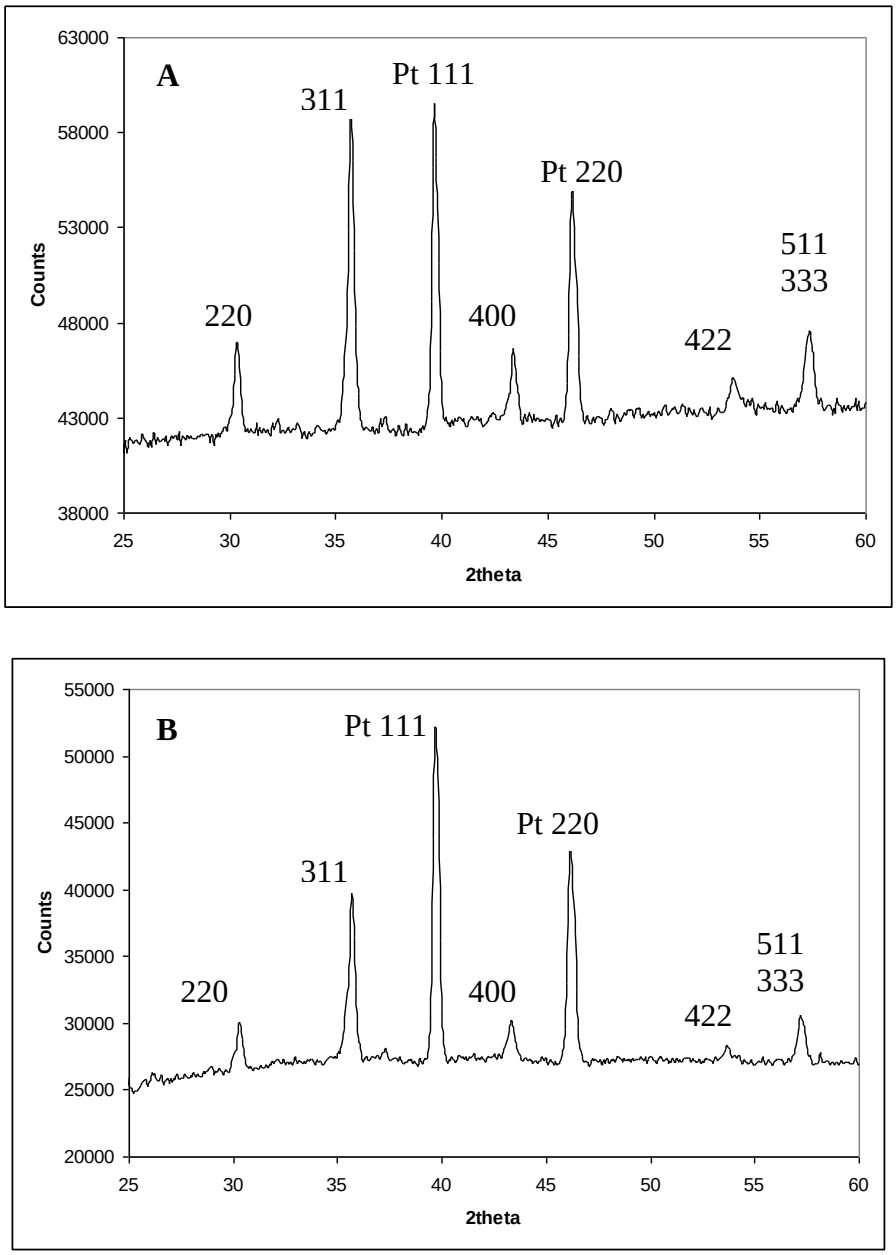

Figure 2.1. X-ray diffraction pattern of Fe_3O_4 from titration of iron(II) chloride with sodium hydroxide. (A) non microwave-assisted synthesis. (B) microwave-assisted synthesis.

2.3.2 pH binding studies

The sorption of selenite and selenate to both sets of synthetic nanomaterials can be seen in Figure 2.2. The binding of selenite to both synthetic Fe_3O_4 nanomaterials was practically pH independent as shown in Figure 2.2. The sorption of selenate had the highest binding at pH 2 to 4 for both synthetic types of Fe_3O_4. A decrease in selenate binding occurred at pH 5 for both particles and a more significant decrease was seen at pH 6. The decrease in binding could be due to the change in surface charge at higher pH values. It has been reported magnetites have a zero-point charge which mostly occurs in the pH range from 5-7 [24]. When the pH increases the surface of the particle will become less positively charged resulting in a lower binding affinity for anion binding. It has been shown selenate has a lower binding affinity to iron oxide surfaces than selenite [25]. The lower binding affinity of selenate in addition to the change of surface charge at increasing pH values, could explain the decrease in binding at pH 5 and 6. The remaining experiments were conducted at a pH of 4 for maximum binding of selenate to the nano-magnetite materials. The nano-magnetite has also been shown to be more stable at pH of 4 as opposed at pH 2 to 3 where dissolution of the particle occurs to a greater extent [26].

A

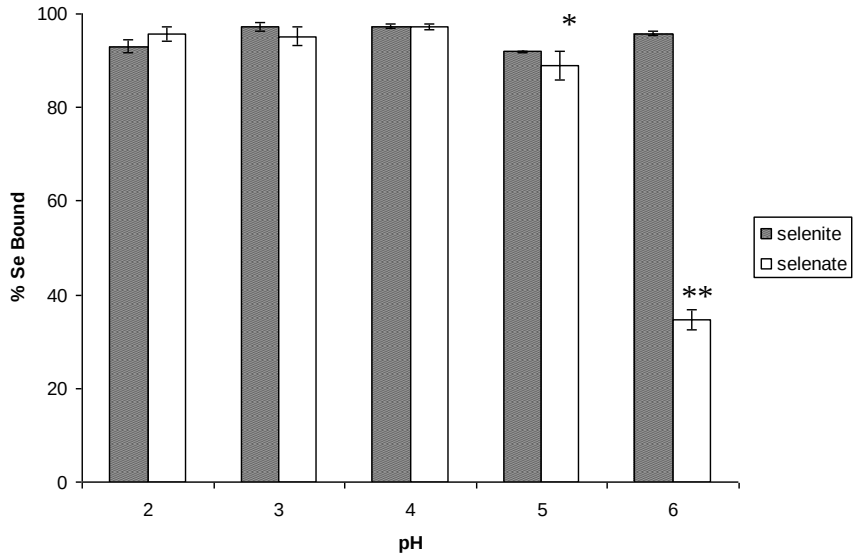

B

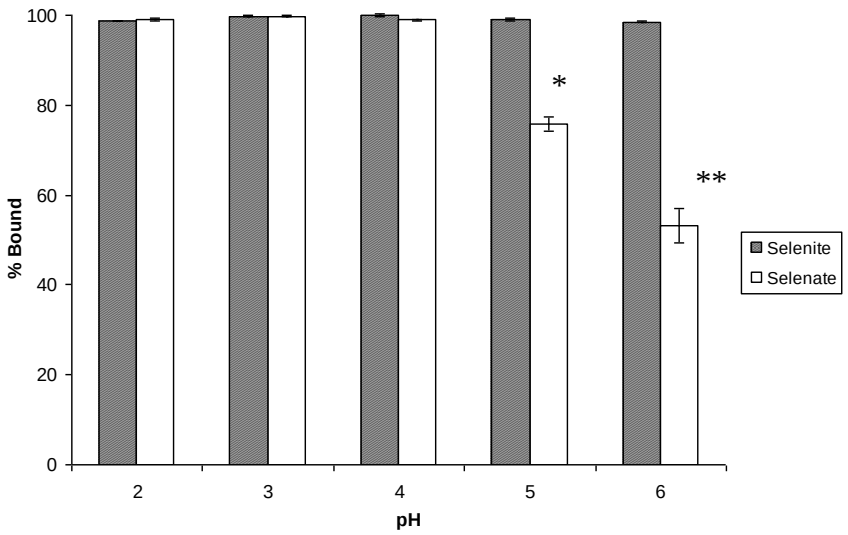

Figure 2.2. Percentage bound of selenite and selenate at a concentration of 100 ppb to the nanomaterial under varying pH conditions ranging from pH 2 to 6. (A) non microwave-assisted Fe_3O_4. (B) microwave-assisted Fe_3O_4. Error bars represent Standard Error of three replicate. * represents statistical differences at $p \leq 0.05$.

2.3.3 Time dependency studies

The binding of selenium oxoanions to non microwave-assisted and microwave-assisted synthetic Fe_3O_4 nanomaterials as a function of time is shown in Figure 2.3. Statistical analysis with one-way ANOVA determined that there was no significant difference in the binding of selenite or selenate to either non-microwave-assisted or microwave-assisted synthetic Fe_3O_4 in a time range of 5 to 60 min. Su and Suarez [27] have shown selenite and selenate binding equilibrates within 25 min of contact time to iron oxides and goethitite. It is interesting to note the rapid binding of selenite to synthetic Fe_3O_4 with average particle size of 4 nm within 10 min of contact time has been shown by Lopez de Arroyabe Loyo *et al.* [28]. Martinez *et al.* [20] have shown both selenite and selenate binding to a natural magnetite with a particle size <5 μm took over 24 h to reach binding capacity. This observation suggests that even though the synthetically

produced nanomaterials used in this study are almost 7 times larger than those produced and used by Lopez de Arroyabe Loyo *et al.* [28], the fact these particles are at nanoscale produces faster binding times than micrometer sized particles. The Fe_3O_4 nanomaterial is non-porous so the smaller the particle, the larger surface area with more available binding sites for selenium oxoanion binding to occur. This suggests the binding is occurring on the surface without the occurrence of a redox reaction. This would indicate the oxidation states of both selenite and selenate will remain the same. This is further proved by Extended X-ray Absorption Fine Structure (EXAFS) produced by Lopez de Arroyabe Loyo *et al.* [28] where no shift of backscattering contribution was observed of the coordination shell of Se and Fe between 2.3 to 2.6 Å.

A

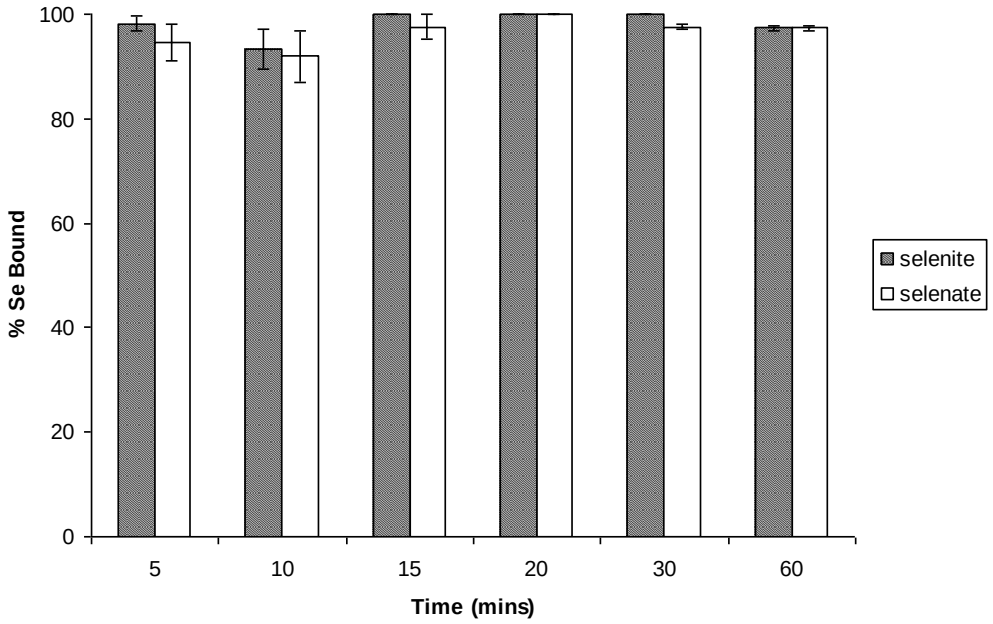

B

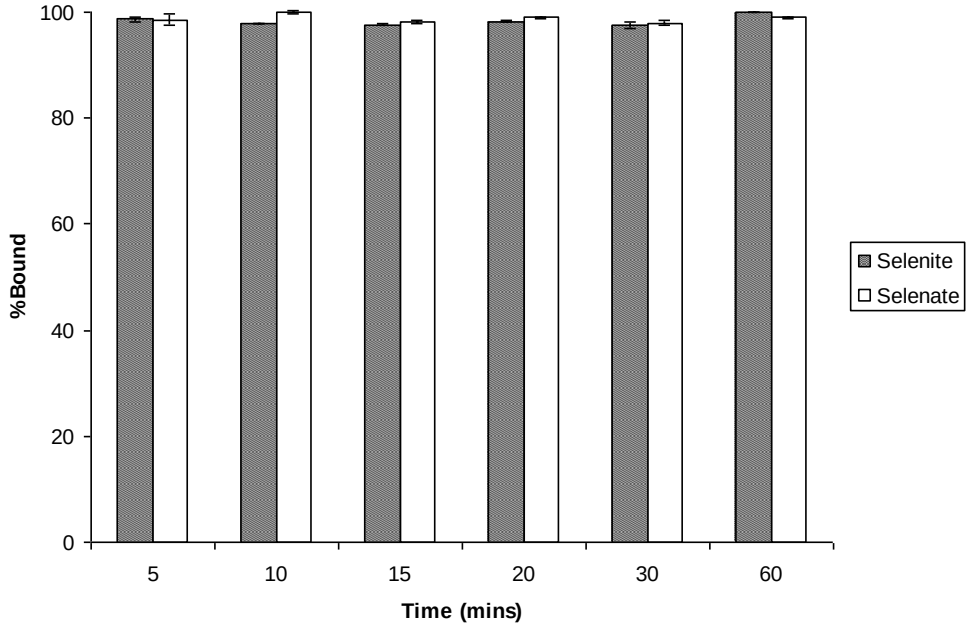

Figure 2.3. Time dependence of percentage bound of selenite and selenate to the nanomaterial at a pH of 4. (A) non microwave-assisted Fe_3O_4. (B) microwave-assisted Fe_3O_4. Error bars represent Standard Error of three replicate.

2.3.4 Competitive anion studies

The results of the competition study on selenite and selenate to both non microwave-assisted and microwave-assisted synthesized nanomaterials in the presence of varying concentrations of Cl^-, NO_3^-, SO_4^{2-}, or PO_4^{3-} added can be seen in Figures 2.4-2.7. As shown in Figure 2.4A-B, the addition of Cl^- in concentration from 0.1 to 100 ppm had no significant effect on the percentage of both selenite and selenate binding to either Fe_3O_4 nanomaterial. This indicates the Cl^- ion has a low binding affinity for Fe_3O_4. A similar observation of Cl^- not acting as a competitive anion for the iron oxide surface was reported by Jeong *et al.* [29]. These similarities in results indicate that chloride has a low binding affinity for iron oxide surface and complexes formed between chloride and iron oxide surface are weaker than those between iron oxide and selenium.

A

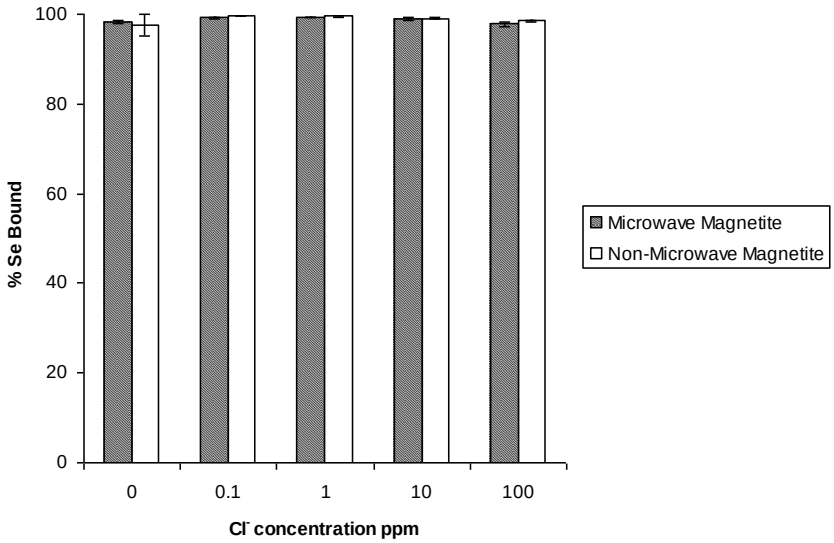

B

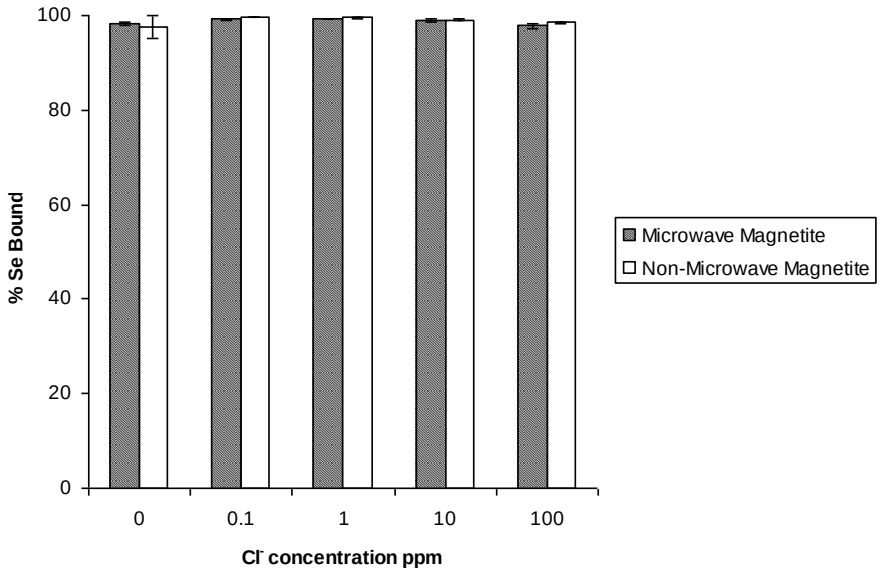

Figure 2.4. The effects of the Cl^- ion ranging in concentration from 0.1-100 ppm on the sorption of selenite and selenate to non microwave-assisted and microwave-assisted Fe_3O_4. (A) Selenate. (B) Selenite. Error bars represent Standard Error of three replicate..

The inclusion of NO_3^- also did not affect the binding of selenite to either of the two synthetically different Fe_3O_4 as can be seen in Figure 2.5B. This non-competitive effect of the nitrite anion could be behaving the same as the chloride anion. While the addition of NO_3^- did not have an effect on selenate binding to the non microwave-assisted synthetic Fe_3O_4, the anion did lower selenate binding by 30% on the microwave-assisted synthetic Fe_3O_4 material. One possible explanation for the decrease in selenate binding to only the microwave-assisted synthetic Fe_3O_4 material is the size of the material. Dhillon and Dhillon [30] have stated that competitive effect of sorbed anions could occur either by physical competition for reactive sites or through electrostatic competition results from a change in electrostatic potential. As explained in the X-ray diffraction analysis of the two different synthetically produced nanomaterials, the microwave-assisted synthetic technique resulted in a smaller average particle size of Fe_3O_4 than that of the non microwave-assisted synthetic technique. A smaller particle size would result in larger surface area and a higher number of reactive sites. This greater number of binding sites along with selenate having a lower binding affinity than observed for selenite could allow the NO_3^- to compete to a higher extent with the selenate oxoanion present in solution.

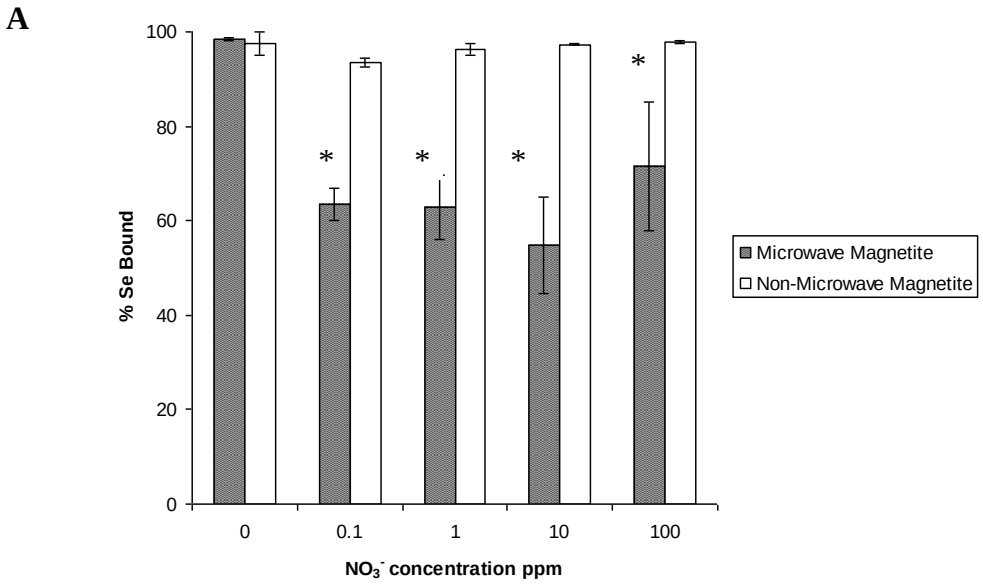

B

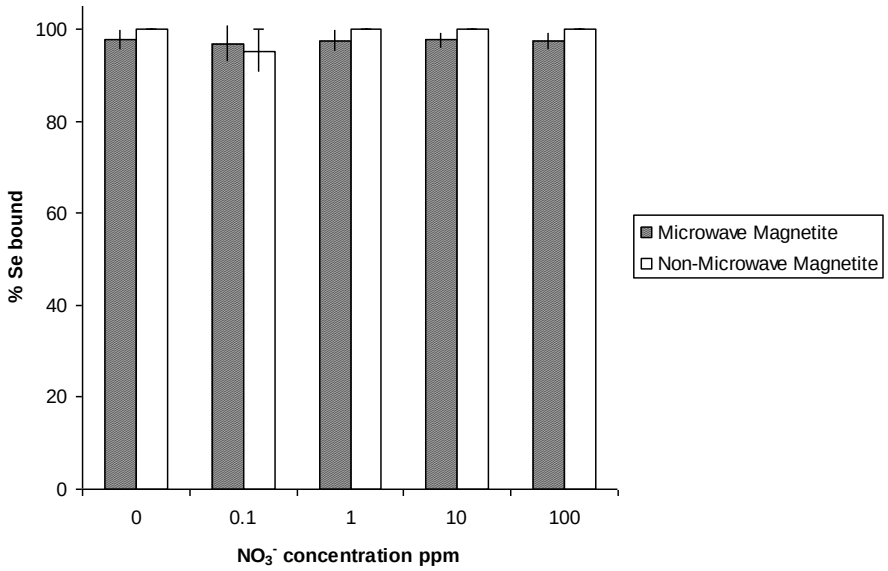

Figure 2.5. The effects of the NO_3^- ion ranging in concentration from 0.1-100 ppm on the sorption of selenite and selenate to non microwave-assisted and microwave-assisted Fe_3O_4. (A) Selenate. (B) Selenite. Error bars represent Standard Error of three replicate. * represents statistical differences at $p \leq 0.05$.

The effects of the addition of SO_4^{2-} on selenite or selenate binding to the two synthetic nanomaterials can be seen in Figure 2.6. Selenite did not experience a significant decrease in binding in the presence of SO_4^{2-} in a range of 0.1-100 ppm which is shown in Figure 2.6B. Goh and Lim [31] and Zhang *et al.* [32] have shown similar results with selenite binding being hardly affected by addition of SO_4^{2-}oxoanion to iron oxide containing tropical sand and iron-coated granular activated carbons (GAC), respectively. There was a decrease of selenate binding to both microwave-assisted and non microwave-assisted synthesized nanomaterials beginning at 1 and 10 ppm, respectively. In the presence of 1 ppm sulfate, the molar ratio of selenate to sulfate is 1 SeO_4^{2-} : 14.9 SO_4^{2-}. The non microwave-assisted material still has around 100 % binding while the microwave assisted material has 60% binding. This indicates the Fe_3O_4 materials have a high affinity for selenate despite the differences in surface area. At 10 ppm of sulfate present,

the molar ratio of selenate to sulfate is 1 SeO_4^{2-} : 149 SO_4^{2-}. Again, at these ratios selenate binding decreased for both Fe_3O_4 particles to 15 and 80% binding for non microwave-assisted and microwave-assisted synthetic Fe_3O_4, respectively. When in the presence of 100 ppm sulfate the molar ratio of selenate to sulfate is SeO_4^{2-} : 1488 SO_4^{2-}. Even though the binding percentages are 6% and 20% for non microwave-assisted and microwave-assisted nanomaterials, respectively, binding occurring at this molar ratio is still indicative of the high affinity for selenate to Fe_3O_4 materials. It is known the chemistry of selenate and sulfate is quite similar. This similarity in chemistry could be the explanation of the decreased sorption of selenate in the presence of sulfate. Zhang *et al.* [32] described this effect by explaining both anions tend to form weak bonds with surface sites which could be more easily released. The smaller particle size of the microwave-assisted synthesized Fe_3O_4, as described above, could explain why binding started to decrease at a lower concentration of SO_4^{2-} (1 ppm) as opposed to the non microwave-assisted synthetic Fe_3O_4 binding (10 ppm).

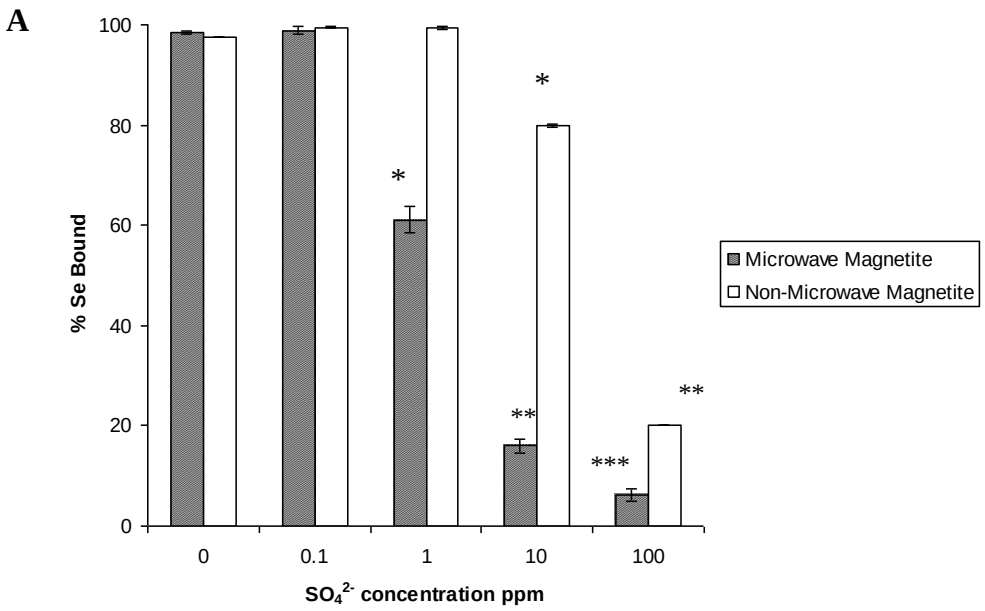

B

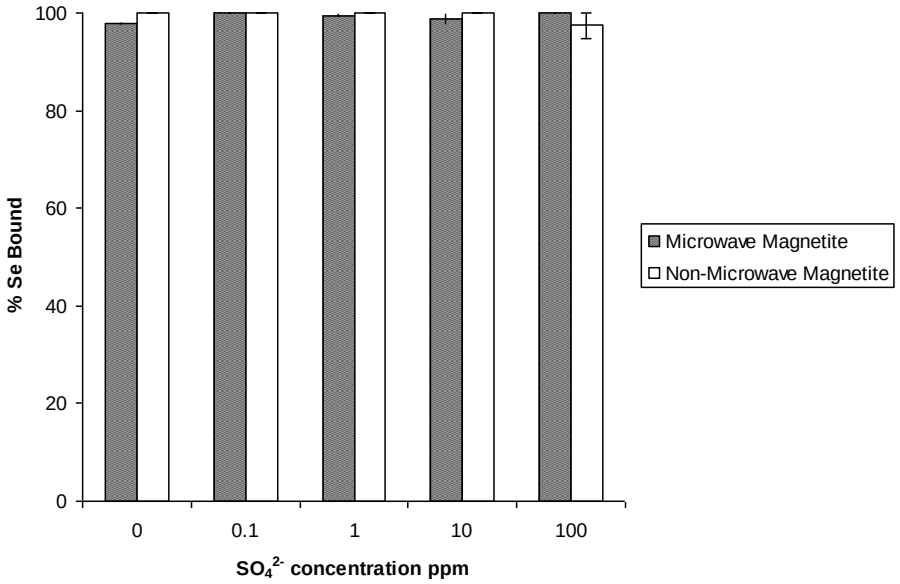

Figure 2.6. The effects of the SO_4^{2-} ion ranging in concentration from 0.1-100 ppm on the sorption of selenite and selenate to non microwave-assisted and microwave-assisted Fe_3O_4. (A) Selenate. (B) Selenite. Error bars represent Standard Error of three replicate. * represents statistical differences at $p \leq 0.05$.

The competitive effect of the addition of PO_4^{3-} anion on selenite and selenate binding to both synthetic Fe_3O_4 nanomaterials can be seen in Figure 2.7. The addition of PO_4^{3-} had a greater affect on the binding of selenate to the synthetic Fe_3O_4 nanomaterials than any other anion investigated in this study. A decrease in selenite binding to microwave-assisted and non microwave-assisted synthetic Fe_3O_4 nanomaterials was observed to begin at the introduction of 10 and 100 ppm of PO_4^{3-}, respectively. In the presence of 100 ppm PO_4^{3-}, the molar ratio of selenite to phosphate is 1 SeO_3^{2-} : 1000 PO_4^{3-}. Even at this large molar ratio of sulfate to selenite ions present, there is still selenite binding occurring to the non microwave-assisted synthetic material. This indicates a high affinity for selenite is shown at this molar ratio. A decrease in binding of selenate to microwave-assisted synthetic Fe_3O_4 was observed to occur not only with a

lower concentration of PO_4^{3-} introduced, but at a greater extent than that of the non microwave-assisted synthetic Fe_3O_4 nanomaterial. These trends have been observed by Goh and Lim [31] and Zhang *et al.* [32-33] in tropical sand containing iron oxides and iron-coated GAC, respectively. As explained previously, the differences in the selenium binding percentages between the non microwave-assisted and microwave-assisted nanomaterials could be a result of the smaller particle size of the microwave-assisted synthetic Fe_3O_4 nanomaterial. A significant decrease of less than 1% and 0% selenate binding to non microwave-assisted synthetic and microwave-assisted synthetic Fe_3O_4, respectively was observed to occur at the addition of 100 ppm of PO_4^{3-}. The inclusion of 100 ppm PO_4^{3-} in solution results in a molar ratio of 1 SeO_4^{2-} : 1505 PO_4^{3-}. There had to be 1505 times the concentration of phosphate present to for selenate binding to decrease to almost 0%. It has been described in the literature that the PO_4^{3-} oxoanion is very adsorptive to the surfaces of iron oxides in low concentration range [29].

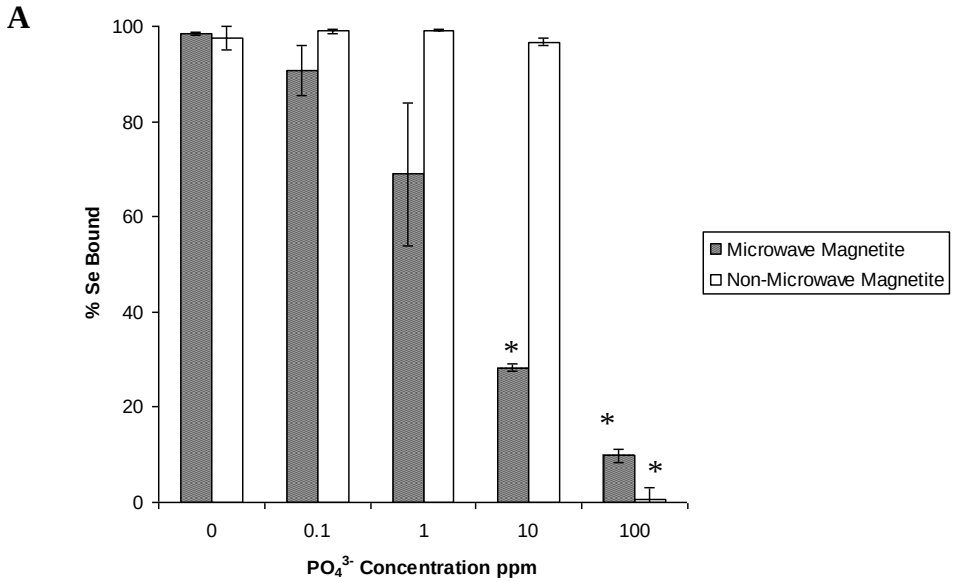

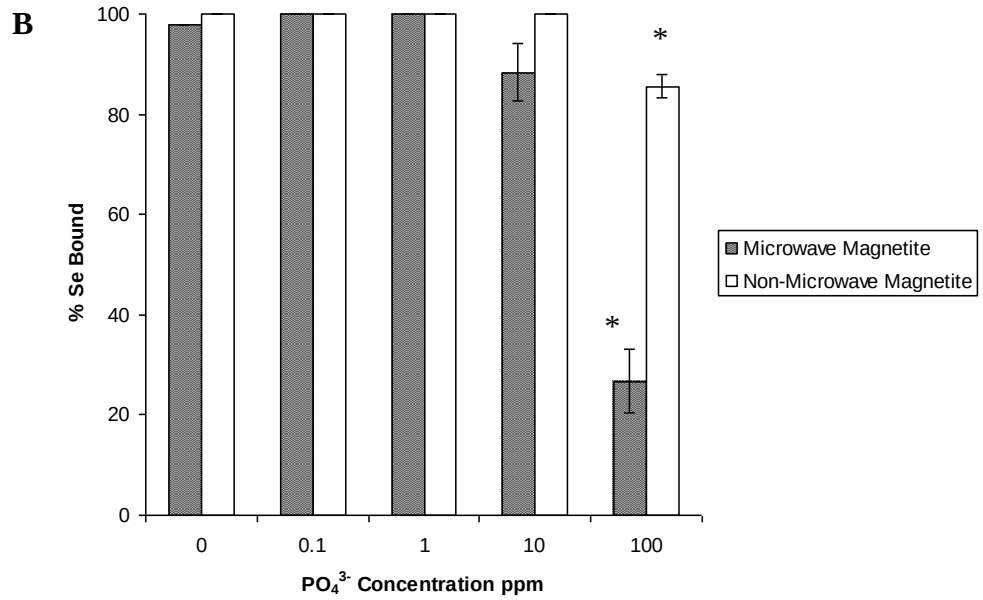

Figure 2.7. The effects of the PO_4^{3-} ion ranging in concentration from 0.1-100 ppm on the sorption of selenite and selenate to non microwave-assisted and microwave-assisted Fe_3O_4. (A) Selenate. (B) Selenite. Error bars represent Standard Error of three replicate. * represents statistical differences at $p \leq 0.05$.

2.3.5 Adsorption isotherms

The binding capacities of both the non microwave-assisted and microwave-assisted synthesized Fe_3O_4 nanomaterials were based on the fitting of selenite and selenate sorption studies to Langmuir isotherms equation. The results can be seen in Table 2.2. The non microwave-assisted synthesized Fe_3O_4 nanomaterial had a capacity of 1923 and 1428 mg Se/kg of Fe_3O_4 for selenite and selenate, respectively. The microwave-assisted synthetic nanomaterial was determined to have a higher capacity for both selenite and selenate of 2380 and 2369 mg Se/kg of Fe_3O_4, respectively than that of the non-microwave assisted nanomaterial. The higher capacity of the microwave-assisted material could be the result of its smaller size than that of the non microwave-assisted synthetic material. As explained earlier, the smaller particle would result in a greater number of surface sites for selenium oxoanion binding to occur. This increase

would allow for a higher capacity of the nanomaterial. Goh and Lim [31] reported 145 mg Se/ kg of tropical soil for selenite removal which is a much lower adsorption value for selenite than the synthetic magnetite produced in this study. Naturally occurring magnetite was also observed to have lower capacities for both selenite and selenate of 352.95 and 484.63 mg Se/ kg of magnetite [20]. This observation in the differences in capacities of naturally occurring and the synthetic magnetite prepared for these studies could be explained by the size differences of the magnetite as stated previously. The reported capacities of selenite and selenate to iron-coated GAC adsorbents at room temperature were 637 and 220 mg Se/ g of Fe-GAC, respectively were also lower than the capacities reported in this study [32-33].

Table 2.2. Capacities based on Langmuir isotherm experiments for both selenite and selenate binding to non microwave-assisted and microwave-assisted Fe_3O_4 nanomaterials.

Nanomaterial	**Adsorbate**	**Q_e (mg Se/kg of Fe_3O_4)**	**R^2**
Non microwave-assisted Fe_3O_4	SeO_3^{2-}	1923±119.877	1.0
	SeO_4^{2-}	1428±71.4	0.997
Microwave-assisted Fe_3O_4	SeO_3^{2-}	2380±7.14	1.0
	SeO_4^{2}	2369±16.58	0.990

2.4 Conclusions

The results of this work show that both non-microwave assisted and microwave-assisted synthesized Fe_3O_4 are capable of binding both selenite and selenate oxoanions. The binding of both oxoanions to the nanomaterial had an optimum pH of 4 and reached equilibrium within 5 min of contact time. These results are consistent with the anion binding to materials with similar surface properties. The anions SO_4^{2-} and PO_4^{3-} affected the binding of both oxoanions to the greatest extent. The non microwave-assisted synthesized Fe_3O_4 nanomaterial had a capacity of 1923 and 1428 mg Se/kg of Fe_3O_4 for selenite and selenate, respectively. The microwave-

assisted synthetic material was determined to have a higher capacity for both selenite and selenate of 2380 and 2369 mg/kg of Fe_3O_4, respectively than that of the non microwave-assisted material.

3. Adsorption of selenite and selenate by a high and low pressure aged manganese oxide nanomaterial

Abstract

Elevated concentrations of selenium oxoanions in aquatic systems can lead to bioaccumulation of excess selenium and improper biological functions in animals. This study investigated the effects of pH, reaction time, competitive anions, and adsorption capacity through the use of Langmuir isotherms of selenite and selenate to engineered Mn_3O_4 nanomaterials aged using two different techniques. The synthesis were performed using a traditional synthesis technique from the titration of Mn(II) ions with sodium hydroxide. The first aging technique used a traditional heating source in an open vessel at 90ºC for 60 min, while the second technique used a microwave oven with a closed vessel at 90ºC for 30 min. The phases and average grain sizes of the materials were determined through X-ray diffraction and Scherrer's equation. The optimal binding occurred at pH 4 within 10 min of contact time for both materials. The addition of Cl^-, NO_3^-, SO_4^{2-}, and PO_4^{3-} all decreased selenate binding while only SO_4^{2-} and PO_4^{3-} decreased selenite binding. The binding capacities were found to be 507 and 800 mg Se/kg of non microwave-assisted Mn_3O_4, for selenite and selenate, respectively. The microwave-assisted Mn_3O_4 displayed binding capacities of 1000 and 934.5 mg Se/kg of nanomaterial for selenite and selenate, respectively.

3.1 Introduction

Selenium is known to be an essential micronutrient for both animal and human health. It has been reported that selenium deficiency in humans occurs when daily consumption of selenium is less than 0.1 mg/kg of body weight, while consumption of levels above 1 mg/kg of body weight are considered toxic [1]. The Environmental Protection Agency has set the maximum contamination level (MCL) in drinking water at 50.0 ppb because of this narrow range between essential and toxic amounts of selenium described above [2]. Ground and surface water can be exposed to high concentrations of selenium from the leaching of mineral rocks, soils, and sediments [3]. There are also a variety of ways selenium can occur in the environment through anthropogenic causes, such as thermal power stations, oil refineries, smelting plants, glass production, and solar batteries [4]. The most frequently found selenium species in natural waters and sediments are the inorganic oxoanions selenite (SeO_3^{2-}, Se^{4+}, Se(IV)) and selenate (SeO_4^{2-}, Se^{6+}, Se(VI)) [5]. Both of these selenium oxoanions are known to bioaccumulate and can cause embryotoxic and teratogenic effects to waterfowl [6-7].

Treatment technologies for the removal of selenium from aqueous solutions that have been tested include chemical precipitation, catalytic reduction, anion-exchange, bacterial reduction, membrane filtration, solar ponds, and phytoremediation [8-11]. Most of these techniques, however, have not proven to be cost efficient. Recently, there have been many studies for the use of sorbents as an alternative technique to remove selenium from aqueous solutions. These sorbents include modified rice husk, hardened cement paste, cement paste minerals, aluminum-based water treatment residuals, and biopolymeric materials [5, 12-14]. In addition, many mineral surfaces such as aluminum oxides, montmorillonite, iron oxyhydroxides, and hematite are being tested for their selenium sorption abilities since the adsorption of

contaminants and trace element ions often control the cycling of these elements in the environment [6,15-18]. However, many of the aforementioned studies have not investigated the ability of these types of materials for the sorption of both selenium oxoanions [16-18]. In addition, many previously studied materials have had the disadvantage of small adsorption capacities or slow adsorption rates [19].

One way to overcome the small capacity problems and possibly slow adsorption rates is through the use of nanoparticles, which have been shown to have high adsorption capacities [4]. Zhang *et al*. [4] reported that nano-TiO_2 has a capacity for selenite binding of 2.6 mg Se(IV)/g TiO_2, reaching equilibrium within 5 min. One material that has not been investigated for its ability to remove selenium oxoanions from solution effluents is Mn_3O_4. If synthesized at the nanometer scale, the Mn_3O_4 material would have a remarkable increase in surface area which could lead to a large adsorption capacity and faster adsorption times than previously studied materials [20].

In this investigation, nanosynthesized manganese oxide (Mn_3O_4), by both non microwave- and microwave-assisted aging techniques, was examined for its ability to remove the selenium oxoanions, selenite and selenate, from aqueous solutions. The crystal structures of both synthetic manganese oxide nanomaterials were determined to be hausmannite, independent of the aging technique used. The potential of both nanomaterials to adsorb the selenium oxoanions was investigated in the pH range of 2 to 6, as was the time dependency for adsorption to occur. Furthermore, the capacities of the nanomaterials to bind selenite or selenate were also tested using Se solutions in the range of 0.25-10.00 ppm. Finally, the addition of the anions Cl^-, NO_3^-, SO_4^{2-}, and PO_4^{3-} were tested as potential interferences on the selenium oxoanion binding to the

nanomaterials. Analytical techniques such as X-ray diffraction and the use of Inductively Coupled Plasma-Mass Spectrometry were used to characterize and determine the Se removal.

3.2 Methodology

3.2.1 Synthesis and characterization of the manganese oxide nanomaterial

The manganese oxide nanomaterials were synthesized from two separate 1.0 L solutions of 30 mM of Mn(II) (from $MnSO_4$, EM Science) following the same conditions as described in Chapter 2. The resulting Mn_3O_4 nanomaterials from each synthetic aging technique were characterized using powder X-ray diffraction (XRD) under the same operating conditions previously described in Chapter 2. The resulting patterns were then fitted using crystallographic data from the literature and the FullProf Suit program to perform a Le Bail fitting to determine the phase of the two synthetic nanomaterials [21]. The average grain size of each material was also determined by performing a Guassian fitting to three different diffraction peaks on both patterns, and then applying the full width half maxima (FWHM), obtained from the Scherrer's equation.

3.2.2 Sorption studies and analysis

The pH profiles, time dependencies, competitive anion effects, and adsorption isotherms were performed with each of the synthetic Mn_3O_4 nanomaterials for both selenite and selenate using the same experimental conditions as in Chapter 2. The supernatants collected from all sample studies were analyzed using the Perkin Elmer Elan DRC II ICP-MS with ELAN software under the operating conditions described in Chapter 2, Table 2.1. Statistical analysis of the collected data of binding percentages of the selenium oxoanions to both sets of synthetic Mn_3O_4

were analyzed with one-way analysis of variance (ANOVA) using SPSS software, version 12.0 (SPSS, Chicago, IL) as described in Chapter 2.

3.3 Results and Discussion

3.3.1 X-ray diffraction characterization of nanomaterial

Both the non microwave-assisted and microwave-assisted synthetic nanomaterials were characterized by powder X-ray diffraction and are concurrent with the 112, 200, 013, 211, 004, 220, 204, 015, 312, 303, and 321 reported diffraction peaks of the phase of hausmannite (Mn_3O_4), as can be seen in Figure 3.1 [21]. The additionally observed 111 and 200 peaks present in both patterns correspond to the platinum sample holder used for pattern collection. The average grain sizes of the non microwave-assisted and microwave-assisted synthetic materials were determined to be 25 and 34 nm, respectively. These average grain sizes of both nanomaterials were determined by first taking the average of three different, full width half maximums (FWHM) from each diffraction pattern. These averages where then inputted into the Scherrer's equation, providing the average grain size of the nanomaterials. The differences seen in the calculated grain sizes show that the difference between both the relative intensities and widths, as seen in Figure 3.1, are due to the difference in the average grain sizes of the two Mn_3O_4 nanomaterials. Both of the synthetic aging techniques described are advantageous because previously reported hydrothermal techniques have required 48-72 hours to produce similar materials [22].

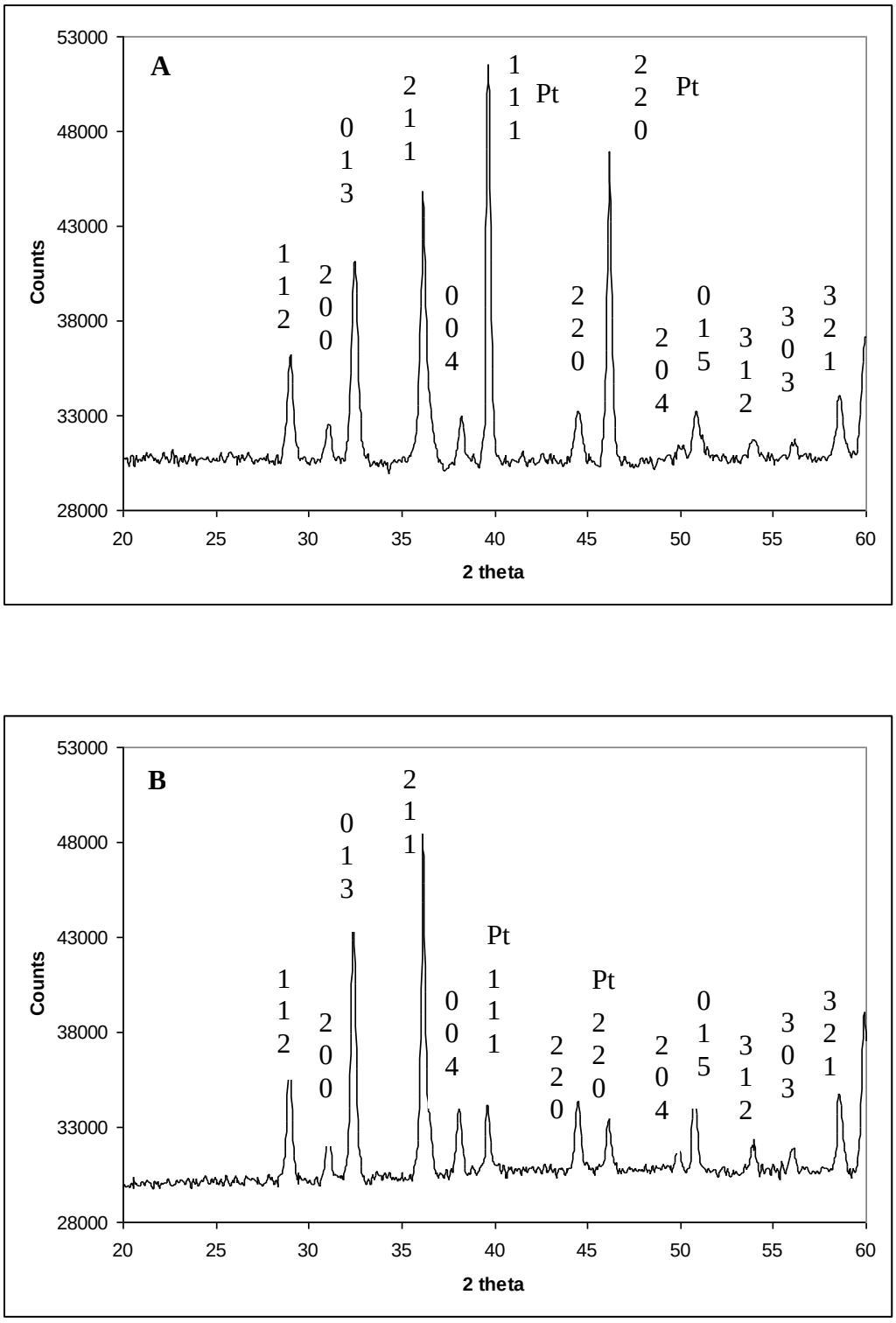

Figure 3.1. X-ray diffraction pattern of Mn_3O_4 from titration of manganese sulfate ($MnSO_4$) with sodium hydroxide. (A) non microwave-assisted synthesis. (B) microwave-assisted synthesis.

3.3.2 pH binding studies

The pH dependence results of selenite and selenate to both synthetic nanomaterials are shown in Figure 3.2. Selenite binding to both nanomaterials was highest in the pH range of 2 to 3. However, it has been previously shown that the Mn_3O_4 nanomaterial is not stable at such a low pH range due to dissolution of the nanomaterial [23]. The non microwave-assisted synthetic nanomaterial had a higher binding percentage of selenite than that of the microwave-assisted nanomaterial. The difference in binding percentages could be attributed to the size difference of the nanomaterials. The smaller surface area could create a higher number of active sites on the nanomaterial surface which would allow for more selenium oxoanion binding to occur. As described earlier, the non microwave-assisted synthetic Mn_3O_4 had a smaller radius and thus a smaller surface area than that of the microwave-assisted synthetic Mn_3O_4 nanomaterial. The binding percentage of selenite to both nanomaterials was greater than that of selenate. This difference in binding percentages has been seen in previous studies, indicating that selenite has a higher and stronger binding affinity to manganese materials than selenate [24]. Both synthetic materials had the highest binding percentage of selenate at pH 3; however, as described above, this is not a desirable pH. Therefore, the highest percentage of binding at a stable pH for both nanomaterials occurred at pH 4. The increased binding of selenium at a lower pH range may indicate that the adsorption was dependent on the variable charge developed on the surface of the Mn_3O_4 materials, as has been previously suggested for other synthetic manganese oxides, including birnessite and cryptomelane [25]. However, there was a significant difference in the binding of selenate to the non microwave-assisted synthetic nanomaterial than to that of the microwave-assisted synthetic nanomaterial at pH 4. As shown in Figure 3.2, the non microwave-assisted synthetic material had a selenate binding percentage of 35% while the

microwave-assisted synthetic material bound 75% of selenate present at pH 4. Again the difference in binding percentages between the two nanomaterials could be due to the difference in average grain size.

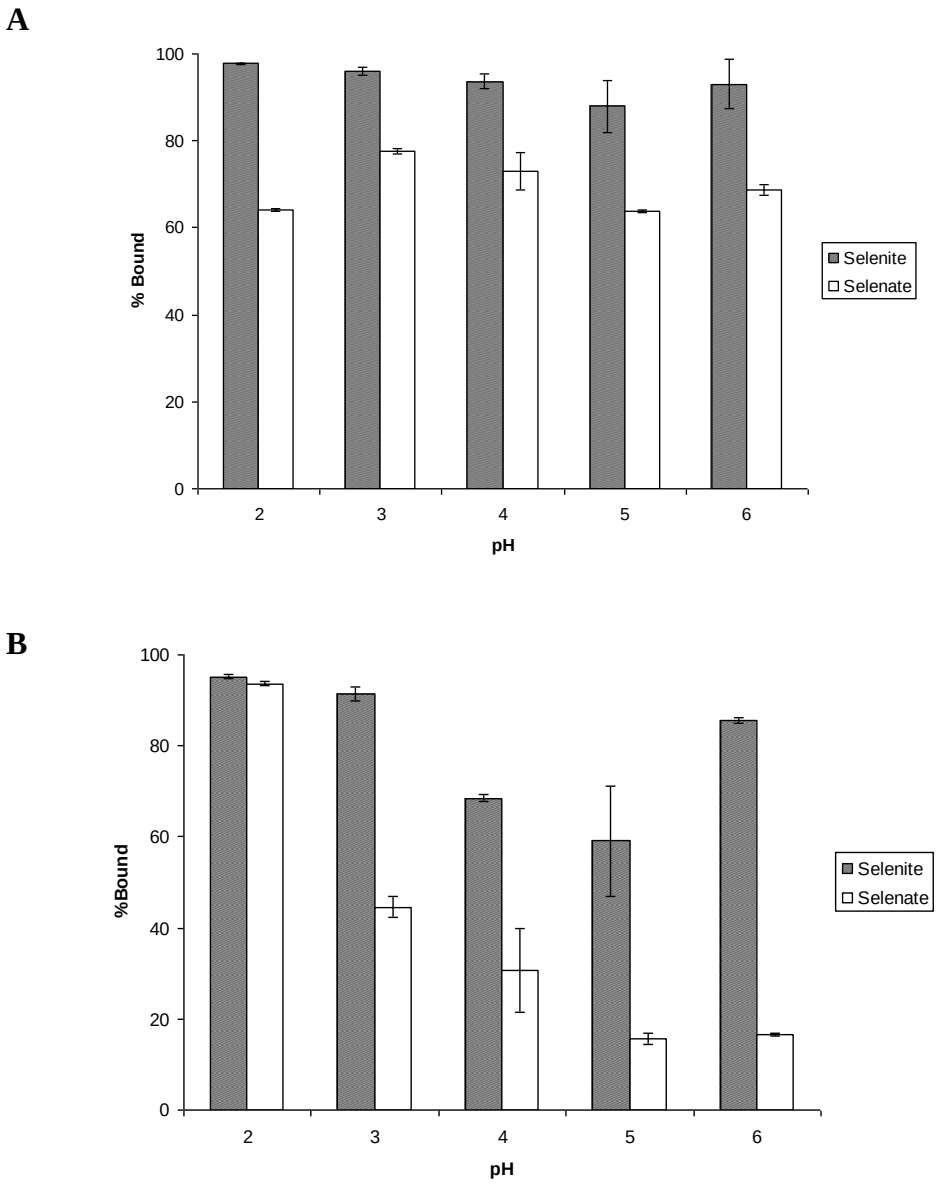

Figure 3.2. Percentage bound of selenite and selenate at a concentration of 100 ppb to the nanomaterial under varying pH conditions ranging from pH 2 to 6. (A) non microwave-assisted Mn_3O_4. (B) microwave-assisted Mn_3O_4. Error bars represent Standard Error of three replicate.

3.3.3 Time dependency studies

The amount of selenite and selenate bound to both synthetic Mn_3O_4 nanomaterials as a function of time can be seen in Figure 3.3. It was observed that the maximum binding occurred within 10 min of contact time for both selenium oxoanions to the Mn_3O_4 nanomaterials. A fast binding equilibrium, as observed in this study, suggests that the sorption of the selenium oxoanions occurs on the surface of the hausmannite nanomaterial without the occurrence of a redox reaction [23]. These results further support the assertion that the difference in binding percentages of the selenate to the different synthetic nanomaterials is occurring due to the differences in the average particle size between the two nanomaterials. The equilibrium time for the selenium oxoanion binding to Mn_3O_4 in this present study is faster than previously reported materials for selenium removal. Liu *et al*. [26] reported that selenite adsorption to a thermally activated, layered double hydroxide material took 30 min to reach equilibrium. Dash and Parida [15] showed manganese nodule-leached residues took 3 hr to reach equilibrium for selenite removal.

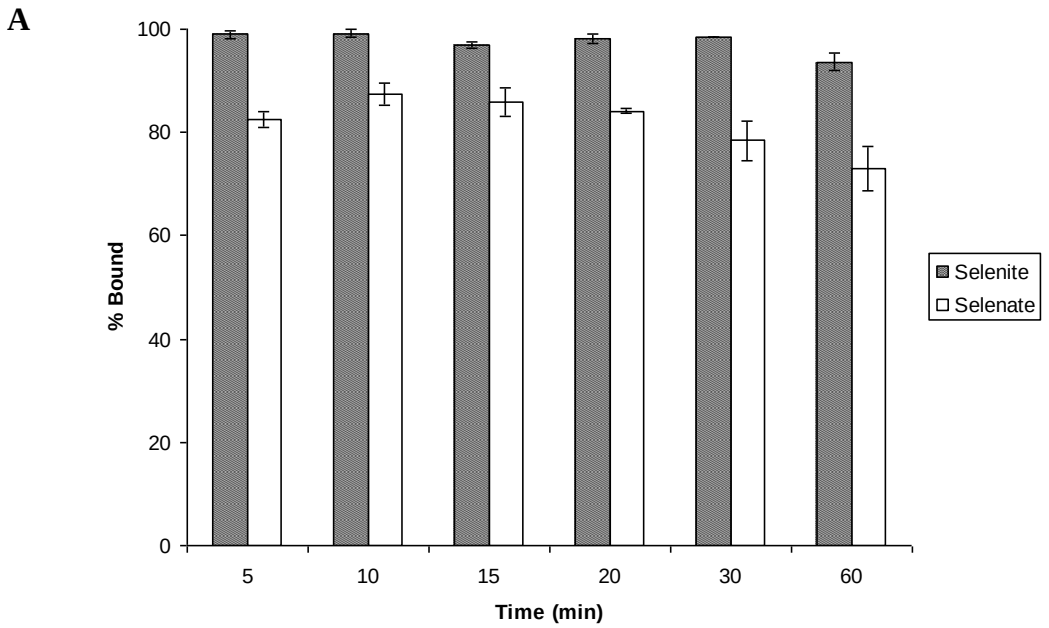

B

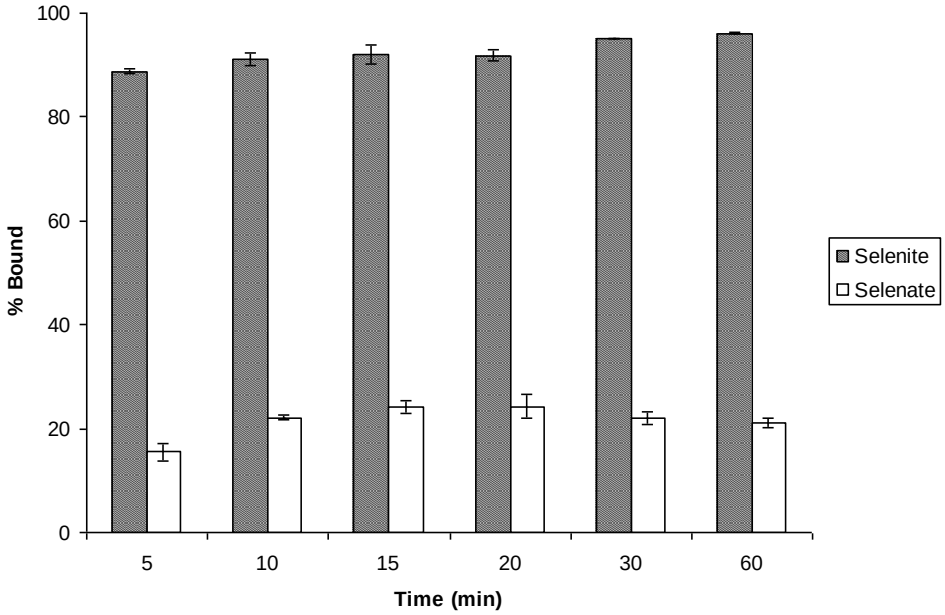

Figure 3.3. Time dependence of percentage bound of selenite and selenate to the nanomaterial at a pH of 4. (A) non microwave-assisted Mn_3O_4. (B) microwave-assisted Mn_3O_4. Error bars represent Standard Error of three replicate.

3.3.4 Competitive anion studies

The results of the addition of possible competitive anions (Cl^-, NO_3^-, SO_4^{2-}, PO_4^{3-}) on selenium oxoanion, binding to both non microwave-assisted and microwave-assisted synthesized Mn_3O_4 nanomaterials, are shown in Figures 3.4-3.7. The addition of the Cl^- ion in the range of 0.1 to 100 ppm had no significant effect on the binding of selenite to either synthetic nanomaterial. This observation indicates the selenite oxoanion has a stronger affinity towards the manganese oxides than the Cl^- ion. However, the addition of Cl^- did have a significant effect on the binding of selenate, beginning at a concentration of 0.1 ppm Cl^- added for both Mn_3O_4 synthetic nanomaterials, as seen in Figure 3.4A. Less than 10% of selenate binding occurred in the presence of Cl^- in the range of 0.1- 100 ppm. The occurrence of such a lower binding percentage could be explained by selenate having a lower binding affinity to the surface of the manganese

nanomaterial. Maliyekkal *et al.* [27] have previously shown that the fluoride ion binds to a manganese-oxide-coated alumina sorbent and is not affected by the addition of a larger anion of SO_4^{2-} (~200 ppm). This would indicate small halogen anions such as Cl^- are capable of having a higher binding preference to manganese oxides than oxoanions with similar chemistry to selenate.

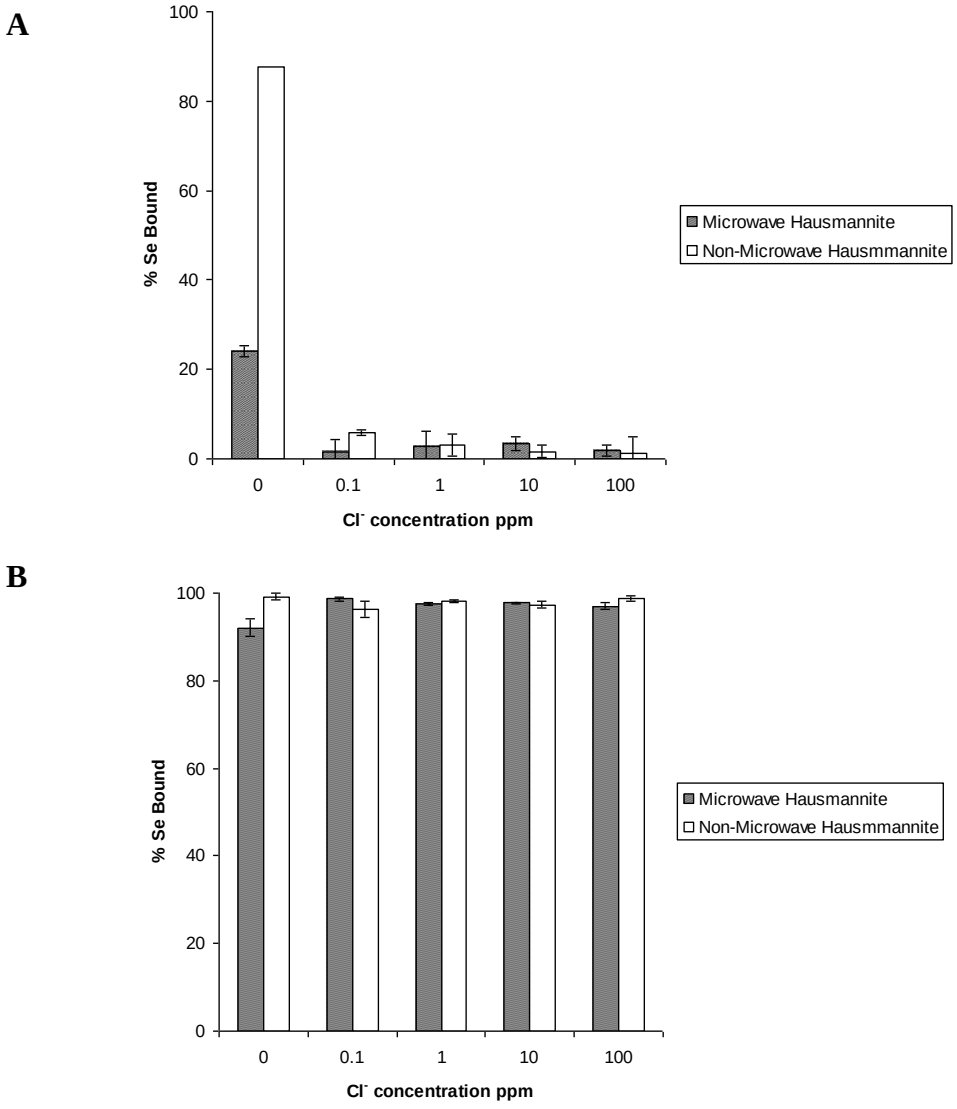

Figure 3.4. The effects of the Cl^- ion ranging in concentration from 0.1-100 ppm on the sorption of selenite and selenate to non microwave-assisted and microwave-assisted synthetic Mn_3O_4. (A) Selenate. (B) Selenite. Error bars represent Standard Error of three replicate.

The addition of NO_3^-, as can be seen in Figure 3.5B, had no significant effect on the binding of selenite to the non microwave-assisted synthetic Mn_3O_4 nanomaterial, and only a slight decrease on the microwave-assisted synthetic Mn_3O_4 nanomaterial. This observed slight decrease of selenite binding in the presence of NO_3^- has been previously shown to occur by Dash and Parida [15]. The decrease in selenate binding in the presence of NO_3^- was significant, as can be seen in Figue 3.5A, and was more evident in the non microwave-assisted nanomaterial. The binding was reduced to less than 10% bound for both nanomaterials in the presence of 0.1-100 ppm NO_3^-. This indicates that the NO_3^- is competing with selenate for the active surface sites on both of the synthetic nanomaterials. This does not correspond with previous studies showing that the addition of NO_3^- has not had such a significant effect on the binding of other anions to aluminum and iron oxides, as shown by Jeong *et al* [28]. However, it has been stated that selenate adsorbs relatively weakly to metal oxide surfaces [29]. This would indicate that the selenate binding complexes formed to the manganese oxides in this study are so weak they are easily displaced by the addition of another anion, such as the presence NO_3^-.

A

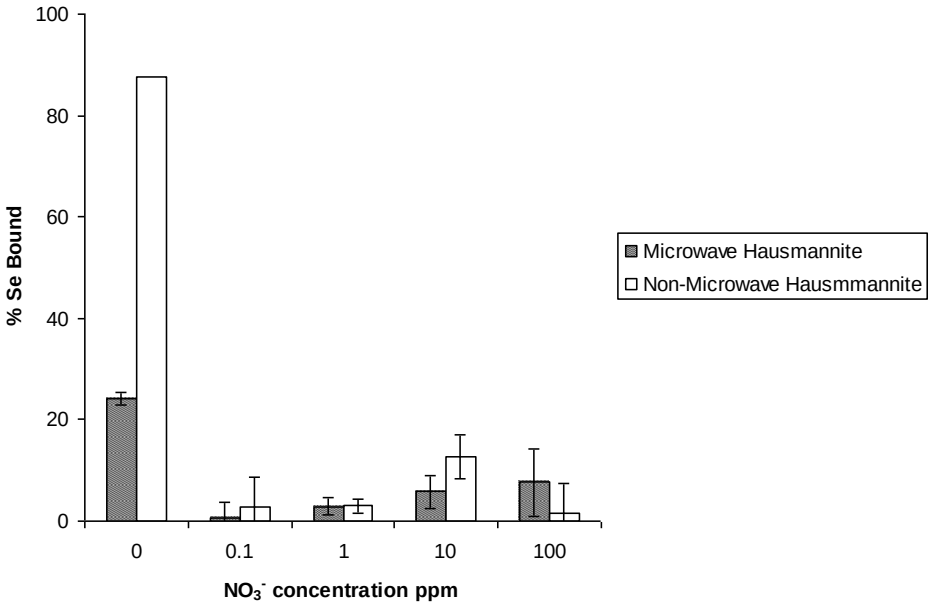

B

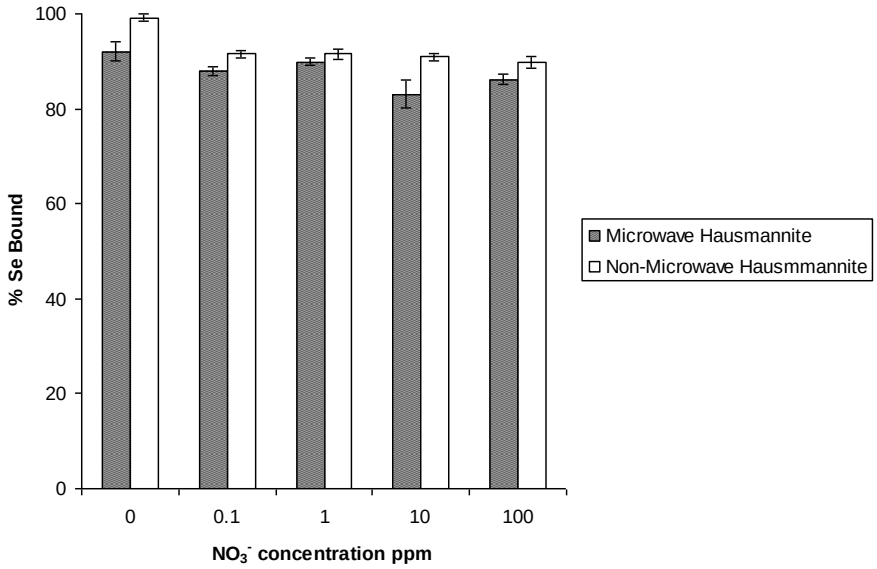

Figure 3.5. The effects of the NO_3^- ion ranging in concentration from 0.1-100 ppm on the sorption of selenite and selenate to non microwave-assisted and microwave-assisted synthetic Mn_3O_4. (A) Selenate. (B) Selenite. Error bars represent Standard Error of three replicate.

As shown in Figure 3.6B, there was no significant effect on selenite binding to either synthetic nanomaterial in the presence of SO_4^{2-} in the range of 0.1-10 ppm. However, binding decreased to around 70% selenite bound for both nanomaterials in the presence of 100 ppm SO_4^2. The addition of SO_4^{2-} has been shown to bind and compete with arsenite binding to a manganese oxide-coated alumina, but only when SO_4^{2-} is present at higher concentrations, such as in this study [30]. There was, however, a significant decrease in the binding of selenate in the presence of SO_4^{2-} at concentrations between 0.1-100 ppm, as can be seen in Figure 3.6A, for both synthetic nanomaterials. Despite the major reduction of binding, it is interesting to note binding is still occurring even at the high ratio of sulfate to selenate present. For example, at 100 ppm SO_4^{2-} present in solution, the molar ratio of selenate to sulfate is 1 SeO_4^{2-} : 1488 SO_4^{2-}. The observation of selenate binding still occurring at this large molar ratio of SO_4^{2-} to SeO_4^{2-}

indicates the high affinity of Mn_3O_4 nanomaterial to bind selenate. This decrease in binding could be attributed to the similar chemistry between selenate and sulfate anions, possibly resulting in similar binding affinities for both anions to the Mn_3O_4 nanomaterial [31]. Also, it has been shown that sulfate and selenate have similar sorption characteristics to soil minerals, as well as chemical properties [32]. These similarities in sorption could also explain the high decrease in binding due to direct competition for binding sites on the surface of the nanomaterial.

A

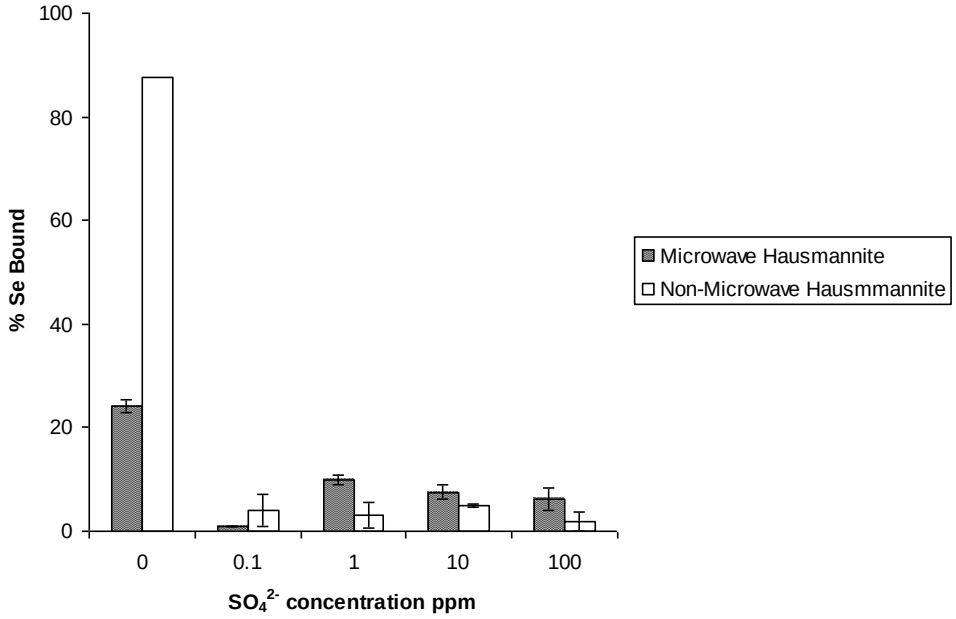

B

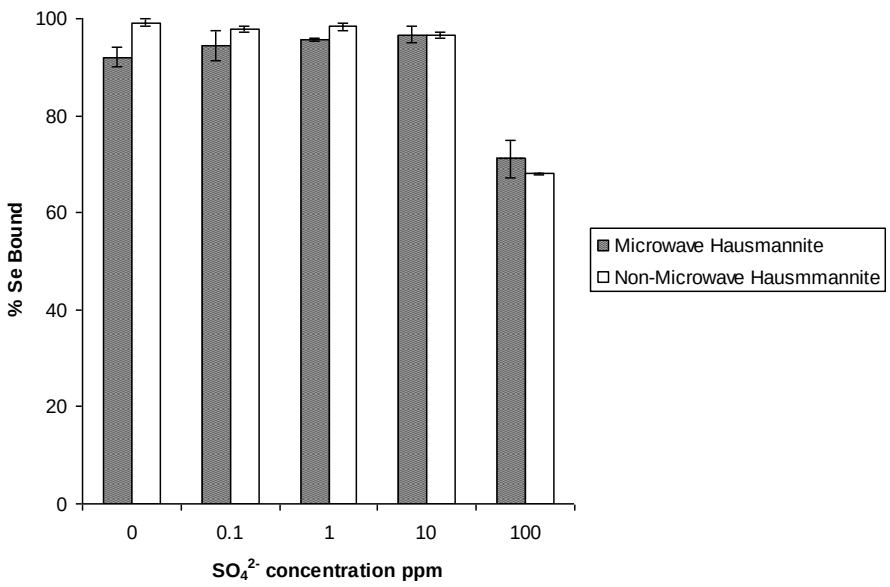

Figure 3.6. The effects of the SO_4^{2-} ion ranging in concentration from 0.1-100 ppm on the sorption of selenite and selenate to non microwave-assisted and microwave-assisted synthetic Mn_3O_4. (A) Selenate. (B) Selenite. Error bars represent Standard Error of three replicate.

The addition of the PO_4^{3-} anion had a significant effect on the binding of selenite to both nanomaterials at concentrations of 1-100 ppm as shown in Figure 3.7B. At 1 ppm PO_4^{3-} present, selenite binding decreased by 30% and 10% for non microwave-assisted and microwave-assisted Mn_3O_4, respectively. This difference in the percentage decrease of selenite binding between the two synthetic nanomaterials could be due to the size difference in the particles. The non microwave-assisted synthetic nanomaterial with the smaller grain size would have more available active sites for sorption to occur, therefore increasing the chances of selenite binding to occur, as opposed to that of the microwave-assisted nanomaterial. When in the presence of 10 ppm PO_4^{3-}, the binding of selenite decreased to 25% and 30% of selenite bound to non microwave-assisted and microwave-assisted Mn_3O_4, respectively. The difference between the

binding percentages of the two synthetic nanomaterials was only 5%. There was no observed binding of selenite to either nanomaterial with the addition of 100 ppm PO_4^{3-} to the solution. The molar ratio between selenite and phosphate in the presence of 100 ppm PO_4^{3-} was 1 SeO_3^{2-} : 1000 PO_4^{3-}. Even though the non microwave-assisted nanomaterial's larger surface area resulted in higher binding percentages of selenite bound at a concentration of 0.1 ppm PO_4^{3-} this was not the case once 100 ppm PO_4^{3-} was added to solution. This decrease in binding of selenite in the presence of the PO_4^{3-} ion could be occurring due to the analogous behavior of sorption of selenite and phosphate, which has been previously observed [32]. Dash and Parida [15] have also shown the ability of PO_4^{3-} to bind and cause direct competition with selenite at equimolar concentrations. The decrease of selenate binding was more pronounced in the presence of 0.1 ppm PO_4^{3-} than that of selenite at the same concentration. Selenate binding decreased to less than 40% for both synthetic Mn_3O_4 nanomaterials. There was no observed selenate binding to the microwave-assisted nanomaterial in the range of 1-100 ppm of PO_4^{3-} present in solution. However, selenate binding was observed for the non microwave-assisted nanomaterial in this range. The observed binding to only the non microwave-assisted nanomaterial at this concentration of PO_4^{3-} could be explained by the size difference between the particles, as mentioned earlier. At a molar ratio of 1 SeO_4^{2-} : 1505 PO_4^{3-} , there was very slight binding still occurring for the non microwave-assisted synthetic Mn_3O_4. Again, the observed selenate binding to the Mn_3O_4 nanomaterial at such a large molar ratio of phosphate to selenate indicates a high affinity for selenate to the Mn_3O_4 nanomaterial. It has been shown by Mustafa *et al.* [33] that PO_4^{3-} does have the ability to bind to a β-MnO_2 material. The ability of phosphate to bind to manganese oxides, combined with the observed weak selenate binding, could be the reason for the low binding of selenate in the presence of the PO_4^{3-} observed in the current study. The PO_4^{3-}

is displacing the weak binding complexes formed between the selenate and synthetic hausmannite nanomaterials.

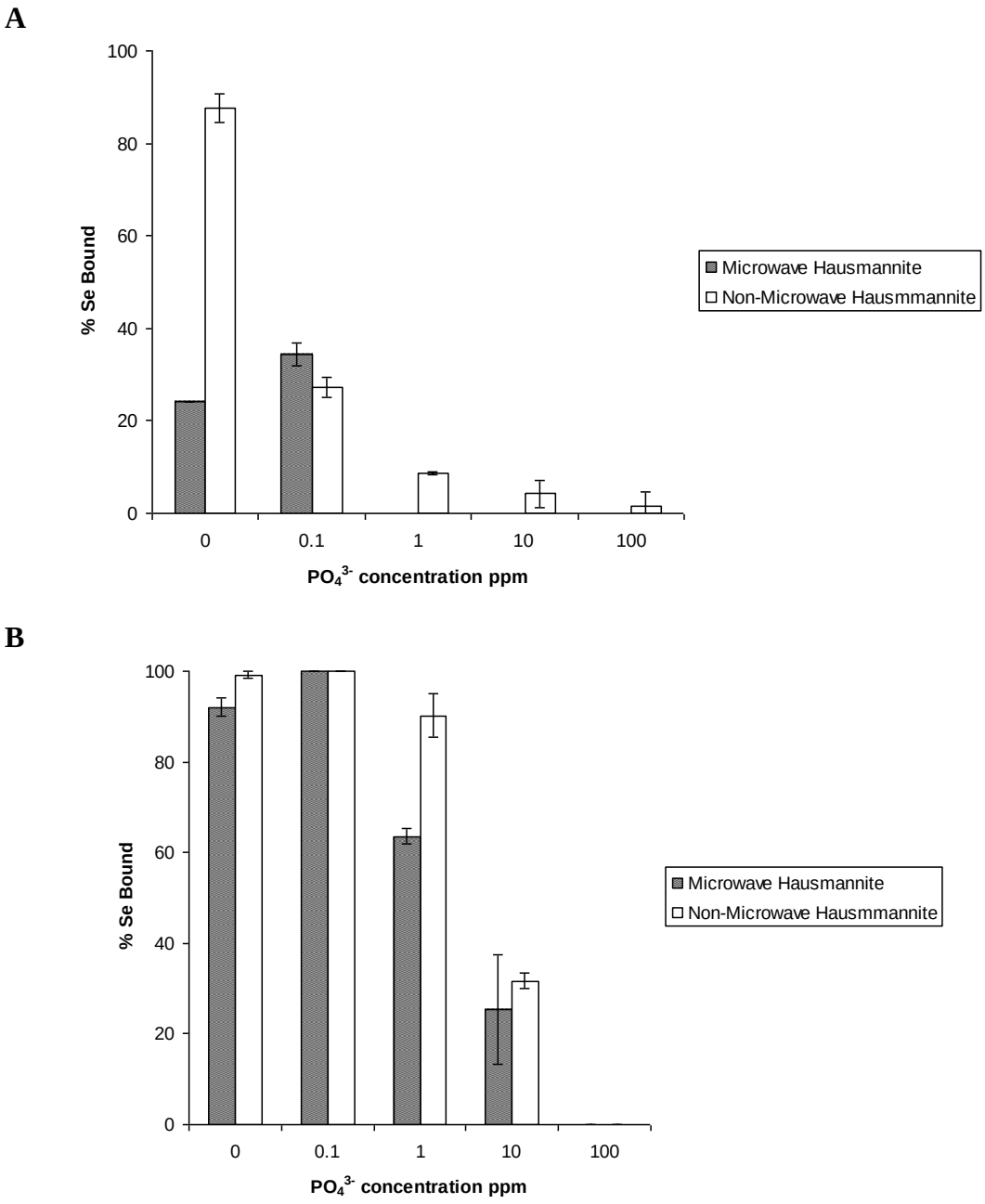

Figure 3.7. The effects of the PO_4^{3-} ion ranging in concentration from 0.1-100 ppm on the sorption of selenite and selenate to non microwave-assisted and microwave-assisted synthetic Mn_3O_4. (A) Selenate. (B) Selenite. Error bars represent Standard Error of three replicate.

3.3.5 Adsorption isotherms

The binding capacities of both synthetic nanomaterials for both selenium oxoanions taken from the Langmuir isotherm equation are shown in Table 3.1. The non microwave-assisted synthesized Mn_3O_4 nanomaterial had a capacity of 507 and 800 mg/kg for selenite and selenate, respectively. The microwave-assisted synthetic material was determined to have a higher capacity for both selenite and selenate of 1000 and 934.5 mg/kg, respectively, than that of the non microwave-assisted material. The capacity for selenite of the microwave-assisted synthetic Mn_3O_4 and the capacity for selenate of both synthetically-prepared Mn_3O_4 reported in this study were higher than that of an iron coated granular activated carbon (Fe-GAC), which has been shown in the literature to have capacities for selenite and selenate of 637 and 221 mg Se/kg Fe-GAC, respectively [34,35]. The higher capacities observed for the Mn_3O_4 materials could be attributed to the blockage of active pore sites on the Fe-GAC material once it has been coated with iron.

Table 3.1. Capacities based on Langmuir isotherm experiments for both selenite and selenate binding to non microwave-assisted and microwave-assisted Mn_3O_4 nanomaterials.

Nanomaterial	Adsorbate	Q_e (mg Se/kg of Mn_3O_4)	R^2
Non-microwave-assisted Mn_3O_4	SeO_3^{2-}	507±44.6	0.994
	SeO_4^{2-}	800±40.0	1.0
Microwave-assisted Mn_3O_4	SeO_3^{2-}	1000±8.0	0.995
	SeO_4^{2-}	934.5±39.1	0.998

3.4 Conclusions

This research has shown the capability of a synthetic nano-hausmannite phase material prepared from two separate synthetic techniques to remove both selenium oxoanions, selenite and selenate, from aqueous solutions under an optimum pH of 4, within 10 min of contact time with the nanomaterials. While the introduction of Cl^- and NO_3^- anions had no significant effect on

selenite binding, selenate binding was decreased to less than 15% beginning at 0.1 ppm of either additional anion present. The addition of SO_4^{2-} and PO_4^{3-}, however, decreased selenite sorption beginning at concentrations of 100 ppm and 1 ppm added, respectively. Selenate binding decreased to less than 40% and 15% after the inclusion of 0.1 ppm PO_4^{3-} or SO_4^{2-}, respectively. The results of these studies indicate nano-hausmannite is more promising as a sorbent for selenite rather than selenate, in the presence of other anions.

4. Removal of selenite and selenate from aqueous solutions using a magnetic iron/ manganese oxide nanomaterial

Abstract

Selenium (Se) is naturally occurring in the environment and is an essential nutrient in mammals. However, environmental Se can be increased to toxic levels through different industrial practices. The potential adsorption of the Se oxoanions, selenite and selenate, from aqueous solutions onto nanosynthesized $MnFe_2O_4$ was investigated using batch techniques and DRC-ICP-MS spectrscopy. The nanomaterial (NM) was laboratory synthesized through slow titration of a mixture of Fe^{2+} and Mn^{2+} ions. X-ray diffraction and Scherrer's equation were used to determine the phase of the material and crystallite size, respectively. The effects of pH, reaction time, competitive anions, and the adsorption capacity of the synthesized NM to bind selenite and selenate were investigated. The Langmuir isotherm was used to determine the binding capacity of the NM. Results showed that the phase of the nanomaterial was similar to Jacobsite with a size of 27.5 nm. Results also showed that the sorption of either 100 ppb of selenite or selenate was pH independent in the pH range 2 to 6 and occurred within 5 min of contact time. The introduction of Cl^- and NO_3^- anions individually added to solution had no significant effect on the sorption of either selenite or selenate. However, it was found that the addition of SO_4^{2-} had a competitive effect only on the sorption of selenate, first seen at 10 ppm and more pronounced at 100 ppm of SO_4^{2-}. In the presence of 100 ppm of PO_4^{3-} the adsorption of selenate decreased to 87% while selenite sorption decreased to 20%. From the Langmuir isotherm equation it was determined that the nano-Jacobsite had a selenite and selenate binding capacity of 6573.76 and 769.23 mg Se/kg of NM, respectively.

4.1 Introduction

Selenium is a necessary element for mammals and is naturally occurring in the environment. Selenium in natural waters generally has a concentration of < 10 ppb (parts per billion); however, in San Joaquin Valley, California, concentrations of Se ranging from 140 to 1400 ppb have been observed [1]. Such Se concentrations are considered to be toxic in aquatic ecosystems where the range between Se deficiency and toxicity is extremely narrow [2]. Selenium concentrations in aqueous environments are increasing not only because of natural sources, but also by anthropogenic practices such as agricultural irrigation drainage, coal burning power plants, combustion of fossil fuels, and mining operations [3-5]. Aqueous Se exists predominantly as two oxoanionic species: selenite (SeO_3^{2-}, Se^{4+}, Se(IV)) and selenate (SeO_4^{2-}, Se^{6+}, Se(VI)). Both Se oxoanions have shown to be toxic and are known to bioaccumulate [1]. Selenium bioaccumulation can lead to serious health conditions in waterfowl, fish, birds, and mammals, including humans [6]. The toxic effects of high levels of Se in wildlife have been reported to include tissue damage, reproductive failure, teratogenic effects, and even elimination of fish communities [3].

There have been several treatment technologies for the removal of Se from aqueous environments including anion-exchange, reverse osmosis, micro-algal-bacterial treatment, and phytoremediation [7-8]. These forms of treatment can be more costly than they are effective. Several adsorbents, many containing naturally occurring minerals and metal oxides, have been tested for their ability to remove these Se oxoanions from aqueous solutions [2,4,7,9-15]. These sorbents include iron-coated granular activated carbons, pure and coated montmorillonite, aluminum oxides, aluminum-based water treatment residuals, iron-coated sand, zerovalent iron, various forms of iron oxyhydroxides (α-,β-,γ-, and δ-FeOOH), ferrihydrite, hardened cement

paste, cement minerals, magnetite, and hematite [2,4,7,9-15]. However, many of these studies only focus on the sorption behavior of one Se oxoanion [4,7,11-12,14-15]. Also, the effects of competitive anions such as Cl^-, NO_3^-, SO_4^{2-}, or PO_4^{3-} have not been thoroughly investigated for many of these adsorption treatment techniques. The aforementioned anions occur naturally in aqueous environments and could potentially compete with selenite and selenate for sorption sites on adsorption materials [11].

Nanomaterials provide a unique opportunity for the removal of hazardous materials from the aqueous environments. Iron based materials and NM are efficient at the removal of arsenic, Se and other oxoanions from solutions. For example, iron coated sand has shown to be able to remove between 1.10 and 1.34 mg Se(IV) /g Fe-sand (or 1100-1300 ug/g) and between 1.026 and 1.10 mg Se(VI)/g Fe-sand (or 1026 and 1100 ug/g) [10]. Parida *et al.* [12] showed that the adsorption capacity of iron oxyhydroxide/ferrihydrites for selenite have the order β-FeOOH < α-FeOOH < γ-FeOOH < δ-FeOOH < amorphous ferrihydrite. In another study by Jordan *et al*. [14] the ability of Se(IV) to bind onto magnetite was studied in the presence of silicic acid, which showed a high binding at low pH and decreasing binding with increasing pH up to pH 10, where the binding was almost completely eliminated. Although the sorptive properties of iron oxide and hydroxide materials for oxoanions have been studied, the sorption properties of substituted NM have not been studied to any great extent. One of these types of materials that has not been studied for the adsorption of Se oxoanions is Jacobsite. This is a Fe_3O_4 material with the formula $MnFe_2O_4$ which, like magnetite, is a magnetic metal oxide mineral. Magnetic materials are advantageous for adsorption because they can be removed from aqueous effluents after sorption through magnetic separation [16, 17]. Jacobsite nanoparticles could be a possible solution for overcoming the small surface area or small adsorption capacities that limit the application of

previously used magnetic materials for the removal of contaminants from aqueous effluents [16]. Previous studies using surface-modified and non-modified Jacobsite nanoparticles have been proven to be effective sorbents for As(III) and (V) and Cr(VI) which showed to have binding capacities of 718 μg/g, 2125 μg/g, and 31.1 mg/g, respectively [18-19].

In this study, we have synthesized a $MnFe_2O_4$ NM and investigated its ability to remove selenite and selenate from aqueous solutions. The synthesized NM was determined to have the crystal structure of Jacobsite at the nanoscale. The capability of the nanomaterial to adsorb selenite and selenate was determined in the pH range from 2 to 6. Additionally, the binding time and isotherm studies were performed using concentrations of selenite and selenate from 0.25-10 ppm. The effects of interfering anions Cl^-, NO_3^-, SO_4^{2-}, or PO_4^{3-} from 0.1-100 ppm on the binding of Se onto Jacobsite were studied.

4.2 Methodology

4.2.1 Synthesis and characterization of the manganese oxide nanomaterial

The synthesis of the Jacobsite ($MnFe_2O_4$) NM was carried out using 1.0 L containing 20.0 mM of Fe(II) (from $FeCl_2$, EM Science) and 10 mM of Mn(II) (from $MnSO_4$, EM Science) and titrated slowly with a 1.0 M NaOH solution. The titration was performed for 1 h by adding 90 mL of NaOH drop by drop to the metal solution to obtain a 1:3 ratio of M^+:OH^-. Upon completion of the titration the solution was heated to 90° C for 1 h on a heating plate. The solution was allowed to cool to room temperature and centrifuged at 3000 rpm (Fisher Scientific 8K, Houston, TX) for 5 min and then washed twice with deionized water (DI) to remove any byproducts that resulted from the reaction. After washing, the nanomaterial was dried at 100° C in a VWR 1305U oven (VWR, West Chester, PA) until completely dried. Characterization of the NM was completed using powder X-ray diffraction (XRD) under the same operating

conditions described in Chapter 2. The resulting pattern was then fitted using crystallographic data from the literature and the FullProf Suit program to perform a Le Bail fitting to determine the phase of the NM [20]. The average grain size of each material was also determined as described in Chapter 2.

4.2.2 Sorption studies and analysis

All sorption studies consisting of pH profiles, time dependencies, competitive anion effects, and adsorption isotherms were performed with the synthetic $MnFe_2O_4$ nanomaterials for both selenite and selenate using the same experimental conditions as in Chapter 2. The supernatants collected from all sample studies were analyzed using the Perkin Elmer Elan DRC II ICP-MS with ELAN software under the operating conditions described in Chapter 2, Table 2.1. Statistical analysis of the collected data of binding percentages of the selenium oxoanions to both sets of synthetic $MnFe_2O_4$ were analyzed with one-way analysis of variance (ANOVA) using SPSS software, version 12.0 (SPSS, Chicago, IL) also as described in Chapter 2.

4.3 Results and Discussion

4.3.1 Characterization of the synthesized nanomaterial

As shown in Figure 4.1, the X-ray diffraction pattern of the synthesized nanomaterial are in agreement with the 220, 311, 222, 400, 511, and the 333 diffraction peaks of Jacobsite ($MnFe_2O_4$) [20]. The 111 and 200 diffraction peaks correspond to the platinum sample holder. Through the determination of the full width at half maximum (FWHM) of the diffraction peaks applied to the Scherrer's equation, the average grain size of the material was determined to be 27 nm. This number is based on the calculation average of three different diffraction peaks. The synthesis technique described in the methodology overcomes some of the cumbersome steps

shown in previous magnetic material preparation, special chemicals and procedures [16]. In addition, the simplicity of the protocol makes it a cost effective synthesis technique.

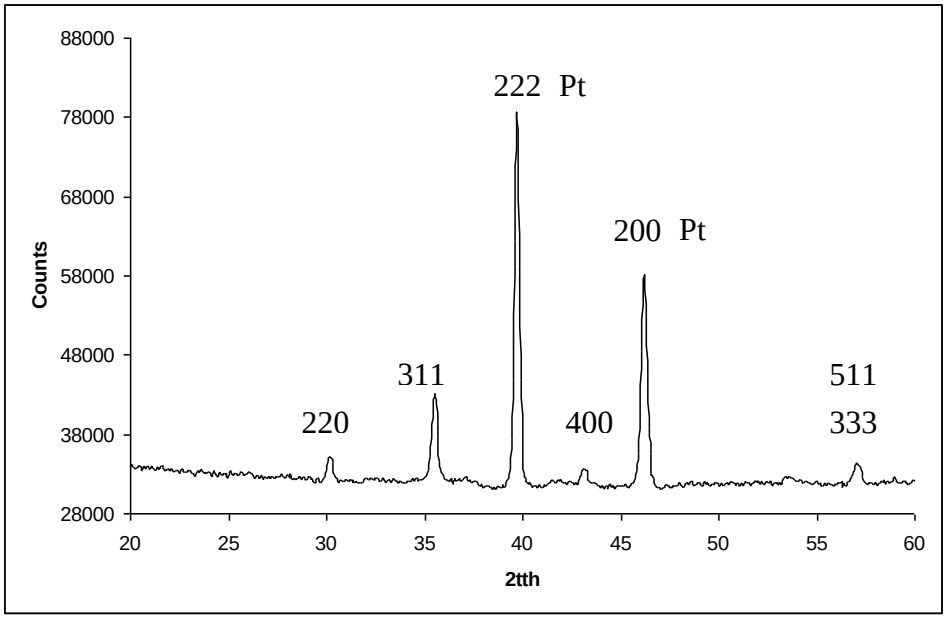

Figure 4.1. X-ray diffraction pattern of $MnFe_2O_4$ from titration of manganese(II) sulfate and iron(II) chloride.

4.3.2 pH binding studies

The binding of selenite and selenate to the nanomaterial over the pH range of 2 through 6 is shown in Figure 4.2. The pH profile study indicated that the binding to the nano-Jacobsite is pH independent in the range of 2 through 6 for both selenite and selenate at 100 ppb concentration. The study also showed that nearly 100% of both Se oxoanions was bound to the $MnFe_2O_4$ material in this pH range at room temperature. The pH independent binding behavior in acidic environments appears to be a characteristic of anionic binding as has been observed with other materials, such as aluminum oxide hydroxide and montmorillonite clays [21-22]. Previous pH dependency studies have also shown that selenium binds greater to iron oxides in acidic environments [23-25]. Rovira *et al.* [24] suggested that sorption of both Se oxoanions

increased at acidic pH because the surface charge on the iron oxides hematite and goethite is positive. The only difference between the $MnFe_2O_4$ nanomaterial and a Fe_3O_4 is that one of the Fe^{2+} in the crystal structure has been substituted with a Mn^{2+} ion and thus one would expect similar behavior between the two types of materials. In addition, under acidic conditions there would be more H^+ present on the surface of the material creating a higher positive charge surface on the $MnFe_2O_4$ or on a Fe_3O_4 nanomaterial. This could enhance the attraction of the selenium anions to the surface of the material which could increase the adsorption of the Se oxoanions.

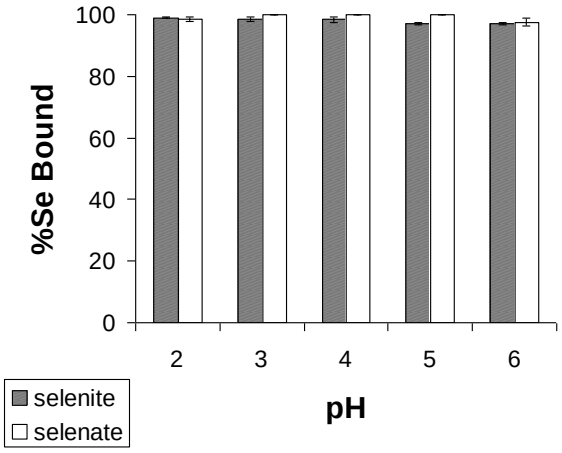

Figure 4.2. Percentage bound of selenite and selenate at a concentration of 100ppb to the nanomaterial under varying pH conditions ranging from pH 2 through pH 6. Error bars represent Standard Error of three replicate.

4.3.3 Time dependency studies

The effect of contact time as a function of the percentage of binding of the Se oxoanions to the nanomaterial can be seen in Figure 4.3. As shown in this figure, the binding maximizes to 96% and 98% of the selenite and selenate in solution, respectively within the first 5 minutes of contact time. Increments beyond that time up to 60 minutes were no significant. This type of fast equilibrium has also been reported for both selenite and selenate binding to iron oxides [25-26]. Additionally, it has been shown that nano-Jacobsite is a rapid sorbent for As(III), As(IV),

and Cr(VI) in acidic conditions [18-19]. In this study, such rapid binding of selenium oxoanions to nano-Jacobsite could be occurring because the active sites are located on the surface of the material as the nano-Jacobsite is nonporous. If the active binding sites are indeed on the surface of the nanomaterial, then the oxoanions will have easy access to these sites, which would result in fast sorption. It has also been suggested by Parsons *et al.* [19] that rapid binding is indicative of adsorption/ion-exhange binding without the occurrence of any redox mechanism.

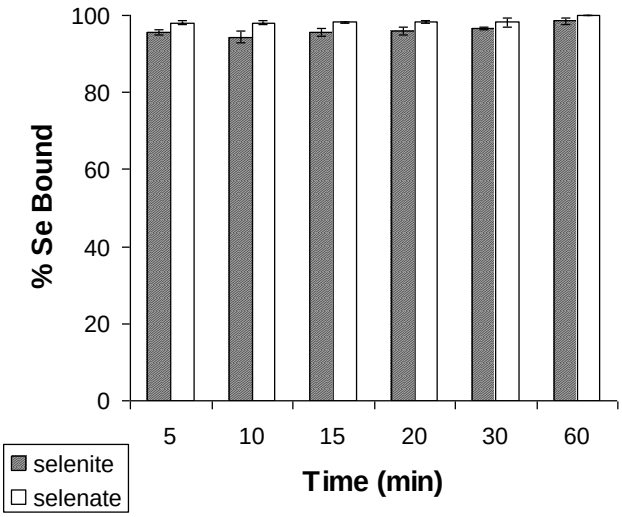

Figure 4.3. Time dependence of percentage bound of selenite and selenate at concentration of 100ppb to the nanomaterial at a pH of 4. Error bars represent Standard Error of three replicate.

4.3.4 Interference studies

The effect of adding potential interfering anions (Cl^-, NO_3^-, SO_4^{2-}, PO_4^{3-}) on the binding of selenite and selenate to the nano-Jacobsite can be seen in Figures 4.4-4.7. As shown in Figure 4.4, the Cl^- ion present in a range from 0.1 to 100 ppm had no significant effect on the percentage of both selenite and selenate binding to the nano-Jacobsite. It can also be seen in Figure 4.4, that binding remained constant for both the selenite and selenate even in the presence of 1000 times the concentration of Cl^-. There was also no significant observable effect of the binding of either

Se oxoanions to the nanomaterial in the presence of NO_3^- in the range from 0.1 to 100 ppm as shown in Figure 4.5. The low binding affinities of both Cl^- and NO_3^- to iron oxides have been observed before [27-28]. This could be occurring because the possible complexes formed between the nano-Jacobsite and Cl^- and NO_3^- are much weaker than those formed between the Se oxoanions even when present at much higher concentrations than selenite or selenate.

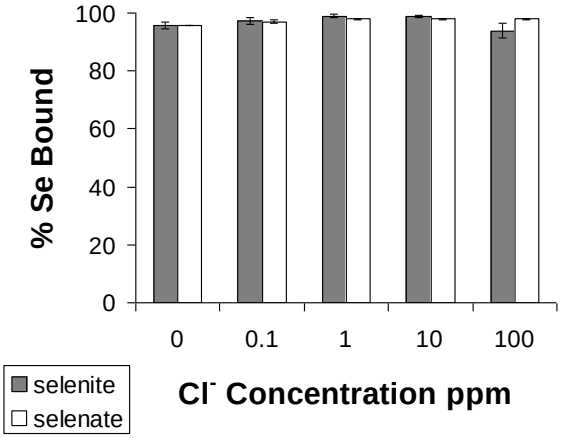

Figure 4.4. Effect of Cl^- ion ranging from 0.1-100ppm on sorption of selenite and selenate to nanomaterial. Error bars represent Standard Error of three replicate.

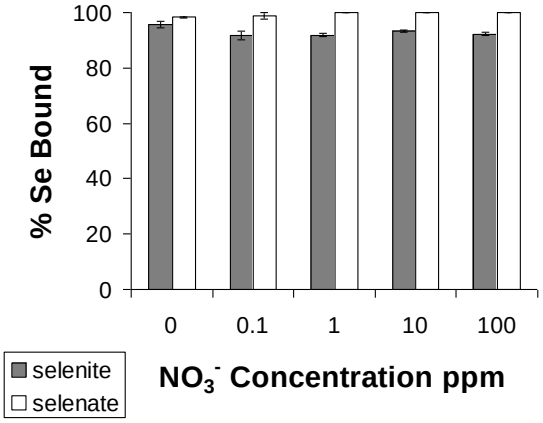

Figuer 4.5. Effect of NO_3^- ion ranging from 0.1-100ppm on sorption if selenite and selenate to nanomaterial. Error bars represent Standard Error of three replicate.

As shown in Figure 4.6, the sorption of selenite was not affected by the introduction of SO_4^{2-} to solution in the range between 0.1 and 10 ppm. However, there was a slight observable decrease in selenium binding at 100 ppm of SO_4^{2-}. Goh and Lim [29] reported a minor reduction of selenite binding when SO_4^{2-} increased in an iron containing soils. In the current study, the addition of SO_4^{2-} at 10 ppm reduced the selenate binding to 90% which is a mole ratio of 1 SeO_4^{2-} to 149 SO_4^{2-}. Even at this large molar ratio of SO_4^{2-} to SeO_4^{2-}, the observed binding is still 90%, which is very impressive and indicate a high affinity of the nanomaterial to SeO_4^{2-}. In the presence of 100 ppm SO_4^{2-} only 35% of selenate was observed to bind to the nanomaterial as shown in Figure 4.6. Again, observing the molar ratio between the SeO_4^{2-} and the SO_4^{2-} , which in this case works out to be 1 SeO_4^{2-} : 1487 SO_4^{2-}, still indicates a high affinity of the nanomaterial to bind the SeO_4^{2-} over the SO_4^{2-}. The observed reduction in selenate binding to the nanomaterial in presence of SO_4^{2-} may be the result of the similar chemistry between selenate and sulfate anions. However, the material does show preferential binding of the SeO_4^{2-} over the SO_4^{2-}. Wijnja and Schulthess [30] have shown using Raman and attenuated total reflection-Fourier transform infrared (ATR-FTIR) spectroscopy that selenate and sulfate adsorption have similar binding behavior on metal (hydr)oxide surfaces. The similar mechanism of binding to adsorbent surfaces suggests that higher concentrations of SO_4^{2-} present in solution could be competing for active binding sites on the nano-Jacobsite.

As shown in Figure 4.7, the binding of either selenium oxoanions to the nanomaterial with concentrations of 0.1-10 ppm of PO_4^{3-} present was not significantly affected. However, at a concentration of 100 ppm PO_4^{3-} (1.0529 M) in solution, the binding was shown to decrease to 81% for selenite with a more dramatic decrease to only 13% binding for selenate to the nano-Jacobsite. However, when the molar concentration ratios of SeO_4^{2-} and PO_4^{3-} are compared, the

ratio is 1 mole SeO_4^{2-}: to 1337 mole PO_4^{3-} . This illustrates the preferential binding of the SeO_4^{2-} to the nanomaterial, as seen in Figure 4.7. There is more than 1000 times the concentration of PO_4^{3-} yet 13% of the SeO_4^{2-} is still binding to the nanomaterial. Similarly, the molar concentration of SeO_3^{2-} and PO_4^{3-} was determined to be 1 SeO_3^{2-} to 1350 PO_4^{3-} and only a 15-20% decrease in the binding of the SeO_3^{2-} was observed. Such a high molar ratio shows the selectivity of the nano-Jacobsite towards SeO_3^{2-}. Goh and Lim [27] using iron containing soils found that PO_4^{3-} had a lower influence on selenite sorption than that of selenate sorption on soil surfaces. This would suggest the selenite oxoanion had stronger adsorption ability to the nano-Jacobsite than selenate. It has been suggested by Smith *et al.* [31] that by increasing PO_4^{3-} concentration in solution could result in an effect of the mass action of the system. Goh and Lim [29] go further to explain this result as the PO_4^{3-} oxoanion may be accumulating or precipitating on the surface of the iron oxides causing a change in the surface potential. The change in the surface potential to a negative charge would then repel the selenium oxoanions and prevent binding of the selenium oxoanions on the surface of the nano-Jacobsite.

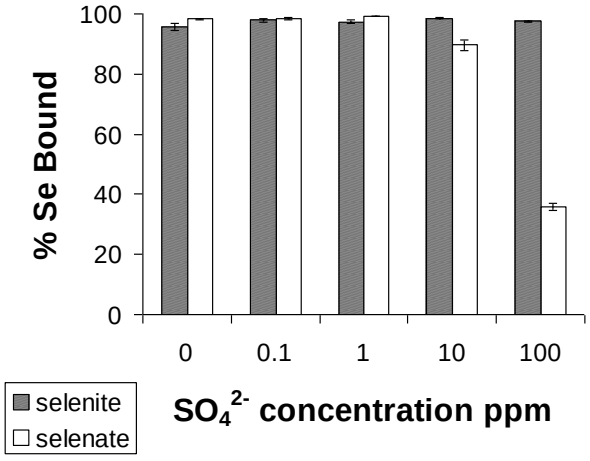

Figure 4.6. Effect of SO_4^{2-} ion ranging from 0.1-100ppm on sorption of selenite and selenate to nanomaterial. Error bars represent Standard Error of three replicate.

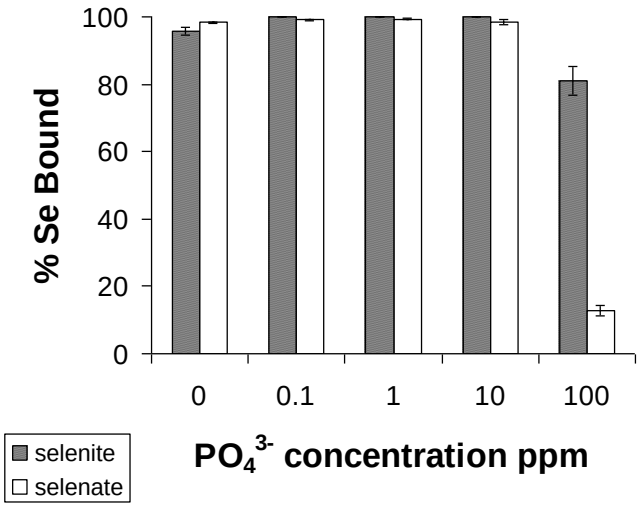

Figure 4.7. Effect of PO_4^{3-} ion ranging from 0.1-100ppm on sorption of selenite and selenate to nanomaterial. Error bars represent Standard Error of three replicate.

4.3.5 Adsorption isotherms

The capacities of the nano-Jacobsite extracted from the Langmuir isotherm are shown in Table 4.1. From the linear fit of both the selenite and selenate it can be seen that the capacity of the NM increased as the concentration of either oxoanions increased. The capacity was found to be of 6573.76 and 769.23 mg Se/kg of nano-Jacobsite for selenite and selenate, respectively, as shown in Table 2. The difference in binding capacities of iron oxides for selenite and selenate has also been shown by Rovira *et al.* [24] and Goh and Lim [29]. Martinez *et al.* [23] reported that the capacity values for natural magnetite were, respectively 352.95 and 484.63 mg Se/kg magnetite for selenite and selenate, after 25-30 h to reach equilibrium. This demonstrates that capacity values for nano-Jacobsite are greater than that of natural magnetite. Kuan *et al.* [32] reported that the capacity of aluminum-oxide-coated sand (AOCS) for selenite and selenate was 1080 and 920 mg Se/kg AOCS, respectively. The capacity of nano-Jacobsite for selenite is higher than that of AOCS but lower for selenate. However, the equilibrium time for AOCS to

reach capacity is 60 min making the nano-Jacobsite a more desirable material to use with an equilibrium time of 15 min.

Table 4.1. Capacity based on Langmuir isotherm experiments for both selenite and selenate binding to $MnFe_2O_4$ nanomaterial.

Adsorbate	Q_e (mg Se/kg of $MnFe_2O_4$)	R^2
SeO_3^{2-}	6573.78±121.52	0.999074
SeO_4^{2-}	769.23±43.41	0.99769

4.4 Conclusions

This research has shown the ability of a synthetic nano-Jacobsite phase material with an average grain size of 27 nm to remove both selenite and selenate from aqueous solutions independently of pH in the range of 2 to 6. Optimum binding of both selenite and selenate occurred within 5 min of contact time with the nano-Jacobsite at pH 4. The introduction of Cl^- and NO_3^- anions had no significant effect on the ability of the material to remove both selenium oxoanions from solution. However, the additions of either SO_4^{2-} or PO_4^{3-} at concentrations of 10 ppm and 100 ppm, respectively were shown to decrease Se adsorption. This work has also shown that nano-Jacobsite has a higher capacity for Se oxoanions removal than naturally occurring magnetite material.

The material of this chapter is in press as:

C.M. Gonzalez, J. Hernandez, J.G. Parsons, J.L. Gardea-Torresdey, Removal of selenite and selenate from aqueous solutions using a magnetic iron/manganese oxide nanomaterial, Microchemical Journal (2010) In Press.

5. X-ray absorption spectroscopy studies for the determination of adsorption binding modes of selenium oxoanions onto iron and manganese based nanomaterials

Abstract

Increasing concentrations of selenium oxoanions in the environment are placing many animals at risks for reproduction failure and deformities. The understanding of binding mechanisms of selenium oxoanions to iron and manganese based oxide minerals could lead to enhanced understanding of selenium mobility in the environment. In this study, the binding mechanisms of selenium oxoanions, selenite and selenate, to non microwave-assisted and microwave-assisted synthetic Fe_3O_4, Mn_3O_4, and $MnFe_2O_4$ nanomaterials were investigated through the use of X-ray absorption spectroscopy. The X-ray absorption near-edge structure (XANES) spectroscopy studies revealed the oxidation state of selenite and selenate remains the same after binding occurs to all nanomaterials in pH 2, 4, or 6 environments. The binding modes of selenite and selenate were determined to be bidentate binuclear and were independent of nanomaterials, synthetic technique, and pH.

5.1. Introduction

Selenium contamination in the environment has become of concern today due to its toxic effects on human and animal health. The increasing concentrations of selenium in the Western United States, such as Wyoming and South Dakota, are raising concern for the possible effects on wildlife in those regions [1]. It has been reported the risks for animals in regions with high concentrations of selenium include bioaccumulation, reproduction failure, deformities, and die-off of migratory waterfowl, fish, insects, and plants [2]. The high mobility of the selenium oxoanions in water systems is proving to be a challenging factor in water treatment [3].

In the environment, the transport and cycling of contaminants and trace element ions are often controlled by adsorption processes onto mineral surfaces [4]. The adsorption of aqueous selenium onto mineral surfaces is an important factor in mobility and bioavailability of selenium in the environment [5]. The most common geosorbent for selenium oxoanions are iron oxide minerals with their structures strongly affecting their reactivity with oxoanions [4]. Manganese oxides have also been shown to be adsorbents for selenium oxoanions, but have been studied to a lesser extent [6]. An understanding of the binding mechanisms for which selenium oxoanions binds to iron and manganese oxide minerals could result in a better understanding of selenium mobility in the environment and lead to enhanced forms of adsorption water treatment techniques.

Hayes *et al.* [7] have demonstrated the bonding mechanisms of selenite and selenate with the iron oxide goethite form bidentate binuclear binding complexes through use of Extended X-ray Absorption Fine Structure (EXAFS) spectroscopy. The use of ultra small Fe_3O_4 particles were shown to not reduce selenite after binding through the use of X-ray absorption near-edge structure (XANES); however the XANES of selenate binding to the particles were not investigated [3]. Foster *et al.* [6] studied the sorption of only selenite onto manganese oxide using X-ray absorption fine structure (XAFS) spectroscopy and determined selenite forms both bidentate mononuclear and monodentate surface complexes. The binding mechanism of the manganese oxide hausmannite Mn_3O_4 for selenium oxoanions have yet to be determined. Gonzalez *et al.* [8] have shown the iron/manganese oxide nanomaterial Jacobsite ($MnFe_2O_4$) is capable of adsorbing both selenite and selenate; however, the binding mechanisms for this nanomaterial have yet to be reported.

In this study, selenium oxoanion binding to non microwave-assisted and microwave-assisted Fe_3O_4 and Mn_3O_4 as well as non-microwave assisted synthetic $MnFe_2O_4$ nanomaterials was investigated using synchrotron-based XAS. The oxidation state of selenium oxoanions after binding to the aforementioned synthetic nanomaterials at pH 2, 4, or 6 was determined by XANES spectroscopy. EXAFS spectroscopy was employed to determine the coordination environment as well as the interatomic distances of selenium oxoanions to the nanomaterials. The combination of both XANES and EXAFS data was used to determine possible types of binding modes for the selenium oxoanion binding to the nanomaterials and if synthetic technique affected these binding modes.

5.2. Experimental

5.2.1 Solution and sample preparation

100 ppm solutions of selenite and selenate were prepared by dissolving reagent grade Na_2SeO_3 (Aldrich) and Na_2SeO_4 (Alfa Aesar), respectively, in Millipore (18 mΩ) water. Synthetic Fe_3O_4, Mn_3O_4, and $MnFe_2O_4$, were prepared as previously described in chapters 2-4. The pH of the 100 ppm selenite or selenate solutions were adjusted to pH 2, 4, or 6 using dilute hydrochloric acid or sodium hydroxide prior to reactions. In 5 mL polyethylene reaction tubes containing 10 mg of either non-microwave assisted synthetic or microwave assisted synthetic Fe_3O_4 or Mn_3O_4 or non-microwave assisted synthetic $MnFe_2O_4$, a 4 mL aliquot of 100 ppm selenite or selenate was added and then rocked (Specimix, Thermo Scientific) for 60 min at room temperature. Once the reaction time was completed, all sample tubes were centrifuged at 3000 rpm for 7 min. The resulting supernatants were discarded and solids were oven dried for X-ray analyses at Stanford Synchrotron Radiation Laboratory (SSRL, Palo Alto, CA).

5.2.2 XANES and EXAFS

The XAS studies to investigate the oxidation state of selenium adsorbed at the surface of the nanomaterials and possible bonding mechanisms were performed at SSRL on Beam Line 7-3 using a liquid helium cryostat (4-200 K). A Canberra 29-element array germanium detector and Si(220)φ 90 monochromator were used to obtain the Fluorescence spectra for the Se-K edge spectra. The operating conditions of the beam line were beam energy of 3 GeV with a beam current of 50-100 mA. The sample spectra for all Fe_3O_4, Mn_3O_4, and $MnFe_2O_4$ nanomaterials as well as the model compounds sodium selenite (Na_2SeO_3) and selenate (Na_2SeO_4) were collected at room temperature and were calibrated using selenium foil.

The sample XAS data collected was then analyzed using WinXAS software [9]. The edge position of an internal selenium foil (12658 eV) was used to calibrate the edge energy. The first and second degree derivatives of the inflection point of the selenium foil was used for the calibration of the sample spectrum. A polynomial fitting subtraction was implemented to remove the background of the spectrum, while a first degree polynomial was used on the pre-edge region, and a third degree polynomial was used on the post-edge region of the spectrum. Based on the energy of the photoelectrons ejected from the samples, the conversion into *k* space was achieved. A Fourier transformation into interatomic distance space was accomplished by resulting scattering curves from *k* space weighted to 3. The coordination numbers as well as the Debye-Waller factors were obtained by the least squares fit of EXAFS data. The Se-Fe_3O_4, Se-Mn_3O_4, and Se-$MnFe_2O_4$ were than fitted to the XANES and EXAFS spectra of the model compounds.

5.3. Results and Discussion

5.3.1 Results of XANES studies

The XANES of the interaction of selenite and selenate reacted with the $MnFe_2O_4$, Fe_3O_4, and Mn_3O_4 microwave-assisted and non-microwave assisted synthetic nanomaterials at pH 2, 4, and 6 are shown in Figures 5.1-5.4. As can be seen in each of the individual figures, the oxidation state of the selenium after being reacted with the nanomaterial remains the same. The oxidation state of the selenium was determined through looking at the white line position. The white line is a sharp feature which is the highest absorption peak in the XAS spectrum due to electronic transitions [10]. As shown in Figure 5.5, the white line for selenite and selenate appear at different energy positions separated by approximately 2.9 eV. The separation between the selenite (Se(IV)) and selenate (Se(VI)) white line features is further apart than the energy resolution of the beamline, which is between 1 and 2 eV. It is because of this separation between the selenate and the selenite white line that allows for the determination of the oxidation state. Based on this information, it can be seen the oxidation state of selenite or selenate after each of the reactions with all the nanomaterials remains unchanged. The presence of selenite and selenate in the samples would show a shoulder feature in the absorption edge, which is not observed in any of the samples. However, there was a change in the local coordination geometry between the model compounds and the selenium coordinated to the nanomaterials. The selenite samples show an increase in the white line feature at 12.662 keV, and a damping of the absorption feature at approximately 12.471 keV. These small changes indicate a change in the local geometry around the Se(IV) ion. Similarly, the selenate bound to the nanomaterials also demonstrated a change in the atomic geometry showing a small increase in the white line feature at 12.665 keV. Additionally, there was an observed disappearance of the XANES features at

approximately 12.673 and 12.681 keV which strongly indicates a change in the local coordination geometry as well. These XANES features observed in the model compounds are due to the coordination geometry of the crystalline samples. The observed increase in the white line features has been associated with the hydration or the breaking apart of the crystals to form ions [11]. This result indicates that the selenium present in the samples after reaction with the nanomaterials is present in the ionic and amorphous form.

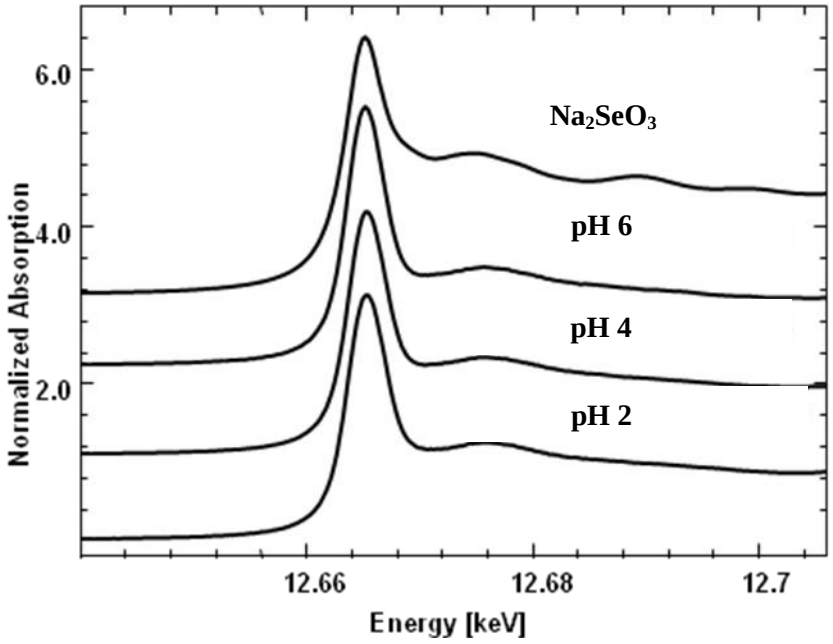

Figure 5.1. XANES spectra of sodium selenite model compound and of selenite (SeO_3^{2-}) binding to the non microwave-assisted synthetic $MnFe_2O_4$ nanomaterial at pH 2, 4, and 6.

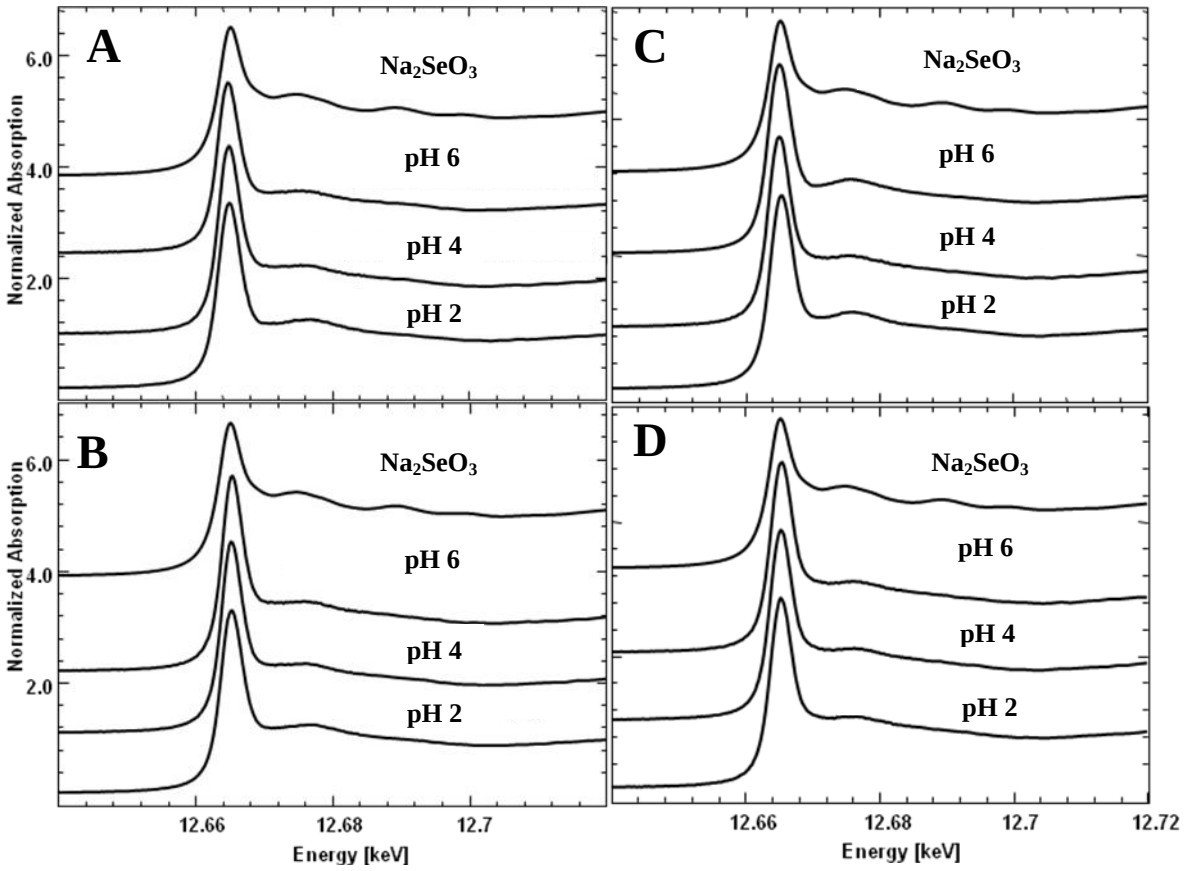

Figure 5.2. XANES spectra of sodium selenite model compound and of selenite (SeO_3^{2-}) binding to (A) microwave-assisted synthetic nanomaterials of Mn_3O_4 at pH 2, 4, and 6, (B) non microwave- assisted synthetic nanomaterials of Mn_3O_4 at pH 2, 4, and 6, (C) microwave-assisted synthetic nanomaterials of Fe_3O_4 at pH 2, 4, and 6, (D) non microwave-assisted synthetic nanomaterials of Fe_3O_4 at pH 2, 4, and 6.

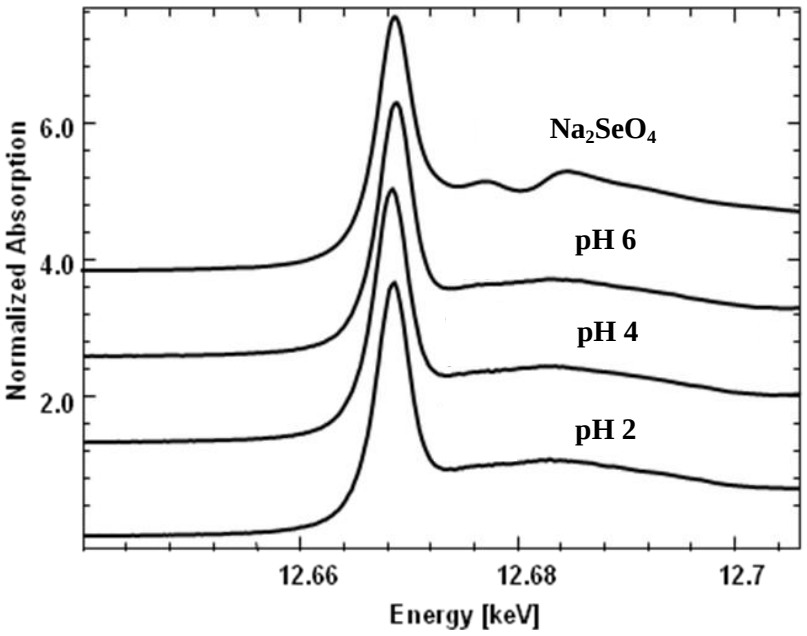

Figure 5.3. XANES spectra of sodium selenate model compound and of selenate (SeO_4^{2-}) binding to non microwave-assisted synthetic $MnFe_2O_4$ nanomaterial at pH 2, 4, and 6.

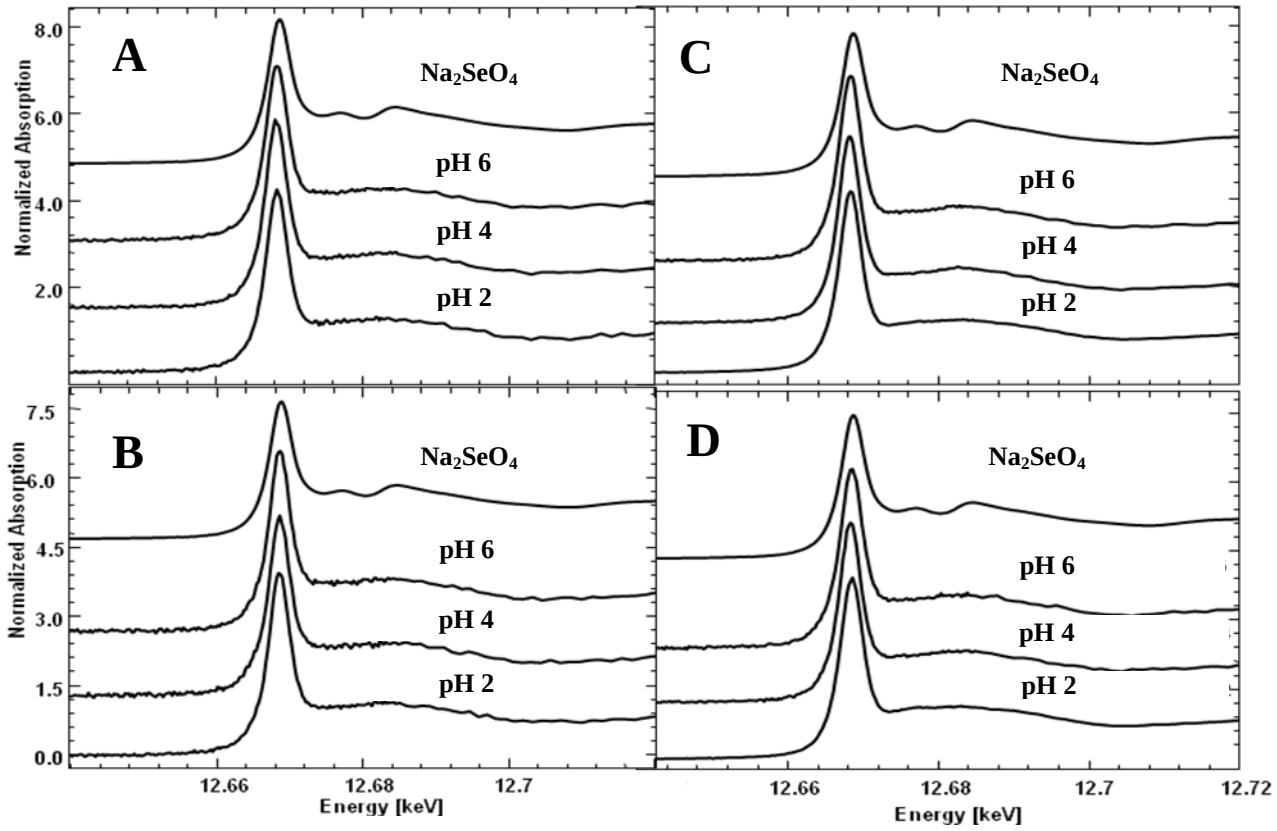

Figure 5.4. XANES spectra of sodium selenate model compound and of selenate (SeO_4^{2-}) binding to (A) microwave-assisted synthetic nanomaterial of Mn_3O_4 at pH 2, 4, and 6, (B) non microwave-assisted synthetic nanomaterial of Mn_3O_4 at pH 2, 4, and 6, (C) microwave-assisted synthetic nanomaterial of Fe_3O_4 at pH 2, 4, and 6, (D) non microwave-assisted synthetic nanomaterial of Fe_3O_4 at pH 2, 4, and 6.

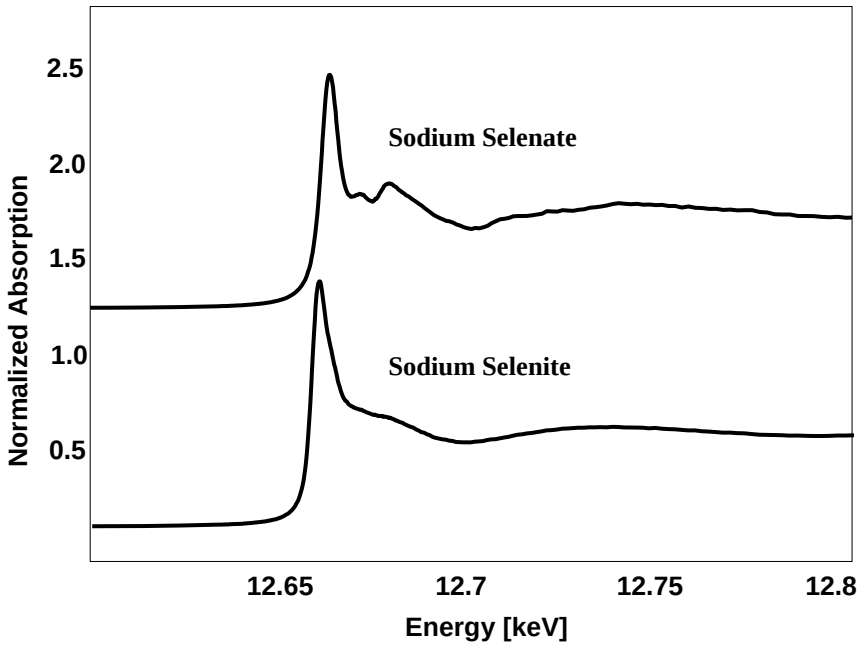

Figure 5.5. XANES spectra of sodium selenite and sodium selenate model compounds taken from 12.603 to 12.809 keV.

5.3.2 Results from the EXAFS studies

A representative Fourier transformed EXAFS spectra for the reaction of selenite and selenate with the $MnFe_2O_4$, Fe_3O_4, and Mn_3O_4 microwave-assisted and non-microwave assisted synthesized nanomaterials at pH 2, 4 and 6 are shown in Figures 5.6-5.9. The Fourier transformed EXAFS are presented as the dotted line and the Fourier transformed fitting of the back transformed EXAFS spectra are shown as solid lines. The actual fitting results are presented in Table 5.1-5.3. The model compound spectra for selenite and selenate are shown in Figure 5.10. As can be seen in Figure 5.10, the position of the main oscillation for both the selenite and the selenate samples are located at approximately the interatomic distance of 1.67 and 1.65 Å, for selenite and selenate, respectively. However, the coordination number does vary from 4 neighboring atoms for selenate and 3 neighboring atoms for selenite.

As can be seen in the representative spectra in Figures 5.6 and 5.7A-B, there are at least two interactions occurring for selenite binding to the $MnFe_2O_4$ and Fe_3O_4 nanomaterials. These interactions are located at 1.71 Å and around 3.30-3.40 Å in the EXAFS data and are shown in Tables 5.1-5.2. The shorter of the two interactions represents the possibility of three Se-O interactions of the selenite with the microwave-assisted and non microwave-assisted synthetic Fe_3O_4 and non microwave-assisted $MnFe_2O_4$ nanomaterials. The determined Se-O interatomic distance falls within the literature determined range for this type of binding which is 1.68–1.72 Å [7]. The other longer observed interaction represents a Se-Metal interaction, which in these nanomaterials appears to be the metal iron or manganese ions present in the nanomaterials. The presence of the two iron atoms on the surface of the nanomaterial structures in the fitting of the spectra gives a strong indication of the type of binding occurring in the samples. There are three possible types of binding modes for the selenium oxoanion binding to the nanomaterials. The

first possible binding mode is a mononuclear monodentate, the second possible binding mode is the binuclear bidentate, and third possible binding mode is mononuclear bidentate as shown in Figure 5.11A, B, and C, respectively. The data obtained from the EXAFS fitting for the selenite binding to the microwave-assisted and non microwave-assisted synthetic Fe_3O_4 and the non microwave-assisted $MnFe_2O_4$, indicates the presence of two heavier atoms in the EXAFS. This observation is indicative that the binding mode of selenium oxoanions to the nanomaterials is binuclear bidentate and has been previously reported in the literature for similar materials [7].

The binding of the selenite to the microwave-assisted and non microwave-assisted Mn_3O_4 nanomaterials was low, and only the first shell EXAFS could be extracted and fitted with any certainty and can be seen in Figure 5.7C-D and Table 5.3. However, the first shell EXAFS of the Mn_3O_4 nanomaterials showed similar data as those of the first shell EXAFS of the microwave-assisted and non microwave-assisted synthetic Fe_3O_4 and the non microwave-assisted $MnFe_2O_4$ nanomaterials. The reported XANES data of the Mn_3O_4 nanomaterials showed similar data as previously discussed to the $MnFe_2O_4$ and Fe_3O_4 nanomaterials, indicating that the binding mode of selenium oxoanions to the Mn_3O_4 nanomaterials may also be binuclear bidentate. Furthermore, it is interesting to note the binding mode is independent of the nanomaterial as well as the synthetic technique of the nanomaterial at pH of 2, 4, and 6.

The selenate binding to the synthetic nanomaterials showed similar data to that of selenite. As can be seen in Figures 5.8-5.9A-B and Tables 5.1-5.2, the binding of selenate to the microwave-assisted and non microwave-assisted synthetic Fe_3O_4 and non microwave-assisted $MnFe_2O_4$ nanomaterials showed a first shell coordination environment consisting of four oxygen atoms with an interatomic distance of 1.65 Å. Similar to the selenite binding, a second coordination sphere was observed for the selenate binding to the nanomaterials at approximately

3.3-3.40 Å and indicates the presence of two heavier atoms. The presence of the two atoms in the second coordination sphere indicates that the binding of the selenate to the $MnFe_2O_4$ and Fe_3O_4 nanomaterials is binuclear bidentate, as was observed with the selenite samples, as shown in Figure 5.11B.

Selenate binding to the microwave-assisted synthetic Mn_3O_4 nanomaterial was low, as was observed with the selenite samples, and therefore only the first shell EXAFS could be extracted as can be seen in Figure 5.9C and Table 5.3. This data showed the presence of 4 oxygen atoms at an interatomic distance of approximately 1.64 Å. However, the XANES data from the selenate samples reacted with the Mn_3O_4 nanomaterials data as previously discussed showed similar data to that of the selenate data obtained from the $MnFe_2O_4$ and Fe_3O_4 nanomaterials indicating similar binding behavior which would be binuclear bidentate. Again, as with the selenite data, the selenate binding mode appears to be independent of the binding nanomaterial and of the synthesis technique of the nanomaterial. The non microwave-assisted Mn_3O_4 samples reacted with selenate were too dilute to give the EXAFS oscillations for fitting purposes.

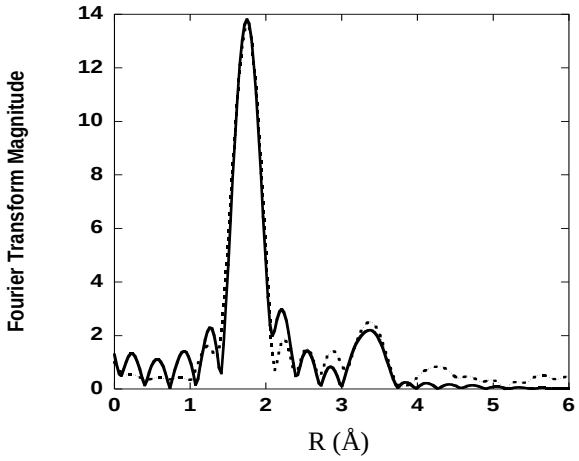

Figure 5.6. Fourier transformed EXAFS of selenite (SeO_3^{2-}) binding to $MnFe_2O_4$.

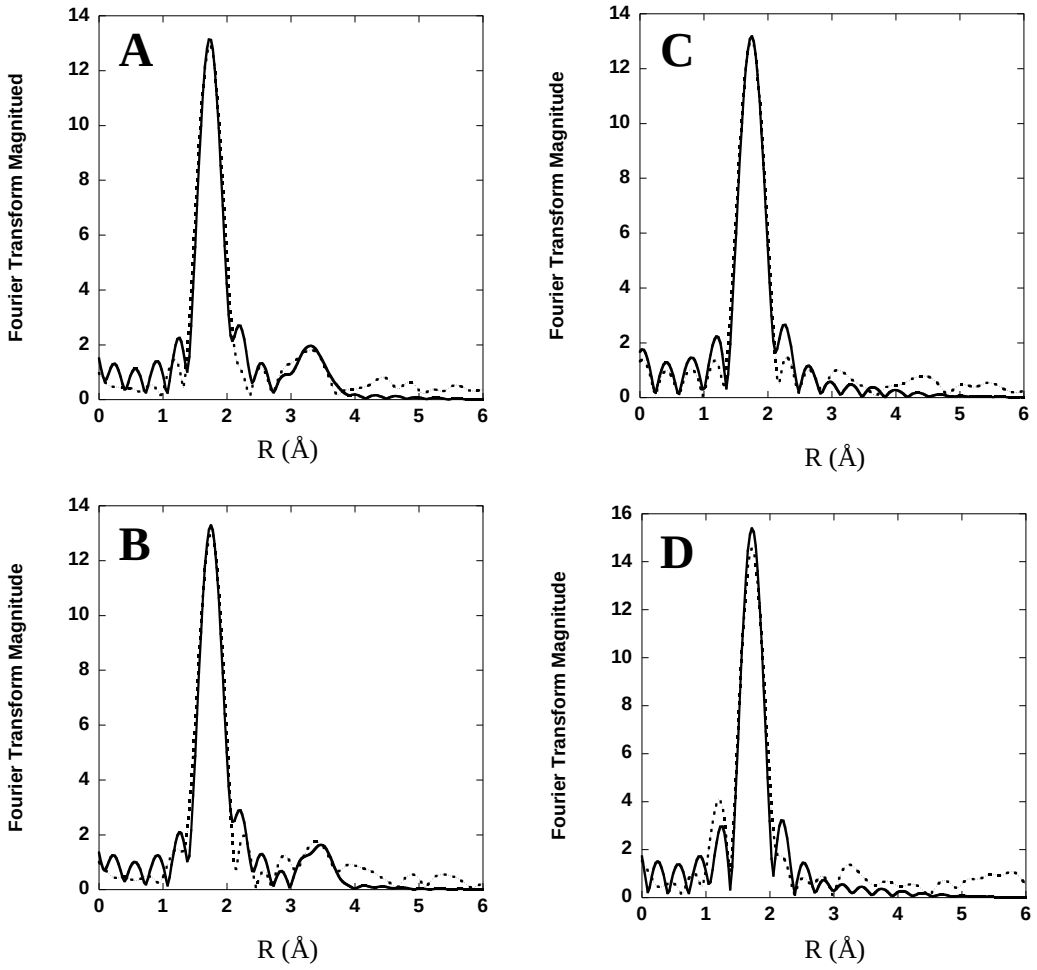

Figure 5.7. Fourier transformed EXAFS of selenite (SeO_3^{2-}) binding to (A) microwave-assisted synthetic Fe_3O_4 nanomaterial, (B) non microwave-assisted synthetic Fe_3O_4 nanomaterial, (C) non microwave-assisted synthetic Mn_3O_4 nanomaterial, (D) non microwave-assisted synthetic Mn_3O_4 nanomaterial.

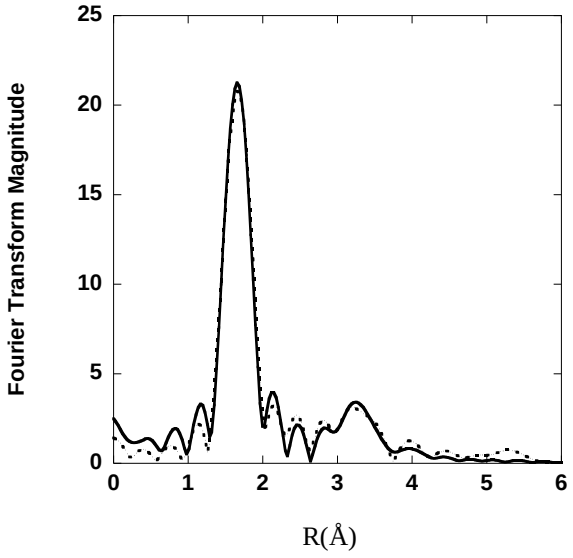

Figure 5.8. Fourier transformed EXAFS of selenate (SeO_4^{2-}) binding to $MnFe_2O_4$.

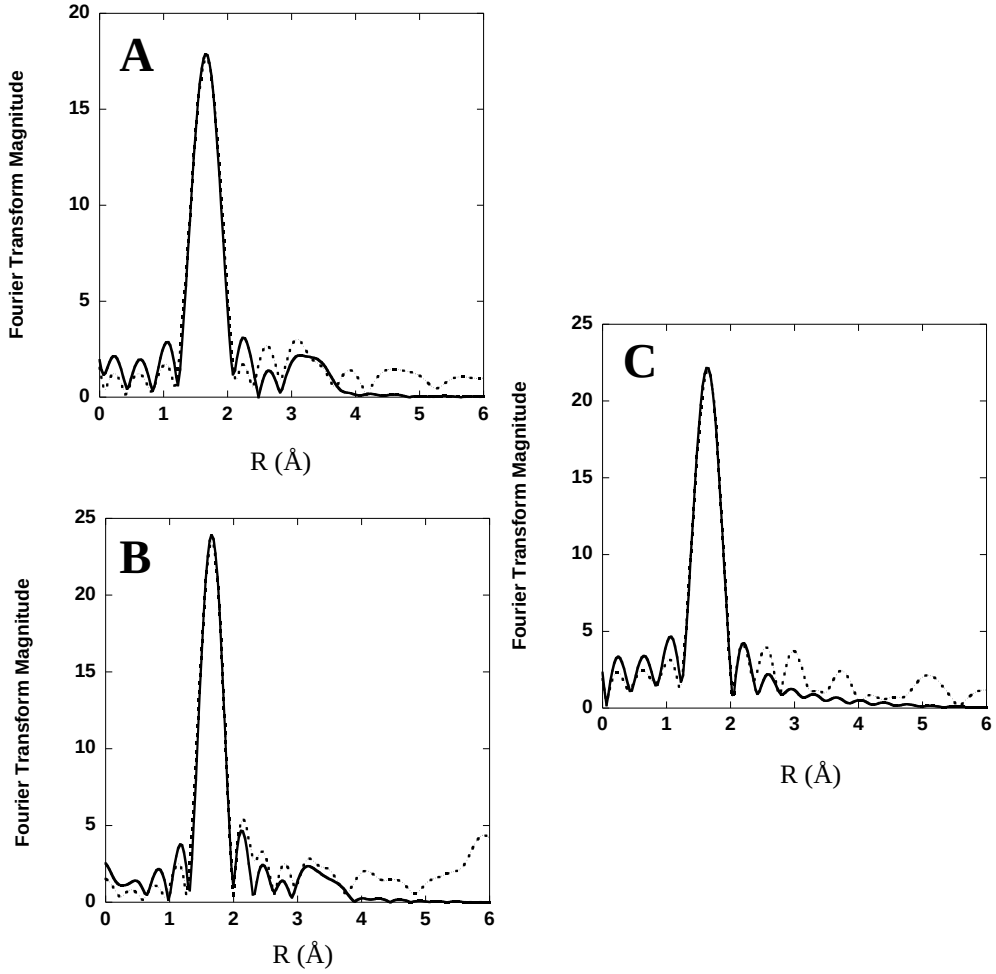

Figure 5.9. Fourier transformed EXAFS of selenate binding to (A) microwave-assisted synthetic Fe_3O_4 nanomaterial, (B) Fourier Transformed EXAFS of selenate binding to non microwave-assisted synthetic Fe_3O_4 nanomaterial, (C) Fourier Transformed EXAFS of selenate binding to microwave-assisted synthetic Mn_3O_4 nanomaterial.

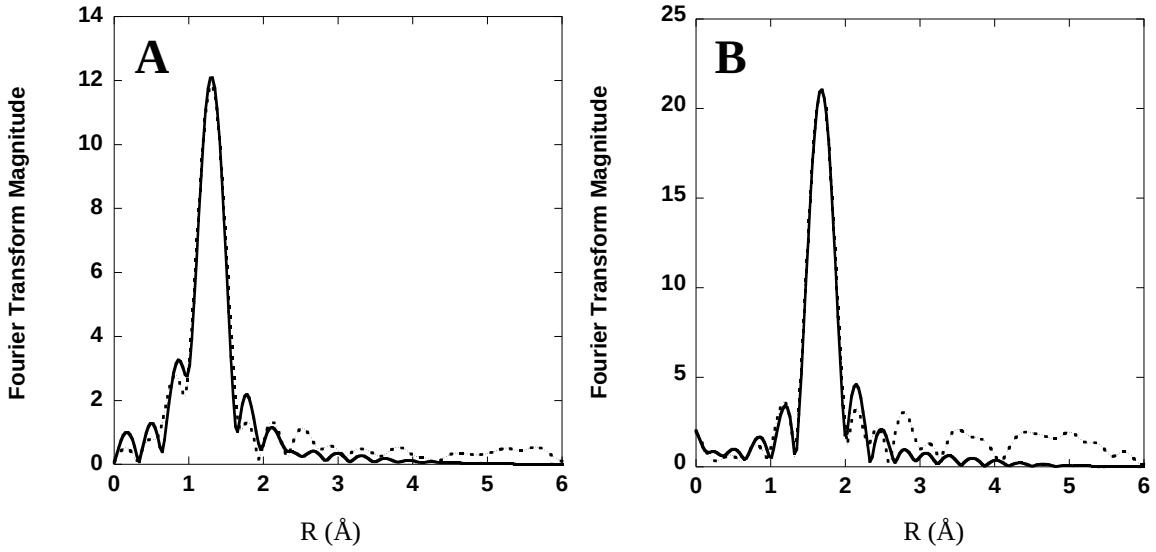

Figure 5.10. Fourier transformed EXAFS of (A) sodium selenite and (B) sodium selenite.

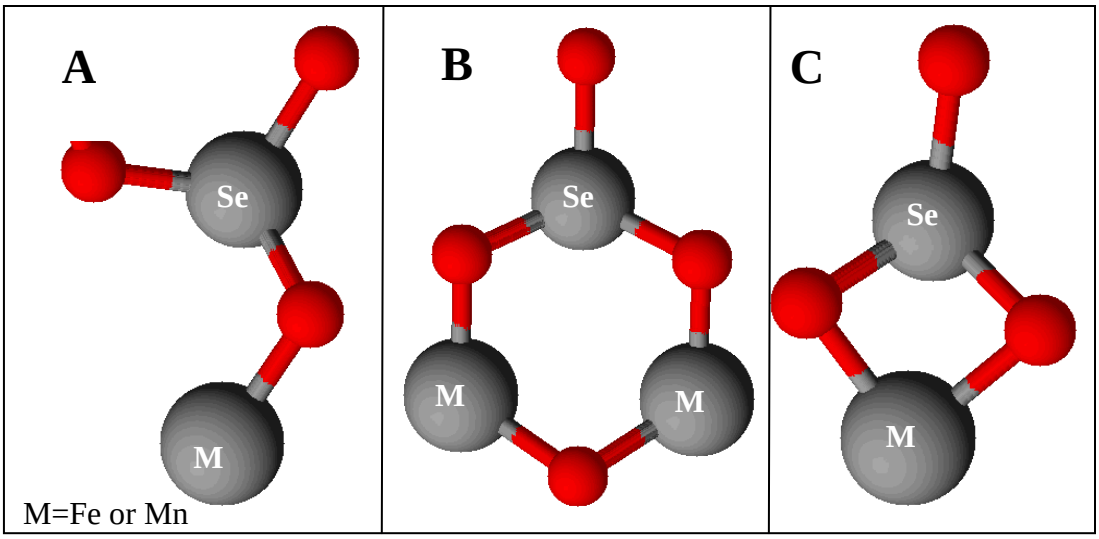

Figure 5.11. Possible binding modes of selenium oxoanions to either microwave-assisted synthesized or non microwave-assisted synthesized Fe_3O_4, $MnFe_2O_4$, and Mn_3O_4 nanomaterials. **(**A) Monodenate mononuclear. (B) Binuclear bidentate. (C) Mononuclear bidentate.

Table 5.1. Fitting of the back transformed EXAFS of the reactions of selenite and selenate with microwave-assisted and non microwave-assisted synthetic Fe_3O_4 nanomaterials.

Sample	**Bond**	**CN**[a]	**R(Å)**[b]	σ^{2c}
Microwave-assisted Fe_3O_4 selenite pH 2	Se-O	3.0	1.70(0)	0.0017
	Se-Fe	1.4	3.32(9)	0.0048
Microwave-assisted Fe_3O_4 selenite pH 4	Se-O	3.0	1.71(4)	0.0025
	Se-Fe	2.0	3.41(1)	0.0065
Microwave-assisted Fe_3O_4 selenite pH 6	Se-O	3.0	1.70(6)	0.0032
	Se-Fe	1.0	3.25(8)	0.0065
Non microwave-assisted Fe_3O_4 selenite pH 2	Se-O	3.0	1.69(7)	0.0017
	Se-Fe	1.0	3.33(3)	0.0072
Non microwave-assisted Fe_3O_4 selenite pH 4	Se-O	3.0	1.71(4)	0.0021
	Se-Fe	1.0	3.38(3)	0.0072
Non microwave-assisted Fe_3O_4 selenite pH 6	Se-O	3.0	1.71(2)	0.0034
	Se-Fe	1.0	3.38(7)	0.0062
Microwave-assisted Fe_3O_4 selenate pH 2	Se-O	4.0	1.65(0)	0.0013
	Se-Fe	2.0	3.34(7)	0.0089
Microwave-assisted Fe_3O_4 selenate pH 4	Se-O	4.0	1.65(3)	0.0025
	Se-Fe	2.0	3.31(2)	0.0073
Microwave-assisted Fe_3O_4 selenate pH 6	Se-O	4.0	1.64(4)	0.0031
	Se-Fe	1.0	3.32(2)	0.0090
Non microwave-assisted Fe_3O_4 selenate pH 2	Se-O	4.0	1.65(3)	0.0020
	Se-Fe	2.0	3.40(1)	0.0047
Non microwave-assisted Fe_3O_4 selenate pH 4	Se-O	4.0	1.63(9)	0.0011
	Se-Fe	2.0	3.34(5)	0.0083
Non microwave-assisted Fe_3O_4 selenate pH 6	Se-O	4.4	1.63(5)	0.0048
	Se-Fe	N/A	N/A	N/A
Sodium Selenite	Se-O	3.0	1.67(1)	0.0024
Sodium Selenate	Se-O	4.0	1.64(1)	0.0019

[a] Coordination number , [b] Interatomic distance, [c] Debe-Waller Factor, N/A=Not Available

Table 5.2. Fitting of the back transformed EXAFS of the reactions of selenite and selenate with non microwave-assisted synthetic $MnFe_2O_4$ nanomaterial.

Sample	**Bond**	**CN**[a]	**R(Å)**[b]	**σ^{2}**[c]
Non microwave-assisted $MnFe_2O_4$ selenite pH 2	Se-O	3.0	1.70(7)	0.0025
	Se-Fe/Mn	2.0	3.37(0)	0.0072
Non microwave-assisted $MnFe_2O_4$ selenite pH 4	Se-O	3.0	1.71(6)	0.0021
	Se-Fe/Mn	2.0	3.37(3)	0.0083
Non microwave-assisted $MnFe_2O_4$ selenite pH 6	Se-O	3.0	1.69(1)	0.0022
	Se-Fe/Mn	2.0	3.33(6)	0.0093
Non microwave-assisted $MnFe_2O_4$ selenate pH 2	Se-O	4.0	1.64(1)	0.0019
	Se-Fe/Mn	2.0	3.32(1)	0.0089
Non microwave-assisted $MnFe_2O_4$ selenate pH 4	Se-O	4.0	1.65(7)	0.0028
	Se-Fe/Mn	2.0	3.33(1)	0.0071
Non microwave-assisted $MnFe_2O_4$ selenate pH 6	Se-O	4.0	1.64(5)	0.0018
	Se-Fe/Mn	2.0	3.34(2)	0.0083

[a] Coordination number , [b] Interatomic distance, [c] Debe-Waller Factor

Table 5.3. Fitting of the back transformed EXAFS of the reactions of selenite and selenate with microwave-assisted and non microwave-assisted synthetic Mn_3O_4 nanomaterials.

Sample	**Bond**	**CN**[a]	**R(Å)**[b]	**σ^{2}**[c]
Microwave-assisted Mn_3O_4 selenite pH 2	Se-O	3.0	1.71(3)	0.0016
Microwave-assisted Mn_3O_4 selenite pH 4	Se-O	3.0	1.70(8)	0.0022
Microwave-assisted Mn_3O_4 selenite pH 6	Se-O	2.8	1.69(7)	0.0019
Non microwave-assisted Mn_3O_4 selenite pH 2	Se-O	3.0	1.71(3)	0.0016
Non microwave-assisted Mn_3O_4 selenite pH 4	Se-O	3.0	1.69(6)	0.00055
Non microwave-assisted Mn_3O_4 selenite pH 6	Se-O	3.0	1.70(5)	0.0020
Microwave-assisted Mn_3O_4 selenate pH 2	Se-O	4.2	1.64(7)	0.0011
Microwave-assisted Mn_3O_4 selenate pH 4	Se-O	4.0	1.63(7)	0.00024
Microwave-assisted Mn_3O_4 selenate pH 6	Se-O	4.0	1.64(3)	0.0010

[a] Coordination number, [b] Interatomic distance, [c] Debe-Waller Factor

5.4 Conclusions

This research has displayed all the nanomaterials bind selenite and selenate without the occurrence of any oxidation state changes at pH of 2, 4, or 6. Also, the binding mode of both selenium oxoanions to all nanaomaterials investigated appears to be binuclear bindentate. Finally, the binding mode is independent of the synthetic technique for all nanomaterials studied.

6. Conclusions

The final conclusions derived from this work can be summarized as follows:

- The results from XRD show that both non microwave-assisted and microwave-assisted Fe_3O_4 and Mn_3O_4, and the non microwave-assisted $MnFe_2O_4$ nanomaterials had the phases of magnetite, hausmannite, and Jacobsite, respectively.
- Application of the Scherrer's equation revealed the average grain sizes of the nanomaterials were 27 and 25 nm for non microwave-assisted and microwave-assisted synthetic Fe_3O_4 nanomaterials, respectively, 25 and 34 nm for non microwave-assisted and microwave-assisted synthetic Mn_3O_4 nanomaterials, respectively, and 27 nm for non microwave-assisted synthetic $MnFe_2O_4$ nanomaterial.
- The optimal binding pH for all nanomaterials was pH 4. This was based on the stability of the materials at the tested pH range of 2-6, as well as the percentage of selenium bound.
- The binding times for selenium oxoanions were observed to be 5 min for $MnFe_2O_4$ and both the synthetic Fe_3O_4 nanomaterials; for both synthetic Mn_3O_4 nanomaterials, binding time was 10 min.
- The addition of the Cl^- ion significantly decreased selenate binding to both synthetic Mn_3O_4 nanomaterials only.
- Selenate binding to both synthetic Mn_3O_4 nanomaterials and microwave-assisted synthetic Fe_3O_4 nanomaterial were significantly decreased in the presence of the NO_3^-.
- The SO_4^{2-} anion significantly decreased the sorption of selenate to all nanomaterials tested, additionally decreasing the binding of selenite to both Mn_3O_4 nanomaterials. The decrease in selenate binding could be due to the similar chemistry and binding behavior to metal oxides between selenate and sulfate.

- The decrease in selenite binding for the Mn_3O_4 nanomaterials in the presence of sulfate could be explained by a weaker affinity of selenite to the Mn_3O_4 nanomaterial than other materials, as well as due to a higher molar ratio of sulfate to selenite.
- The addition of the PO_4^{3-} ion significantly affected the binding of both selenite and selenate to all nanomaterials tested. When at a much higher molar ratio, selenite could be outcompeted for binding sites by the phosphate ion. The selenate complexes formed between all nanomaterials tested could be much weaker than those formed by the phosphate ion.
- The capacities for the Fe_3O_4 nanomaterials based on Langmuir isotherms were found to be 1923 and 1428 mg Se /kg of non microwave-assisted Fe_3O_4 and 2380 and 2369 mg Se/ kg of microwave-assisted Fe_3O_4 for selenite and selenate, respectively. The differences in capacities between the two Fe_3O_4 nanomaterials could be attributed to the variation of the nanomaterial's size. The smaller sized nanomaterial would have a larger surface area resulting in a higher number of active binding sites.
- The capacities based on the Langmuir isotherm adsorption experiments show that the non microwave-assisted synthetic Mn_3O_4 nanomaterial had a capacity of 507 and 800 mg Se/kg of nanomaterial for selenite and selenate, respectively. The microwave-assisted synthetic Mn_3O_4 nanomaterial was determined to have a higher capacity for both selenite and selenate, 1000 and 934.5 mg Se/kg of nanomaterial, respectively, than that of the non microwave-assisted Mn_3O_4 nanomaterial.
- The Langmuir isotherm equation determined that the nano-Jacobsite had a selenite and selenate binding capacity of 6573.76 and 769.23 mg Se/kg of $MnFe_2O_4$, respectively.
- In all cases tested, except for microwave-assisted synthetic Mn_3O_4, selenite sorption capacity of the nanomaterials was greater than selenate sorption capacity. This trend has been

observed with most metal oxides that have been tested for their adsorption capacities for both selenium oxoanions.

- The XANES studies revealed the oxidation state of both selenite and selenate does not change after binding to Fe_3O_4, Mn_3O_4, or $MnFe_2O_4$ nanomaterials has occurred.
- The EXAFS results displayed that all nanomaterials bind both selenite and selenate in a binuclear bidentate fashion.
- While all materials were found to bind both selenium oxoanions regardless of synthetic technique, the addition of competitive anions does not make Mn_3O_4 a promising sorbent for selenium oxoanion removal.
- Fe_3O_4 and $MnFe_2O_4$ nanomaterials had the highest observed binding capacities and were the least affected by the addition of competitive anions; they also continued to display a high affinity for both selenite and selenate binding. These materials are the most promising adsorbents tested for selenium oxoanion removal in this work.

Reference

Chapter 1

[1] C.B'Hymer, J.A. Caruso, Selenium speciation analysis using inductively coupled plasma-mass spectrometry, *Journal of Chromatography A* **1114** (2006) 1-20.

[2] M.S. Dzul Erosa, W.H. Höll, J. Horst, Sorption of selenium species onto weakly basic anion exchangers: I. Equilibrium studies, *Reactive & Functional Polymers* **69** (2009) 576–585.

[3] S.Y.Hasanay, Najamuddin, and M. Ikram, Uptake of Traces of Selenite by Manganese Dioxide from Aqueous Solutions, *Sep. Sci. Technol.* **32** (1997) 1945-1957.

[4] E.I. El-Shafey, Removal of Se(IV) from aqueous solution using sulphuric acid-treated peanut shell, *Journal of Environmental Management* **84** (2007) 620-627.

[5] K.M. Parida, B. Gorai, N.N. Das, S.B. Rao, Studies on ferric oxide hydroxides: Adsorption of selenite (SeO_3^{2-}) on different forms of iron oxyhydroxides, *J. Colloid Interface Sci.* **185** (1997) 355-362.

[6] D. Peak, Adsorption mechanisms of selenium oxyanions at the aluminum oxide/water interface, *J. Colloid Interface Sci.* **303** (2006) 337-345.

[7] D. Peak, U.K. Saha, P.M. Huang, Selenite adsorption mechanisms on pure and coated montmorillonite: an EXAFS and XANES Spectroscopic study, *Soil Sci. Soc. Am. J.* **70** (2006) 192-203.

[8] United States Environmental Protection Agency (USEPA). 2006 Edition of the drinking water standards and health advisories, EPA-822-R-06-013, Office of Water, USEPA, Washington, DC.

[9] W.T. Frankenberger, M. Arshad, Bioremediation of selenium-contaminated sediments and water, *BioFactors* **14** (2001) 241–254.

[10] Y. Zhang, J. Wang, C. Amrhein, W. T. Frankenberger, Removal of selenate from water by zerovalent iron, *J. Environ. Qual.* **34** (2005) 487-495.

[11] United States Environmental Protection Agency (USEPA). National Primary Drinking Water Regulations, EPA-816-F-09-004, Office of Water, USEPA, Washington, DC., 2009.

[12] G. Jegadeesan, K. Mondal, S.B. Lalvani, Selenate removal from sulfate containing aqueous solutions, *Environ. Technol.* **26** (2005) 1181-1187.

[13] J.A. Ippolito, K.G. Scheckel, K.A. Barbarick, Selenium adsorption to aluminum-based water treatment residuals, *J. Colloid Interface Sci.* **338** (2009) 48-55.

[14] D. J. Hoffman, Role of Selenium toxicity and oxidative stress in aquatic birds, *Aquat. Toxicol.* **57** (2002) 11-26.

[15] M.S. Dzul Erosa, W.H. Höll, J. Horst, Sorption of selenium species onto weakly basic anion exchangers: I. Equilibrium studies, *Reactive and Funtional Polymers* **69** (2009) 546-585.

[16] W.T. Frankenberger, C. Amrhein, T.W.M. Fan, D. Flaschi, J. Glaer, E. Kartinen, K. Kovac, E. Lee, H.M. Ohlendorf, L. Owens, N. Terry, A. Toto, Advanced treatment technologies in the remediation of seleniferous drainage waters and sediments, *Irrigation and Drainage Systems* **18** (2004) 19-41.

[17] G.S. Banuelos, Z.Q. Lin, L. Wu, N. Terry, Phytoremediation of selenium-contaminated soils and waters: fundamentals and future prospects, *Rev. Environ. Health* **17** (2002) 291-306.

[18] N. Zhang, D. Gang, L. Lin, Adsorptive removal of ppm-level selenate using iron-coated GAC adsorbents, *J. Environ. Eng.* (2010) In Press.

[19] A.W. Cantafio, K.D. Hagen, G.E. Lewis, T.L. Bledsoe, K.M. Nunan, J.M. Macy, Pilot-scale selenium bioremediation of San Joaquin drainage water with *Thauera selenatis*, *Applied Environmental Microbiology* **62** (1996) 3298-3303.

[20] I. Baur, C.A. Johnson, Sorption of selenite and selenate to cement minerals, *Environ. Sci. Technol.* **37** (2003) 3442-3447.

[21] C. Su, D.L. Suarez, Selenate and Selenite Sorption on Iron Oxides: An Infrared and Electrophoretic Study, *Soil Sci. Soc. Am. J.* **64** (2000) 101-111.

[22] M. Zhang, E. J. Reardon, Removal of B, Cr, Mo, and Se from Wastewater by Incorporation into Hydrocalumite and Ettringite, *Environ. Sci. Technol.* **37** (2003) 2947-2952.

[23] T. Roussel, C. Bichara, R.J.M. Pellenq, Selenium and carobon nanostructures in the pores of $AlPO_4$-5, *Adsorption* **11** (2005) 709-714.

[24] A. Sabarudin, K. Oshita, M. Oshima, S. Motomizu, Synthesis of chitosan resin possessing 3,4-diamino benzoic acid moiety for the collection/concentration of arsenic and selenium in water samples and their measurement by inductively coupled plasma-mass spectrometry, *Anal. Chim. Acta* **542** (2005) 207-215.

[25] I. Bonhoure, I. Baur, E. Wieland, C.A. Johnson, Uptake of Se(IV/VI) oxyanions by hardened cement paste and cement minerals: An X-ray absorption spectroscopy study, *Cem. Concr. Res.* **36** (2006) 91-98.

[26] S.L. Lo, T.Y.Chen, Adsorption of Se(IV) and Se(VI) on an iron-coated sand from water, *Chemosphere* **35** (1997) 919-930.

[27] D. Peak, U.K. Saha, P.M. Huang, Selenite adsorption mechanisms on pure and coated montmorillonite: an EXAFS and XANES Spectroscopic study, *Soil Sci. Soc. Am. J.* **70** (2006) 192-203.

[28] M. Martinez, J. Gimenez, J. de Pablo, M. Rovira, L. Duro, Sorption of selenium (IV) and selenium (VI) onto magnetite, *Appl. Surf. Sci.* **252** (2006) 3767-3773.

[29] J.T. Mayo, C. Yavuz, S. Yean, L. Cong, H. Shipley, W. Yu, J. Falkner, A. Kan, M. Tomson, V.L. Colvin, The effect of nanocrystalline magnetite size on arsenic removal, *Science and Technology of Advanced Materials* **8** (2007) 71-75.

[30] J. Hu, I.M.C. Lo, G. Chen, Fast Removal and Recovery of Cr (VI) using surface-modified jacobsite ($MnFe_2O_4$) nanoparticles, *Langmuir* **21** (2005), 11173-11179.

[31] J.G. Parsons, M.L. Lopez, J.R. Peralta-Videa, J.L. Gardea-Torresdey, Determination of arsenic (III) and arsenic (V) binding to microwave assisted hydrothermal synthetically prepared Fe_3O_4, Mn_3O_4, and $MnFe_2O_4$ nanoadsorbents, *Microchem. J.* **91** (2009) 100-106.

[32] K. Sakei, S. Matsumoto, R. Tatsukawa, Selenite adsorption by manganese oxides, *Soil Sci.* **160** (1995) 265-272.

[33] S.K. Apte, S.D. Naik, R.S. Sonawane, B.B. Kale, N. Pavaskar, A.B. Mandale, B.K. Das, Nanosize Mn3O4 (Hausmannite) by microwave irradiation method, *Mater. Res. Bull.* **41** (2006) 647–654.

Chapter 2

[1] C.B'Hymer, J.A. Caruso, Selenium speciation analysis using inductively coupled plasma-mass spectrometry, *Journal of Chromatography A* **1114** (2006) 1-20.

[2] United States Environmental Protection Agency (USEPA). 2006 Edition of the drinking water standards and health advisories, EPA-822-R-06-013, Office of Water, USEPA, Washington, DC.

[3] S. Mandal, S. Mayadevi, B.D. Kulkarni, Adsorption of Aqueous Selenite [Se(IV)] Species on Synthetic Layered Double Hydroxide Materials, *Ind. Eng. Chem. Res.* **48** (2009) 7893-7898

[4] D. J. Hoffman, Role of Selenium toxicity and oxidative stress in aquatic birds, *Aquat. Toxicol.* **57** (2002) 11-26.

[5] D. Strawn, H. Doner, M. Zavarin, S. McHugo, Microscale investigation into the geochemistry of arsenic, selenium, and iron in soil developed in pyritic shale materials, *Geoderma* **108** (2002) 237-257.

[6] W.T. Frankenberger, M. Arshad, Bioremediation of selenium-contaminated sediments and water, *BioFactors* **14** (2001) 241-254.

[7] V. Marvo, S. Stamenov, E. Todorova, H. Chimel, T. Erwe, New hybrid electro-coagulation membrane process for removing selenium from industrial wastewater, *Desalination* **201** (2006) 290-296.

[8] E.I. El-Shafey, Removal of Se(IV) from aqueous solution using sulphuric acid-treated peanut shell, Journal of Environmental Management 84 (2007) 620–627.

[9] M. Zhang, E. J. Reardon, Removal of B, Cr, Mo, and Se from Wastewater by Incorporation into Hydrocalumite and Ettringite, *Environ. Sci. Technol.* **37** (2003) 2947-2952.

[10] T. Roussel, C. Bichara, R.J.M. Pellenq, Selenium and carobon nanostructures in the pores of $AlPO_4$-5, *Adsorption* **11** (2005) 709-714.

[11] A. Sabarudin, K. Oshita, M. Oshima, S. Motomizu, Synthesis of chitosan resin possessing 3,4-diamino benzoic acid moiety for the collection/concentration of arsenic and selenium in water samples and their measurement by inductively coupled plasma-mass spectrometry, *Anal. Chim. Acta* **542** (2005) 207-215.

[12] J.A. Ippolito, K.G. Scheckel, K.A. Barbarick, Selenium adsorption to aluminum-based water treatment residuals, *J. Colloid Interface Sci.* **338** (2009) 48-55.

[13] I. Bonhoure, I. Baur, E. Wieland, C.A. Johnson, Uptake of Se(IV/VI) oxyanions by hardened cement paste and cement minerals: An X-ray absorption spectroscopy study, *Cem. Concr. Res.* **36** (2006) 91-98.

[14] D. Peak, Adsorption mechanisms of selenium oxyanions at the aluminum oxide/water interface, *J. Colloid Interface Sci.* **303** (2006) 337-345.

[15] K.M. Parida, B. Gorai, N.N. Das, S.B. Rao, Studies on ferric oxide hydroxides: Adsorption of selenite (SeO_3^{2-}) on different forms of iron oxyhydroxides, *J. Colloid Interface Sci.* **185** (1997) 355-362.

[16] S.L. Lo, T.Y.Chen, Adsorption of Se(IV) and Se(VI) on an iron-coated sand from water, *Chemosphere* **35** (1997) 919-930.

[17] Y. Zhang, J. Wang, C. Amrhein, W. T. Frankenberger, Removal of selenate from water by zerovalent iron, *J. Environ. Qual.* **34** (2005) 487-495.

[18] L.C.A. Oliveira, V.R.A. Rios, J.D. Fabris, K.Sapag, V.K. Garg, R.M. Lago, Clay-oxide magnetic composites for the adsorption of contaminants in water, *Appl. Clay Sci.* **22** (2003) 169-177.

[19] V. Rocher, J. Siaugue, V. Cabuil, A. Bee, Removal of organic dyes by magnetic alginate beads, *Water Res.* **42** (2008) 1290-1298.

[20] M. Martinez, J. Gimenez, J. de Pablo, M. Rovira, L. Duro, Sorption of selenium (IV) and selenium (VI) onto magnetite, *Appl. Surf. Sci.* **252** (2006) 3767-3773.

[21] R. Lopez de Arroyabe Loyo, S. I. Nikitenko, A. C. Scheinost, M. Simonoff, Immobilization of selenite on Fe_3O_4 and Fe/Fe_3C Ultrasmall particles, *Environ. Sci. Technol.* **42** (2008) 2451-2456.

[22] V. Sreeja, P.A. Joy, Microwave–hydrothermal synthesis of γ-Fe_2O_3 nanoparticles and their magnetic properties, *Mater. Res. Bull.* **42** (2007) 1570–1576

[23] S. Laurent, D. Forge, M. Port, A. Roch, C. Robic, L. V. Elst, R.N. Muller, Magnetic iron oxide nanoparticles: synthesis, stabilization, vectorization, physiochemical characterizations, and biological application, *Chem. Rev.* **108** (2008) 2064-2110.

[24] M. Kosmulski (Ed) Surface Charging and Points of Zero Charge, in: Surfactant Science Series, vol. 145, Taylor & Francis Group, Bocan Rayon, FL, 2009, 222-233.

[25] A. Manceau, L. Charlet, The mechanism of selenate adsorption on goethite and hydrous ferric oxide, *J. Colloid Interface Sci.* **168** (1994) 87-93.

[26] J.G. Parsons, M.L. Lopez, J.R. Peralta-Videa, J.L. Gardea-Torresdey, Determination of arsenic (III) and arsenic (V) binding to microwave assisted hydrothermal synthetically prepared Fe_3O_4, Mn_3O_4, and $MnFe_2O_4$ nanoadsorbents, *Microchem. J.* **91** (2009) 100-106.

[27] C. Su, D.L. Suarez, Selenate and Selenite Sorption on Iron Oxides: An Infrared and Electrophoretic Study, *Soil Sci. Soc. Am. J.* **64** (2000) 101-111.

[28] R. Lopez de Arroyabe Loyo, S.I. Nikitenko, A. C. Scheinost, M. Simonoff, Immobilization of selenite on Fe_3O_4 and Fe/Fe_3C Ultrasmall particles, *Environ. Sci. Technol.* **42** (2008) 2451-2456.

[29] Y. Jeong, F. Maohong, J. Van Leeuwen, J.F. Belczyk, Effect of competing solutes on arsenic(V) adsorption using iron and aluminum oxides, *J. Environ. Qual.* **34** (2005) 487-495.

[30] S.K. Dhillon, K.S. Dhillon, Selenium adsorption in soils as influenced by different anions, *J. Plant Nutr. Soil Sci.* **163** (2000) 577-582.

[31] K. Goh, T. Lim, Geochemistry of inorganic arsenic and selenium in a tropical soil: effect of reaction time, pH, and competitive anions on arsenic and selenium adsorption, *Chemosphere* **55** (2004) 849-859.

[32] N. Zhang, L. Lin, D. Gang, Adsorptive selenite removal from water using iron-coated GAC adsorbents, *Water Res.* **42** (2008) 3809-3816.

[33] N. Zhang, D. Gang, L. Lin, Adsorptive removal of ppm-level selenate using iron-coated GAC adsorbents, *J. of Environ. Eng.* (2010) In Press.

Chapter 3

[1] C. B'Hymer, J.A. Caruso, Selenium speciation analysis using inductively coupled plasma-mass spectrometry, *J. Chromatogr., A* **1114** (2006) 1-20.

[2] United States Environmental Protection Agency (USEPA). 2006 Edition of the drinking water standards and health advisories, EPA-822-R-06-013, Office of Water, USEPA, Washington, DC.

[3] G. Jegadeesan, K. Mondal, S.B. Lalvani, Selenate removal from sulfate containing aqueous solutions, *Environ. Tech.* **26** (2005) 1181-1187.

[4] L. Zhang, N. Liu, L. Yang, Q. Lin, Sorption behavior of nano-TiO_2 for the removal of selenium ions from aqueous solution, *J. Hazard. Mater.* **170** (2009) 1197–1203.

[5] A. Sabarudin, K. Oshita, M. Oshima, S. Motomizu, Synthesis of chitosan resin possessing 3,4-diamino benzoic acid moiety for the collection/concentration of arsenic and selenium in water samples and their measurement by inductively coupled plasma-mass spectrometry, *Anal. Chim. Acta* **542** (2005) 207–215.

[6] D. Peak, Adsorption mechanisms of selenium oxoanions at the aluminum oxide/water interface, J. *Colloid Interface Sci.* **303** (2006) 337-345.

[7] D. J. Hoffman, Role of Selenium toxicity and oxidative stress in aquatic birds, *Aquat. Toxicol.* **57** (2002) 11-26.

[8] M. Kashiwa, S. Nishimoto, K. Takahashi, M. Ike, M. Fujita, Factors affecting soluble selenium removal by a selenate reducing bacterium *Bacillus* sp. SF-1, *J. Biosci. Bioeng.* **89** (2000) 528–533.

[9] W.T. Frankenberger, M. Arshad, Bioremediation of selenium-contaminated sediments and water, *BioFactors* **14** (2001) 241-254.

[10] V. Marvo, S. Stamenov, E. Todorova, H. Chimel, T. Erwe, New hybrid electro-coagulation membrane process for removing selenium from industrial wastewater, *Desalination* **201** (2006) 290-296.

[11] G.S. Banuelos, Z.Q. Lin, L. Wu, N. Terry, Phytoremediation of selenium-contaminated soils and waters: fundamentals and future prospects, *Rev. Environ. Health* **17** (2002) 291-306.

[12] E.I. El-Shafey, Sorption of Cd(II) and Se(IV) from aqueous solution using modified rice husk, *J. Hazard. Mater.* **147** (2007) 546–555.

[13] I. Bonhoure, I. Baur, E. Wieland, C.A. Johnson, Uptake of Se(IV/VI) oxoanions by hardened cement paste and cement minerals: An X-ray absorption spectroscopy study, *Cem. Concr. Res.* **36** (2006) 91-98.

[14] J.A.Ippolito, K.G. Scheckel, K.A. Barbarick, Selenium adsorption to aluminum-based water treatment residuals, *J. Colloid Interface Sci.* **338** (2009) 48-55.

[15] S.S. Dash, K.M. Parida, Studies on selenite adsorption using manganese nodule leached residues, *J. Colloid Interface Sci.* **307** (2007) 333–339.

[16] D. Peak, U.K. Saha, P.M. Huang, Selenite adsorption mechanisms on pure and coated montmorillonite: an EXAFS and XANES Spectroscopic study, *Soil Sci. Soc. Am. J.* **70** (2006) 192-203.

[17] K.M. Parida, B. Gorai, N.N. Das, S.B. Rao, Studies on ferric oxide hydroxides: Adsorption of selenite (SeO_3^{2-}) on different forms of iron oxyhydroxides, *J. Colloid Interface Sci.* **185** (1997) 355-362.

[18] J.G. Catalano, Z. Zhang, P. Fenter, M.J. Bedzyk, Inner-sphere adsorption geometry of Se(IV) at the hematite (100)-water interface, *J. Colloid Interface Sci.* **297** (2006) 665-671.

[19] J. Hu, I.M.C. Lo, G. Chen, Fast Removal and Recovery of Cr (VI) using surface-modified jacobsite ($MnFe_2O_4$) nanoparticles, *Langmuir* **21** (2005) 11173-11179.

[20] S.K. Apte, S.D. Naik, R.S. Sonawane, B.B. Kale, N. Pavaskar, A.B. Mandale, B.K. Das, Nanosize Mn_3O_4 (Hausmannite) by microwave irradiation method, *Mater. Res. Bull.* **41** (2006) 647–654.

[21] T. Ozkaya, A. Baykal, H. Kavasb, Y. Köseoğlu , M.S. Toprak,, A novel synthetic route to Mn_3O_4 nanoparticles and their magnetic evaluation, *Phys. B* **403** (2008) 3760–3764.

[22] M. Salavati-Niasari, F. Davar, M. Mazaheri, Synthesis of Mn_3O_4 nanoparticles by thermal decomposition of a [bis(salicylidiminato)manganese(II)] complex, *Polyhedron* **27** (2008) 3467–3471.

[23] J.G. Parsons, M.L. Lopez, J.R. Peralta-Videa, J.L. Gardea-Torresdey, Determination of arsenic (III) and arsenic (V) binding to microwave assisted hydrothermal synthetically prepared Fe_3O_4, Mn_3O_4, and $MnFe_2O_4$ nanoadsorbents, *Microchem. J.* **91** (2009) 100-106.

[24] A. L. Foster, G. E. Brown, G. A. Parks, X-ray absorption fine structure study of As(V) and Se(IV) sorption complexes on hydrous Mn oxides, *Geochim. Cosmochim. Acta.* **67** (2003) 1937-1953.

[25] K. Saeki, S. Matsumoto, R. Tatsukawa, Selenite Adsorption By Manganese Oxides, *Soil Sci.* **160** (1995) 265-272.

[26] R. Liu, R. L. Frosta, W. N. Martens, Absorption of the selenite anion from aqueous solutions by thermally activated layered double hydroxide, *Water Res.* **43** (2009) 1323-1329.

[27] S. M. Maliyekkal, A. K. Sharma, L. Philip, Manganese-oxide-coated alumina: A promising sorbent for defluoridation of water, *Water Res.* **40** (2006) 3497-3506.

[28] Y. Jeong, F. Maohong, J. Van Leeuwen, J.F. Belczyk, Effect of competing solutes on arsenic(V) adsorption using iron and aluminum oxides, *J. Environ. Qual.* **34** (2005) 487-495.

[29] H. Wijnja, C.P. Schulthess, Vibrational Spectroscopy Study of Selenate and Sulfate Adsorption Mechanisms of Fe and Al (Hydr)oxide Surfaces, *J. Colloid Interface Sci.* **229** (2000) 286-297.

[30] S. M. Maliyekkala, L. Philip, T. Pradeep, As(III) removal from drinking water using manganese oxide-coated-alumina: Performance evaluation and mechanistic details of surface binding, *Chem. Eng. J.* **153** (2009) 101–107.

[31] Y. Zhang, J. Wang, C. Amrhein, W. T. Frankenberger, Removal of selenate from water by zerovalent iron, *J. Environ. Qual.* **34** (2005) 487-495.

[32] C. Su, D.L. Suarez, Selenate and Selenite Sorption on Iron Oxides: An Infrared and Electrophoretic Study, *Soil Sci. Soc. Am. J.* **64** (2000) 101-111.

[33] S. Mustafa, M. I. Zaman, S. Khan, Temperature effect on the mechanism of phosphate anions sorption by β-MnO_2, *Chem. Eng. J.* **141** (2008) 51–57.

[34] N. Zhang, L. Lin, D. Gang, Adsorptive selenite removal from water using iron-coated GAC adsorbents, *Water Res.* **42** (2008) 3809-3816.

[35] N. Zhang, D. Gang, L. Lin, Adsorptive removal of ppm-level selenate using iron-coated GAC adsorbents, *J. Environ. Eng.* (2010) In Press.

Chapter 4

[1] W.T. Frankenberger, M. Arshad, Bioremediation of selenium-contaminated sediments and water, *BioFactors* **14** (2001) 241-254.

[2] D. Peak, Adsorption mechanisms of selenium oxyanions at the aluminum oxide/water interface, *J. Colloid Interface Sci.* **303** (2006) 337-345.

[3] C. B'Hymer, J.A. Caruso, Selenium speciation analysis using inductively coupled plasma-mass spectrometry, *J. Chromatogr., A* **1114** (2006) 1-20.

[4] D. Peak, U.K. Saha, P.M. Huang, Selenite adsorption mechanisms on pure and coated montmorillonite: an EXAFS and XANES Spectroscopic study, *Soil Sci. Soc. Am. J.* **70** (2006) 192-203.

[5] P.M. Chapman, Selenium-A potential time bomb or just another contaminant?, *Hum. Ecol. Risk Assess.* **5** (1999) 1123-1138.

[6] Y. Zhang, J.H. Moore, Selenium Fractionation and speciation in a wetland system, *Environ. Sci. Technol.* **30** (1996) 2613-2619.

[7] N. Zhang, L. Lin, D. Gang, Adsorptive selenite removal from water using iron-coated GAC adsorbents, *Water Res.* **42** (2008) 3809-3816.

[8] G.S. Banuelos, Z.Q. Lin, L. Wu, N. Terry, Phytoremediation of selenium-contaminated soils and waters: fundamentals and future prospects, *Rev. Environ. Health* **17** (2002) 291-306.

[9] J.A.Ippolito, K.G. Scheckel, K.A. Barbarick, Selenium adsorption to aluminum-based water treatment residuals, *J. Colloid Interface Sci.* **338** (2009) 48-55.

[10] S.L. Lo, T.Y.Chen, Adsorption of Se(IV) and Se(VI) on an iron-coated sand from water, *Chemosphere* **35** (1997) 919-930.

[11] Y. Zhang, J. Wang, C. Amrhein, W. T. Frankenberger, Removal of selenate from water by zerovalent iron, *J. Environ. Qual.* **34** (2005) 487-495.

[12] K.M. Parida, B. Gorai, N.N. Das, S.B. Rao, Studies on ferric oxide hydroxides: Adsorption of selenite (SeO_3^{2-}) on different forms of iron oxyhydroxides, *J. Colloid Interface Sci.* **185** (1997) 355-362.

[13] I. Bonhoure, I. Baur, E. Wieland, C.A. Johnson, Uptake of Se(IV/VI) oxyanions by hardened cement paste and cement minerals: An X-ray absorption spectroscopy study, *Cem. Concr. Res.* **36** (2006) 91-98.

[14] N. Jordan, C. Lomenech, N. Marmier, E. Giffaut, J. Ehrhardt, Sorption of selenium(IV) onto magnetite in the presence of silicic acid, *J. Colloid Interface Sci.* **329** (2009) 17-23.

[15] J.G. Catalano, Z. Zhang, P. Fenter, M.J. Bedzyk, Inner-sphere adsorption geometry of Se(IV) at the hematite (100)-water interface, *J. Colloid Interface Sci.* **297** (2006) 665-671.

[16] L.C.A Oliveira, V.R.A. Rios, J.D. Fabris, K.Sapag, V.K. Garg, R.M. Lago, Clay-oxide magnetic composites for the adsorption of contaminants in water, *Appl. Clay Sci.* **22** (2003) 169-177.

[17] N. Karapinar, Magnetic separation of ferrihydrite from wastewater by magnetic seeding and high-gradient magnetic separation, *Int. J. Miner. Process.* **71** (2003) 45-54.

[18] J. Hu, I.M.C. Lo, G. Chen, Fast Removal and Recovery of Cr (VI) using surface-modified jacobsite ($MnFe_2O_4$) nanoparticles, *Langmuir 21* (2005), 11173-11179.

[19] J.G. Parsons, M.L. Lopez, J.R. Peralta-Videa, J.L. Gardea-Torresdey, Determination of arsenic (III) and arsenic (V) binding to microwave assisted hydrothermal synthetically prepared Fe_3O_4, Mn_3O_4, and $MnFe_2O_4$ nanoadsorbents, *Microchem. J.* **91** (2009) 100-106.

[20] S. Kuo, J. Lee, N. Wu, Study on Pseudocapacitance Mechanism of Aqueous MnFe2O4 Supercapacitor, *J. Electrochem. Soc.* **154** (2007) A34-A38.

[21] S. Tananda, M. Kabayama, N. Kawasaki, T. Sakiyama, T. Nakamura, M. Araki, T, Tamura, Removal of phosphate by aluminum oxide hydroxide, *J. Colloid Interface Sci.* **257** (2003) 135-140.

[22] O. Hocine, M. Boufatit, A. Khouider, Use of montmorillonite clays as adsorbents of hazardous polluants, *Desalination* **167** (2004) 141-145.

[23] M.Martinez, J. Gimenez, J. de Pablo, M. Rovira, L. Duro Sorption of selenium (IV) and selenium (VI) onto magnetite, *Appl. Surf. Sci.* **252** (2006) 3767-3773.

[24] M. Rovira, J. Gimenez, M. Martinez, X. Martinez-Llado, J. de Pablo, V. Marti, L. Duro, Sorption of selenium(IV) and selenium(VI) onto natural iron oxides: Goethite and hematite**,** *J. Hazard. Mater.* **150** (2008) 279-284.

[25] M. Duc, G. Lefevre, M. Fedoroff, Sorption of selenite ions on hematite, *J. Colloid Interface Sci.* **298** (2006) 556-563.

[26] C. Su, D.L. Suarez, Selenate and Selenite Sorption on Iron Oxides: An Infrared and Electrophoretic Study, *Soil Sci. Soc. Am. J.* **64** (2000) 101-111.

[27] F. Frau, D. Addari, D. Atzei, R. Biddau, R. Cidu, A. Rossi, Influence of Major Anions on As(V) Adsorption by Synthetic 2-line Ferrihydrite. Kinetic Investigation and XPS Study of the Competitive Effect of Bicarbonate, *Water, Air, Soil Pollut.* **205** (2010) 25-41.

[28] Y. Jeong, F. Maohong, J. Van Leeuwen, J.F. Belczyk, Effect of competing solutes on arsenic(V) adsorption using iron and aluminum oxides, *J. Environ. Qual.* **34** (2005) 487-495.

[29] K. Goh, T. Lim, Geochemistry of inorganic arsenic and selenium in a tropical soil: effect of reaction time, pH, and competitive anions on arsenic and selenium adsorption, *Chemosphere* **55** (2004) 849-859.

[30] H. Wijnja, C.P. Schulthess, Vibrationsal Spectroscopy Study of Selenate and Sulfate Adsorption Mechanisms of Fe and Al (Hydr)oxide Surfaces, *J. Colloid Interface Sci.* **229** (2000) 286-297.

[31] E. Smith, R. Naidu, A.M. Alston, Chemistry of Inorganic Arsenic in Soils: II. Effect of Phosphorous, Sodium, and Calcium on Arsenic Sorption, J. *Environ. Qual.* **31** (2002) 557-563.

[32] Wen-Hui Kuan, Shang-Lien, Lo, M.K. Wang, Cheng-Fang, Lin, Removal of Se(IV) and Se(VI) from water by aluminum-oxide-coated sand, *Water Res.* **32** (1998) 915-923.

Chapter 5

[1] S.S. Dash, K.M. Parida, Studies on selenite adsorption using manganese nodule leached residues, *J. Colloid and Interface Sci.* **307** (2007) 333–339.

[2] J.A.Ippolito, K.G. Scheckel, K.A. Barbarick, Selenium adsorption to aluminum-based water treatment residuals, J. *Colloid Interface Sci.* **338** (2009) 48-55.

[3] R. Lopez de Arroyabe Loyo, S. I. Nikitenko, A. C. Scheinost, M. Simonoff, Immobilization of selenite on Fe_3O_4 and Fe/Fe_3C Ultrasmall particles, *Environ. Sci. Technol.* **42** (2008) 2451-2456.

[4] D. Peak, Adsorption mechanisms of selenium oxoanions at the aluminum oxide/water interface, *J. Colloid Interface Sci.* **303** (2006) 337-345.

[5] H. Wijnja, C.P. Schulthess, Vibrational Spectroscopy Study of Selenate and Sulfate Adsorption Mechanisms of Fe and Al (Hydr)oxide Surfaces, *J. Colloid Interface Sci.* **229** (2000) 286-297.

[6] A.L. Foster, G.E. Brown, G.A. Parks, X-ray absorption fine structure study of As(V) and Se(IV) sorption complexes on hydrous Mn oxides, *Geochim. Cosmochim. Acta* **67** (2003) 1937-1953.

[7] K.F. Hayes, A.L. Roe, G.E. Brown, K.O. Hodgson, J.O. Leckie, G.A. Parks, In situ x-ray absorption study of surface complexes of selenium oxyanions on α-FeOOH, *Science* **238** (1987) 783-786.

[8] C.M. Gonzalez, J. Hernandez, J.G. Parsons, J.L. Gardea-Torresdey, Removal of selenite and selenate from aqueous solutions using a magnetic iron/manganese oxide nanomaterial, *Microchem. J.* (2010) In Press.

[9] T. Ressler, WinXAS: a program for X-ray absorption spectroscopy data analysis under MS-Windows, *J. Synchrotron Radiat.* **5** (1998) 118-122.

[10] D. Bazin, D. Sayers, J. J. Rehr, C. Mottet, Numerical Simulation of the Platinum L_{III} Edge White Line Relative to Nanometer Scale Clusters, *J. Phys. Chem. B* **101** (1997) 5332-5336.

[11] S.M. Webb, J. Gaillard, L.Q. Ma, C. Tu, XAS speciation of arsenic in a hyper-accumulating fern, *Environ. Sci. Technol.* **37** (2003) 754-760.

Curriculum Vita

Christina Marie Gonzalez was born in El Paso, Texas on October 25, 1985 and is the second daughter of David Gonzalez and Helen R. Gonzalez. In the fall of 2004, Christina enrolled in undergraduate studies at the University of Texas at El Paso (UTEP). During her undergraduate studies, Christina had the opportunity to do research to test for metabolic toxins in *Ginkgo biloba* extracts using the Lumitection Analysis method, which involves the use of bioluminescent bacteria under the supervision of Dr. James Becvar. In December 2007, she graduated cum laude from UTEP with a Bachelor's Degree in Chemistry and a minor in Mathematics. In addition to this, Christina also received an award for Outstanding Undergraduate in Chemistry with Highest GPA. In the spring of 2008, she entered the Graduate School of UTEP to obtain her Master of Science degree in environmental/analytical chemistry under the guidance and supervision of Dr. Jorge Gardea-Torresdey, Chair of the Chemistry Department. During her graduate studies, Christina studied the ability of iron and manganese oxide based nanomaterials to remove selenium oxoanions from aqueous solutions. In addition to her research, she was awarded the National Science Foundation Graduate Teaching Fellows in K-12 Education fellowship and was elected by her peers to be Secretary of the Paso Del Notre Society for the Advancement of Chicanos and Native Americans UTEP Chapter. While at UTEP, she authored and coauthored scientific publications and gave several presentations at national and regional conferences.

Publications:

C.M. Gonzalez, J. Hernandez, J.G. Parsons, J.L. Gardea-Torresdey, Removal of selenite and selenate from aqueous solutions using a magnetic iron/manganese oxide nanomaterial, *Microchemical Journal* (2010) In Press.

J.G. Parsons, M.L. Lopez, C.M. Gonzalez, J.R. Peralta-Videa, J.L. Gardea-Torresedey, Toxicity and Biotransformation of uncoated and coated nickel hydroxide nanoparticles on mesquite plants, *Environmental Toxicology and Chemistry* 29 (2010) 1146-1154.

Oral Presentations:

C.M. Gonzalez, J. Hernandez, J.G. Parsons, J.L. Gardea-Torresdey, "Sorption and interference batch studies of selenite (SeO_3^{2-}) and selenate (SeO_4^{2-}) to engineered nano-Jacobsite in aqueous solutions," 239th American Chemical Society National Meeting and Exposition, March 2010.

C.M. Gonzalez, J. Hernandez, J.G. Parsons, J.L. Gardea-Torresdey, Sorption of Selenite (SeO_3^{2-}) and Selenate (SeO_4^{2-}) to engineered nano-Jacobsite, Society for Advancement of Chicanos and Native Americans in Science National Conference, Oct. 2009

Poster Presentations:

C.M. Gonzalez, J. Hernandez, J.G. Parsons, J.L. Gardea-Torresdey, Sorption and Interference Studies of Selenite (SeO_3^{2-}) and Selenate(SeO_4^{-2}) to Engineered Nano-Jacobsite, 65th American Chemical Society Southwest Regional Meeting, Nov. 2009.

C.M. Gonzalez and J.E. Becvar, Analysis of *Ginkgo biloba* extracts for metabolic toxins using Lumitection Analysis Method, Society for Advancement of Chicanos and Native Americans in Science National Conference, Oct 2008.

Permanent Address:

11346 Esmara Ct.

El Paso, Texas 79936

This thesis was typed by Christina Marie Gonzalez